MEASUREMENT OF THERMAL ELECTRON DISSOCIATIVE ATTACHMENT RATES FOR HALOGEN GASES USING A FLOWING AFTERGLOW TECHNIQUE

By

GARY DONALD SIDES

A DISSERTATION PRESENTED TO THE GRADUATE COUNCIL OF
THE UNIVERSITY OF FLORIDA
IN PARTIAL FULFILLMENT OF THE REQUIREMENTS FOR THE
DEGREE OF DOCTOR OF PHILOSOPHY

UNIVERSITY OF FLORIDA

1975

Copyright, 1975, by Gary Donald Sides

ACKNOWLEDGMENTS

The author wishes to express his appreciation to the many people who have contributed to the completion of this research. Special thanks are due Professor Robert J. Hanrahan, Chairman of his Supervisory Committee, whose tireless efforts on his behalf made this research possible. The author also thanks Dr. Thomas O. Tiernan, Co-Chairman of his Supervisory Committee, whose co-operation indeed made this dissertation possible. Special thanks are due Professor E.E. Muschlitz, Jr., who was instrumental in getting an assignment for the author at the Aerospace Research Laboratories. Thanks are also due Dean Miller for his technical assistance, Dr. B. Mason Hughes for his advice and computer programming assistance, Julius Becsey for the loan of his direct grid search subroutine, Dr. E. Grant Jones for reading this dissertation and suggesting improvements, and Alexis VanDenAbell for her administrative assistance. The author also appreciates the excellent support of the skilled machinists, draftsmen and glassblowers at the Aerospace Research Laboratories. In addition, the author wishes to express his gratitude to the Aerospace Research Laboratories and the United States Air Force for allowing this research to be completed.

The author wishes to thank his wife, Sarah, both for typing the dissertation and for tolerating the many inconveniences caused by years of graduate study.

TABLE OF CONTENTS

	Page
ACKNOWLEDGMENTS	iii
LIST OF TABLES	vi
LIST OF FIGURES	vii
ABSTRACT	ix
CHAPTER I. INTRODUCTORY DISCUSSION	1
A. Electron Attachment	1
B. Discussion of Literature Data	5
1. Fluorine	5
2. Chlorine	8
3. Bromine	17
4. Summary of Published Data	21
C. Experimental Approach	23
CHAPTER II. DESCRIPTION OF THE FLOWING AFTERGLOW SYSTEM	26
A. Experimental Apparatus	26
B. Data Acquisition	41
CHAPTER III. MATHEMATICAL MODEL	54
A. Basic Model	54
B. Axial Flow Velocity	56
C. Radial Diffusion of Charged Species	69
D. Inlet Effects	75
E. Reactant/Electron Number Density Ratio	76
F. Ambipolar Diffusion	77
CHAPTER IV. DATA REDUCTION	79
A. Jacobian Matrix Technique	81
B. Grid Search Technique	91

Page

CHAPTER V. EXPERIMENTAL RESULTS 105

A. Microwave Discharge Source 105
1. Electron Energy 105
2. Electron Attachment in Sulfur Hexafluoride 106
3. Electron Attachment in Fluorine 110
4. Sulfur Hexafluoride - Oxygen Negative Ion Charge Transfer 111
B. Filament Source 115
1. Electron Energy 115
2. Electron Attachment in Sulfur Hexafluoride 116
3. Electron Attachment in Fluorine 117
4. Electron Attachment in Chlorine 117
5. Electron Attachment in Oxygen 118
6. Electron Attachment in Bromine 121

CHAPTER VI. DISCUSSION OF RESULTS 128

A. Comparison with Published Data 128
B. Significance of the Results 132
C. Assumptions Made in the Derivation of the Mathematical Model 133
D. Suggestions for Modification of the Flowing Afterglow Apparatus and Further Research 134

APPENDIX I. ANALYSIS OF THE FLUORINE/ARGON MIXTURE 137

APPENDIX II. ELECTROSTATIC LENS SYSTEM 139

APPENDIX III. THERMALIZATION OF ELECTRONS BY ELASTIC COLLISIONS IN AN ARGON AFTERGLOW 145

APPENDIX IV. EXPERIMENTAL DATA 150

LIST OF REFERENCES 160

BIOGRAPHICAL SKETCH 164

LIST OF TABLES

Table		Page
1.	Measured First Appearance Potentials (eV) for Dissociative Electron Attachment in Chlorine	14
2.	Measured First Appearance Potentials (eV) for Dissociative Electron Attachment in Bromine	20
3.	Measured First Appearance Potentials (eV) for Dissociative Electron Attachment in the Halogens	22
4.	Thermal Electron Dissociative Attachment Rates	23
5.	Rate Constants Determined in the Present Experiments ...	126
6.	Comparison of the Present Results with Published Data ..	129
7.	Electron Energy Versus Time Calculations for an Afterglow	149
8.	Data Listings Key	150

LIST OF FIGURES

Figure		Page
1.	Potential Energy Diagram for Dissociative Electron Attachment to Diatomic Molecules	2
2.	Potential Energy Diagram for Electron Attachment to Sulfur Hexafluoride	6
3.	Electron Attachment Probability in Chlorine Versus the Pressure-Reduced Electric Field	9
4.	Calculated Electron Attachment Thresholds Versus Experimental Thresholds Measured by Bradbury	11
5.	Electron Attachment Probability in Chlorine Versus Electron Energy	12
6.	Electron Attachment Cross-Section Versus Electron Energy for Chlorine and Bromine	18
7.	Electron Attachment Coefficient Versus the Pressure-Reduced Electric Field for Chlorine and Bromine	19
8.	Flowing Afterglow Apparatus in the Microwave Discharge Source Configuration	27
9.	Flowing Afterglow Apparatus in the Filament Source Configuration	29
10.	Filament Emission Regulator Circuit	30
11.	Buffer Gas Rotameter Calibration Curves	33
12.	Buffer Gas Volume Flow Rate Versus Flow Tube Pressure	34
13.	Reactant Gas Linear Mass Flowmeter Calibration	37
14.	Comparison of Two Techniques Used to Measure the Reactant Gas Number Density	40
15.	Computer-Interfaced Data Acquisition System	42

Figure		Page
16.	Magnetic Disc Data File Organization	45
17.	Experimental Configuration for the Measurement of Transit Times for Ions in the Flow Tube	58
18.	Sample Trace Obtained in the Measurement of Ion Transit Times in the Flow Tube	60
19.	Measured Ion Transit Times in the Flow Tube Versus Pressure for the Microwave Discharge Source Configuration	63
20.	Filament Source Configuration for the Measurement of Ion Transit Times in the Flow Tube	66
21.	Measured Ion Transit Times in the Flow Tube Versus Pressure for the Filament Source Configuration	68
22.	Dissociative Electron Attachment in Fluorine	85
23.	Dissociative Electron Attachment and Br_3^- Formation in Bromine	104
24.	SF_5^-/SF_6^- Ratio in the Microwave Discharge Source Configuration	107
25.	F^- Ion Signal Versus the Partial Pressure of an Argon Metastable Atom Quenchant, Nitrogen, Injected into the Afterglow	112
26.	Charge Transfer Between SF_6 and O_2^-	114
27.	Dissociative Electron Attachment in Chlorine	119
28.	Electron Attachment in Oxygen	120
29.	Formation of Br_3^- in Bromine	123
30.	Dissociative Electron Attachment in Bromine	124
31.	Electrostatic Lens System	140
32.	Electrostatic Lens Control Circuit	142
33.	Electrostatic Lens Performance	143

Abstract of Dissertation Presented to the Graduate Council
of the University of Florida in Partial Fulfillment of the Requirements
for the Degree of Doctor of Philosophy

MEASUREMENT OF THERMAL ELECTRON DISSOCIATIVE ATTACHMENT RATES FOR HALOGEN GASES USING A FLOWING AFTERGLOW TECHNIQUE

By

Gary Donald Sides

June, 1975

Chairman: Robert J. Hanrahan
Major Department: Chemistry
Co-Chairman: Thomas O. Tiernan
Aerospace Research Laboratories

A flowing afterglow apparatus was designed, constructed and used to measure thermal electron dissociative attachment rates in the halogen gases fluorine, chlorine and bromine. Electrons were produced in a high velocity buffer gas flow using either a microwave discharge source or a filament source. The electrons and positive ions produced in the source were carried past a reactant gas injection port by the high velocity viscous flow of the buffer gas. The halogen gas injected at that port then reacted with the electrons to form halide ions. These ions were sampled at the end of the reaction tube by a quadrupole mass spectrometer. By monitoring the negative ion signal as a function of the halogen gas flow injected into the reaction tube, electron attachment rates could be deduced. The operation of the flowing afterglow system was checked by

measuring the thermal attachment rate for electrons in sulfur heaxafluoride. The average value obtained for this rate constant was $3.9 \pm 1.4 \times 10^{-8}$ cm^3/molecule-sec. The average rate constants obtained for the rates of dissociative electron attachment in fluorine, chlorine and bromine were $3.8 \pm 1.2 \times 10^{-9}$, $3.7 \pm 1.7 \times 10^{-9}$ and $1.1 \pm 0.9 \times 10^{-11}$ cm^3/molecule-sec, respectively. Electrons produced in the source of the flowing afterglow system are rapidly thermalized in the high pressures present in the flow tube. Electron temperatures were estimated to be 300-600°K in the present experiments. The rate of the three-body attachment reaction $Br^- + Br_2 + Ar$ to form Br_3^- was also measured and found to be $1.9 \pm 1.0 \times 10^{-28}$ cm^6/molecule^2-sec. A charge transfer reaction, $SF_6 + O_2^-$, and the three-body attachment of electrons to oxygen were also observed using the flowing afterglow apparatus.

CHAPTER I

INTRODUCTORY DISCUSSION

A. Electron Attachment

Dissociative electron attachment to diatomic molecules is generally thought to proceed by a resonance mechanism in which the electron is first attached to the molecule to form a molecular ion complex.[1] The negative ion formed may then undergo auto-ionization (that is, ejection of the electron) and revert to the neutral molecular state or it may dissociate into an atom and an atomic ion. The sequence of steps in equation form are

$$e^- + AA \rightleftarrows (AA^-)^* \rightarrow A^- + A \qquad (1)$$

This reaction sequence may be discussed in terms of a potential energy diagram as shown in Figure 1. The Franck-Condon region is defined by the line ab. Electrons with an energy between E_1 and E_2 will be attached by the molecule to form the negative ion complex $(AA^-)^*$. The nuclei then begin to separate, their energy following the upper potential curve. During the separation the negative molecular ion is subject to auto-ionization, a process by which it may revert to the neutral state with the ejection of an electron, possibly leaving the neutral molecule vibrationally excited. If the complex ion nuclei separate to

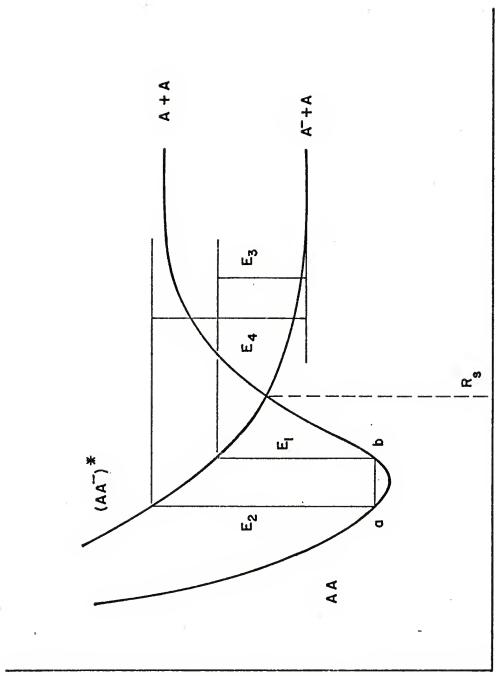

Figure 1. Potential Energy Diagram for Dissociative Electron Attachment to Diatomic Molecules

the radius R_s without undergoing auto-ionization, then the negative ion becomes stable against auto-ionization and the ion dissociates. The fragments of dissociation, A^- and A, have a total kinetic energy between E_3 and E_4.

The rate of dissociative electron attachment will then depend not only upon the rate of electron capture to form the molecular negative ion but also upon the lifetime of this resonance state against auto-ionization and the time required for the nuclei to move a distance R_s apart. The average lifetime of the resonance state against auto-ionization is written as $\hbar/\Gamma$ where Γ is the width (in energy units) for auto-ionization and $\hbar$ is Planck's constant divided by 2π. If τ is the time required by the nuclei to separate to $R=R_s$, then the dissociative attachment cross-section may be written as

$$\sigma_{DA} = \sigma_C \exp[-\bar{\Gamma}\tau/\hbar] \qquad (2)$$

where σ_C is the electron capture cross-section and $\bar{\Gamma}$ is the width for auto-ionization averaged over the nuclear separation R_C ($R=R_C$ at electron capture) to R_s since $\Gamma=\Gamma(R)$ and $\Gamma(R_s)=0$ (that is, auto-ionization is no longer possible for $R>R_s$).[1]

For the halogen gases fluorine, chlorine and bromine, the electron affinities of the halide atoms are greater than the corresponding neutral molecule dissociation energies. This means that the molecular negative ion, formed by a two-body electron-halogen molecule collision, will be produced at an energy much greater than the dissociation energy of the ion. Thus, the ion formed will dissociate within one vibrational period.

This will be the case whether the molecular ion is formed in a repulsive or an attractive state. In order for thermal electron dissociative attachment in the halogen gases to be possible, the molecular negative ion potential curve (repulsive or attractive) must intersect the neutral molecule potential curve in the Franck-Condon region.

The discussion above indicates the mechanism by which electrons undergo dissociative attachment to the halogen molecules chlorine, fluorine and bromine, whose dissociative electron attachment rates were measured in the current research. In this research the rate of electron attachment to sulfur hexafluoride was also measured. Electron attachment to form a molecular negative ion, such as SF_6^-, may be explained by a two-step mechanism in which the electron is first attached to the molecule to form a molecular negative ion.[2] However, the negative ion is vibrationally excited and may eject an electron through auto-ionization unless a process takes place to remove the excess energy. Since relaxation through vibrational transitions is a slow process, it is thought that collisional stabilization is the dominant relaxation mechanism if the pressure is not too low.[1] In equation form the electron attachment to SF_6 may be written

$$SF_6 + e^- \rightleftarrows (SF_6^-)^* \xrightarrow{M} SF_6^- \qquad (3)$$

where M is the species removing the vibrational energy of $(SF_6^-)^*$ through inelastic collisions. If one considers the

molecule SF_6 as a diatomic molecule SF_5-F, then the electron attachment mechanism may be explained in terms of the simple potential energy diagram in Figure 2. The Franck-Condon region is again defined by the line ab. Since the cross-section for the attachment of electrons to sulfur hexafluoride is a maximum for thermal energy electrons,[3] the potential curve for SF_6^- must cross the minimum of the SF_6 curve. Thus, electrons with an energy between 0 and E_2 will be attached to SF_6 to form vibrationally excited SF_6^-. If the vibrational energy is removed by collisional stabilization, then a stable negative ion, SF_6^-, results. If the excited negative ion is not collisionally stabilized, then ejection of the electron may occur. If the initial energy of the electron is between E_2 and E_3, then the negative ion formed may dissociate.[4] It has been shown that the ratio of SF_5^-/SF_6^- in a flowing afterglow is independent of pressure.[2] This would indicate that the $(SF_6^-)^*$ complex probably dissociates within a vibrational period ($\sim 10^{-13}$ sec).[2] It has also been shown experimentally that the ratio of SF_5^-/SF_6^- obtained by the attachment of electrons to sulfur hexafluoride can be used as a measure of the electron temperature or average electron energy.[2,5]

B. Discussion of Literature Data

1. Fluorine

A thorough search of chemistry and physics literature failed to yield any experimental measurements or theoretical

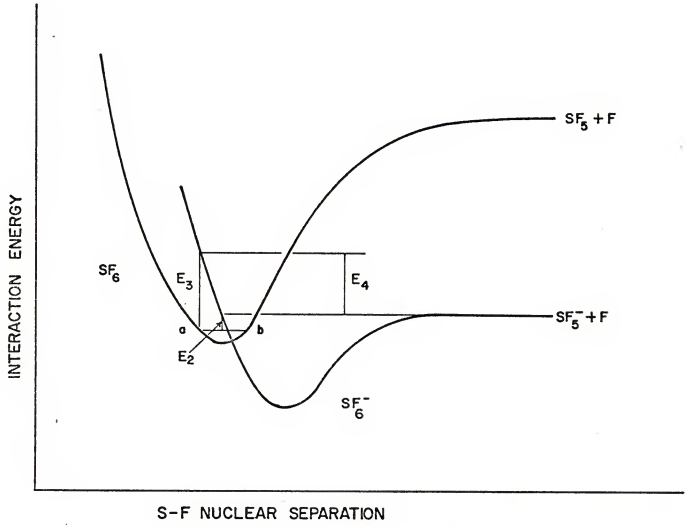

Figure 2. Potential Energy Diagram for Electron Attachment to Sulfur Hexafluoride

estimates for electron attachment cross-sections, rates, coefficients or probabilities in fluorine. Due to the extreme reactivity and corrosive nature of this gas, most researchers seem reluctant to investigate its properties in kinetics instruments.

The minimum appearance potential of F^- ions from the dissociative attachment reaction

$$e^- + F_2 \rightleftarrows (F_2^-)^* \rightarrow F^- + F \qquad (4)$$

can be calculated from the known electron affinity of the fluorine atom, EA(F) = 3.62 eV,[6] and the molecular fluorine dissociation energy, $D(F_2)$ = 1.60 eV,[7] using the equation

$$A(F^-) = D(F_2) - EA(F) + K + E \qquad (5)$$

where $A(F^-)$ denotes the appearance potential of F^- ions and K and E represent the kinetic and excitation energies, respectively, of the products of the reaction. If K and E are zero for the dissociative attachment process, then

$$A(F^-) = 1.60 - 3.62 = -2.02 \text{ eV} \qquad (6)$$

Therefore, the reaction is exothermic and would be expected to have a zero energy threshold. This has been confirmed by Burns[8] who demonstrated that F^- ions are formed by electrons with zero energy and is consistent with the work of Thorburn,[9] who found that the appearance potential of F^- ions, produced by dissociative electron attachment to fluorine, was less

than 2 eV, the lower energy limit of his electron source. In addition, DeCorpo and Franklin[10] have obtained an appearance potential of 0 ± 0.1 eV for F^- ions produced by dissociative electron attachment in fluorine.

2. Chlorine

Though several investigations of the electron attachment mechanism in chlorine have been made, there is still considerable disagreement concerning the threshold value and the attachment cross-section versus energy behavior for this reaction.[9,11-17] In addition, no thermal electron attachment reaction rates have been published.

The electron affinity of chlorine, EA(Cl) = 3.82 eV,[6] and the molecular dissociation energy, $D(Cl_2)$ = 2.48 eV,[7] can be used to calculate the minimum appearance potential for Cl^- ions in the dissociative attachment reaction, assuming K and E to be zero.

$$A(Cl^-) = 2.48 - 3.82 = -1.34 \text{ eV} \qquad (7)$$

The reaction is exothermic and would be expected to have a zero energy threshold.

Bradbury[11] used a drift tube method to measure electron attachment probabilities in chlorine/argon mixtures as a function of the pressure-reduced electric field, E/P, which is directly proportional to the average electron energy in the gas. His data are shown in Figure 3. He obtained a threshold of less than 1 volt/cm-Torr for dissociative electron attachment

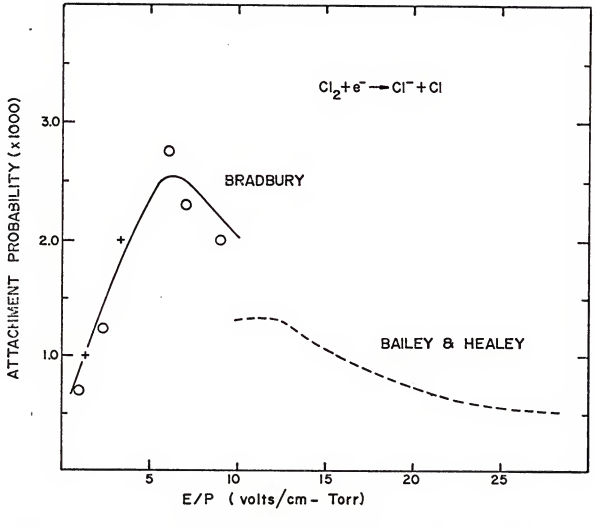

Figure 3. Electron Attachment Probability in Chlorine Versus the Pressure-Reduced Electric Field (After References 11 and 12)

in chlorine. In order to determine the approximate energy of electrons corresponding to E/P = 1 volt/cm-Torr, the calculated dissociative electron attachment threshold energies versus the measured E/P thresholds for the dissociative attachment reactions studied by Bradbury are shown in Figure 4. This plot indicates that the threshold for dissociative electron attachment in chlorine is in the range less than 0.1-1.1 eV, the energy range corresponding to less than 1 volt/cm-Torr. The dashed lines indicate the range of energy values possible for a given measured threshold (measured in E/P units). Although it is recognized that the average electron energy for a given E/P value is a function of the composition of the gaseous medium, the threshold estimate above should be reasonable since a variety of gaseous environments were used in this "calibration" plot.

Bailey and Healey[12] used a drift tube apparatus to determine the attachment probability as a function of the pressure-reduced electric field, E/P, for electrons in chlorine and carbon dioxide or helium mixtures. In addition, they were able to convert these data to attachment probability as a function of electron energy data. The resulting data, shown in Figure 5, indicate a threshold for the reaction of about 0.3 eV.

Thorburn[9] used a mass spectrometer to determine the appearance potential of Cl^- ions formed by the dissociative electron attachment reaction in chlorine. He found the appearance potential to be less than 2 eV, the minimum electron energy obtainable in his source. He also observed an appearance potential, $A(Cl^-)$, at 4.4 ± 0.2 eV which he postulated could

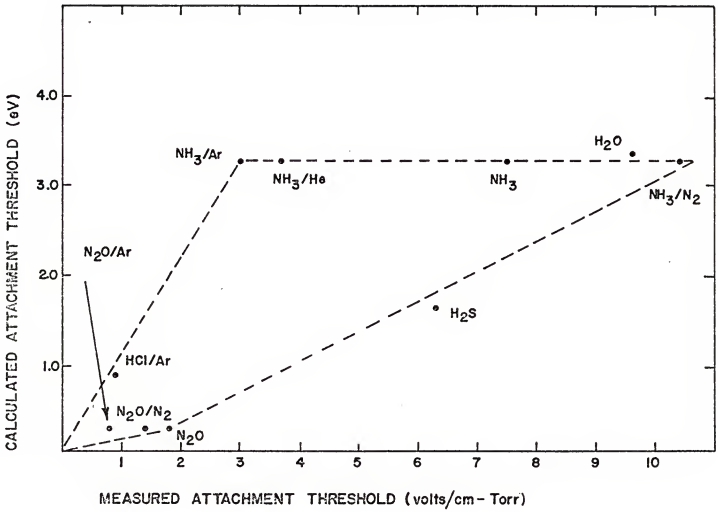

Figure 4. Calculated Electron Attachment Thresholds Versus Experimental Thresholds Measured by Bradbury

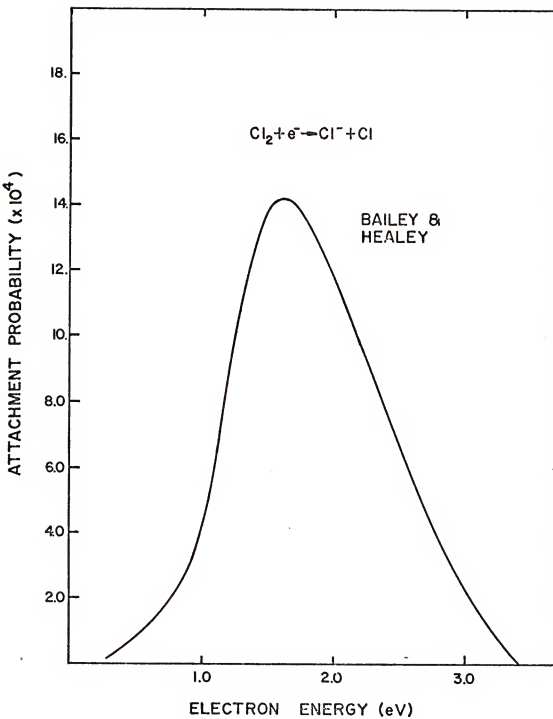

Figure 5. Electron Attachment Probability in Chlorine Versus Electron Energy (After Reference 12)

be explained by dissociative electron attachment in chlorine in which one of the products, Cl^- or Cl, was in an excited state.

Frost and McDowell[13] used a mass spectrometer with a monoenergetic electron source and measured an appearance potential of 1.60 ± 0.05 eV for Cl^- ions in chlorine with a maximum at 2.4 eV. This value falls outside the energy range for the appearance potential, $A(Cl^-)$, deduced from the Bradbury[11] data. Neither does it agree with the expected appearance potential of zero deduced by comparing the dissociation energy of molecular chlorine with the electron affinity of the chlorine atom. The resonance observed by Frost and McDowell is probably one in which the molecular ion is formed in an excited electronic state which then dissociates. This would explain the apparently high appearance potential obtained in their work. Frost and McDowell did not see the process producing Cl^- ions at 4.4 eV that Thorburn[9] observed.

Moe[14] used an RPD electron gun in a trapped electron apparatus and observed four resonance peaks attributed to dissociative attachment in chlorine. These peaks were located at 0, 1.75, 3.07 and 5.9 ± 0.17 eV. The first resonance peak is due to dissociative electron attachment in which the molecular ion potential energy curve intersects the neutral molecule potential energy curve in the Franck-Condon region. The other three resonances are probably ones in which the molecular ion is formed in an excited electronic state which then dissociates. Note that the second resonance at 1.75 ± 0.17 eV is probably

the same resonance observed by Frost and McDowell[13] with a threshold at 1.60 ± 0.05 eV and a maximum at 2.4 eV.

Dunkin et al.[15] have reported the qualitative observation of large dissociative electron attachment rates for chlorine in a flowing afterglow apparatus. This finding supports a zero energy threshold, since electrons in the high pressure helium afterglow are known to be near thermal energies.[2]

Thus, there appears to be some disagreement concerning the energetics of the dissociative attachment of electrons to chlorine. Table 1 summarizes the observations to date of the first appearance potential for Cl^- ions produced by dissociative electron attachment in chlorine.

Table 1

Measured First Appearance Potentials (eV) for Dissociative Electron Attachment in Chlorine

A(Cl^-)	Author(s)
<0.1-1.1	Deduced from Bradbury[11] data
0.3	Deduced from Bailey and Healey[12] data
<2	Thorburn[9]
1.6 ± 0.05	Frost and McDowell[13]
0 ± 0.17	Moe[14]
∿0	Dunkin et al.[15]

These data show the disagreement concerning whether thermal electrons (∿0.03 eV) will undergo dissociative attachment in chlorine.

As was previously mentioned, Bradbury used a drift tube method to determine the attachment probability for electrons in chlorine/argon mixtures as a function of the pressure-reduced electric field as shown in Figure 3. Extrapolating the measured attachment probabilities, h, to E/P=0 yields $h \simeq 5 \times 10^{-4}$ at thermal electron energies. This agrees with a value for $h \simeq 5 \times 10^{-4}$ measured by Wahlin.[16] Electron attachment cross-sections can be calculated from the observed attachment probabilities using the equation

$$\sigma = h/\lambda_1 N_1 \qquad (8)$$

where λ_1 is the electron mean free path at one Torr and N_1 is the number of molecules per cubic centimeter per Torr.[18] Since Bradbury did not state the composition of the Cl_2/Ar mixture used in his experiments, the cross-section was first calculated assuming the thermal electrons to be in 100% chlorine and then calculated assuming 100% argon (that is, much more argon than chlorine), these concentrations representing the two possible extremes. λ_1 for thermal electrons in argon is 0.13 cm.[19] The calculated cross-section for thermal electron dissociative attachment to chlorine is then 1.2×10^{-19} cm^2. The mean free path for thermal electrons in chlorine at one Torr is approximately 0.0005 cm.[12] This results in an attachment cross-section of 3.0×10^{-17} cm^2. Thus, analysis of the Bradbury data yields a thermal dissociative electron attachment cross-section of $1.2 - 300 \times 10^{-19}$ cm^2. This corresponds to

a rate constant of 1.2-300 x 10^{-12} cm^3/molecule-sec for thermal energy electrons.

As was previously mentioned, Bailey and Healey[12] used a drift tube apparatus to determine the attachment probability as a function of E/P for electrons in chlorine and carbon dioxide or helium mixtures. They also measured the electron mean free path, drift velocity and free path velocity as a function of E/P. These data enabled them to calculate attachment coefficients, cross-sections and rate constants as a function of E/P or electron energy. The attachment probability as a function of E/P is shown in Figure 3. The maximum in the Bradbury[11] data is at 6 volts/cm-Torr while that in the Bailey and Healey data is at 11 volts/cm-Torr. The average electron energy in chlorine and carbon dioxide or helium mixtures for a given E/P is expected to be lower than that in a mixture of chlorine and argon, since electrons transfer energy more efficiently to carbon dioxide or helium than argon.[20] Thus, the maximum in the Bailey and Healey data occurs at a higher E/P than the Bradbury data, since the average electron energy is directly proportional to E/P.[20] Bailey and Healey also obtained the attachment probability as a function of electron energy; these data are shown in Figure 5. As previously stated, these data yield a threshold for dissociative attachment near 0.3 eV and a maximum at 1.5 eV. The Bailey and Healey data may also be converted to the attachment cross-section as a function of electron energy and to the attachment coefficient as a function

of E/P. These data are shown in Figures 6 and 7, respectively, and as stated above illustrate a significant attachment cross-section for electrons at energies as low as 0.3 eV.

Bozin and Goodyear[17] measured attachment coefficients in pure chlorine as a function of the pressure-reduced electric field. They obtained these data by observing the variation of pre-breakdown ionization currents with distance between parallel electrodes for E/P between 70 and 150 volts/cm-Torr. Their results are shown in Figure 7. In the E/P regions in which the Bozin and Goodyear and the Bailey and Healey data overlap, the attachment coefficients measured by the latter are much less than those measured by Bozin and Goodyear. Bozin and Goodyear interpret this disagreement as being partially due to the neglect of the effects of ionization ignored by Bailey and Healey.

3. Bromine

There is general agreement among researchers that the dissociative attachment of electrons to bromine is a zero energy threshold process. This is expected in view of the fact that the electron affinity of the bromine atom, EA(Br) = 3.49 eV,[21] is larger than the molecular dissociation energy, $D(Br_2)$ = 1.97 eV.[22] The minimum appearance potential for Br^- ions from the reaction can then be calculated from

$$A(Br^-) = 1.97 - 3.49 = -1.52 \text{ eV} \qquad (9)$$

assuming K and E to be zero. Thus, the reaction is exothermic

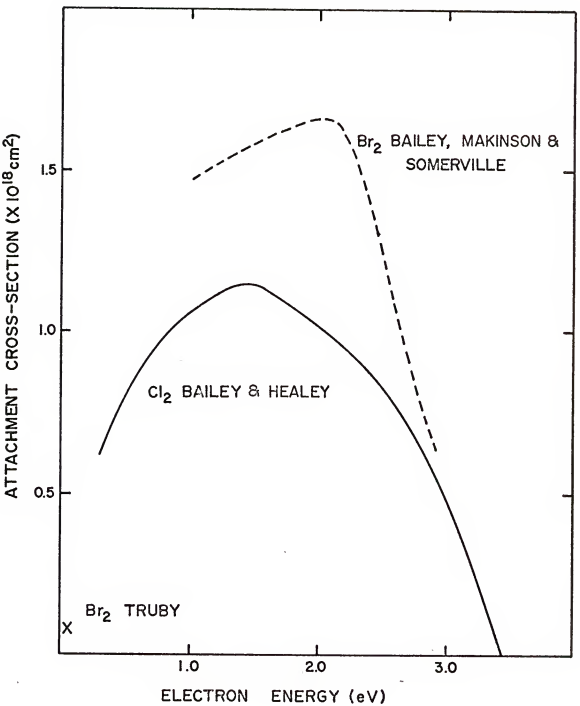

Figure 6. Electron Attachment Cross-Section Versus Electron Energy for Chlorine and Bromine (After References 12, 23 and 24)

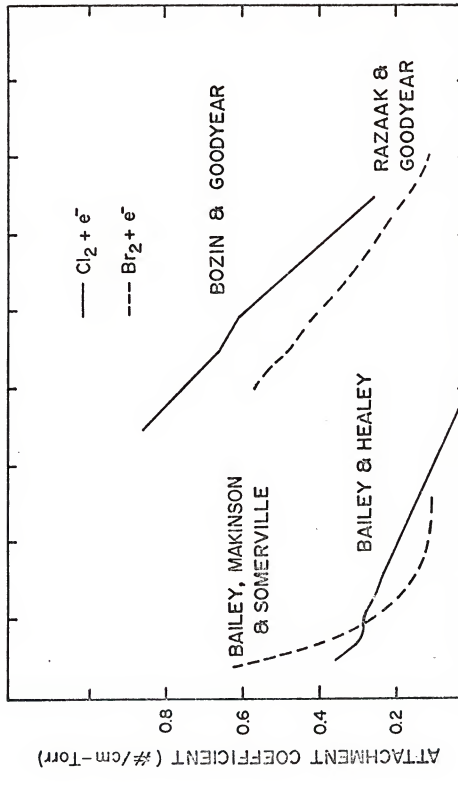

Figure 7. Electron Attachment Coefficient Versus the Pressure-Reduced Electric Field for Chlorine and Bromine (After References 12, 17, 23 and 25)

and a zero energy threshold is not surprising. Table 2 summarizes the first appearance potentials measured for the bromine-electron reaction. All of the data listed in this table are consistent with a zero energy threshold for dissociative electron attachment in bromine.

Table 2

Measured First Appearance Potentials (eV) for Dissociative Electron Attachment in Bromine

$A(Br^-)$	Author(s)
<0.7	Deduced from Bailey et al.[23]
0.03 ± 0.03	Frost and McDowell[13]
0.05 ± 0.17	Moe[14]
∿0.03	Deduced from Truby[24]

Bailey et al.[23] used their drift tube apparatus to investigate electron attachment in bromine and helium or carbon dioxide mixtures. The resulting attachment coefficients versus pressure-reduced electric field data are shown in Figure 7. Since they also measured the electron free velocity and drift velocity in these mixtures, the attachment coefficients may be converted to attachment cross-sections. These data are shown as a function of energy in Figure 6.

Frost and McDowell[13] observed a maximum Br^- ion current due to the dissociative attachment of electrons in bromine at 0.03 eV with the ion signal dropping to zero at 0.72 eV.

Moe[14] used the trapped electron technique mentioned above and noted dissociative electron attachment resonance peaks at 0.05, 0.98 and 3.30 ± 0.17 eV. The first peak is due to attachment in which the potential energy curve for the molecular ion intersects the neutral molecule potential energy curve in the Franck-Condon region while the other peaks are due to attachment yielding molecular ions, which dissociate, in higher energy states.

Razzak and Goodyear[25] measured attachment coefficients in pure bromine as a function of the pressure-reduced electric field using the same method employed for Bozin and Goodyear's[17] chlorine studies. The data obtained by them are shown in Figure 7. The coefficients obtained are again higher than the corresponding measurements by Bailey et al.[23]

Truby[24] used a microwave cavity technique to determine the rate constant for dissociative attachment of electrons in bromine at 296°K. He obtained a value of $k = 0.82 \times 10^{-12}$ cm^3/molecule-sec. This corresponds to a value for the attachment cross-section of 0.80×10^{-19} cm^2.

4. Summary of Published Data

Table 3 summarizes dissociative electron attachment appearance potential measurements, either published or deduced from published data (for references refer to the preceding discussion), for the halogens.

Table 3

Measured First Appearance Potentials (eV) for Dissociative Electron Attachment in the Halogens

Gas	Appearance Potentials
Fluorine	0, <2, 0 ± 0.1
Chlorine	<0.1-1.1, 0.3, <2, 1.6 ± 0.05, 0 ± 0.17, ∿0
Bromine	<0.7, 0.03 ± 0.03, 0.05 ± 0.17, ∿0.03

Appearance potential measurements indicate that both fluorine and bromine have a zero energy dissociative electron attachment threshold as expected; however, there is some disagreement in the case of chlorine. The measurement of the rate of thermal energy electron attachment in chlorine would help settle the controversy.

Table 4 summarizes thermal electron dissociative attachment rate constants, either published or calculated from published data, for fluorine, chlorine and bromine. These data illustrate the need for further halogen thermal electron dissociative attachment studies. Not only are there no data for fluorine but there are also no definitive measurements for chlorine since the rates shown were extrapolated from data for which the electron energy is greater than thermal. In addition, there is a factor of eighteen disagreement between the rate measurement for bromine and a value extrapolated from the data of Bailey *et al.*

Table 4

Thermal Electron Dissociative Attachment Rates

Molecule	$k(cm^3/molecule\text{-}sec)$	Author(s)
Fluorine	none	
Chlorine	$1.2\text{-}300 \times 10^{-12}$	Extrapolated from Bradbury[11]
	$<6 \times 10^{-12}$	Extrapolated from Bailey and Healey[12]
	large	Dunkin et al.[15]
Bromine	1.5×10^{-11}	Extrapolated from Bailey et al.[23]
	0.82×10^{-12}	Truby[24]

C. Experimental Approach

In view of the absence of rate data for the attachment of thermal electrons to the halogen molecules, an apparatus was designed and constructed to obtain this information. A flowing afterglow technique was selected for these experiments after a review of the methods which have been used to measure thermal electron attachment rates. The flowing afterglow method was selected primarily because of the ease with which thermal electrons are produced in the afterglow.[2] In addition, this technique has been used previously to measure a thermal electron attachment rate.[2]

The present experiments were performed in three stages

1. the design and construction of the flowing afterglow apparatus,
2. the use of this apparatus to measure known reaction rates in order to determine whether the apparatus was functioning

properly and 3. the use of the apparatus to measure thermal electron attachment rates for the halogens. The reactions used to check out the flowing afterglow apparatus were

$$e^- + SF_6 \rightleftarrows (SF_6^-)^* \xrightarrow{M} SF_6^- \qquad (3)$$

and

$$SF_6 + O_2^- \rightarrow SF_6^- + O_2 \qquad (10)$$

Both of these reactions were selected because their rates had been measured using a flowing afterglow technique.[2,26] In addition, the thermal electron attachment rate for sulfur hexafluoride has been measured using a variety of experimental techniques.[2,27-30] During the course of experimental measurements in the flowing afterglow apparatus, another known reaction rate, that of the

$$O_2 + e^- \rightleftarrows (O_2^-)^* \xrightarrow{O_2} O_2^- \qquad (11)$$

reaction was also determined as a further check of experimental procedure.[31,32] Once the initial tests of the experimental technique were completed, the thermal electron attachment rates for the reactions

$$e^- + F_2 \rightleftarrows (F_2^-)^* \rightarrow F^- + F \qquad (4)$$

$$e^- + Cl_2 \rightleftarrows (Cl_2^-)^* \rightarrow Cl^- + Cl \qquad (12)$$

$$e^- + Br_2 \rightleftarrows (Br_2^-)^* \rightarrow Br^- + Br \qquad (13)$$

were determined. In addition, the reaction rate for

$$Br^- + Br_2 + Ar \rightarrow Br_3^- + Ar \qquad (14)$$

was determined in the course of the experiments.

CHAPTER II

DESCRIPTION OF THE FLOWING AFTERGLOW SYSTEM

A. Experimental Apparatus

The flowing afterglow apparatus in the microwave discharge source configuration is shown in Figure 8. Electrons are produced by a 2450 MHz microwave discharge (approximately 2 watts) in argon buffer gas in a quartz tube with an inside diameter of 1.1 cm. The microwave power supply[33] is coupled to the buffer gas by an Evenson cavity[34] and the microwave power is monitored by a microwave power meter[35] (not shown). The buffer gas flow is measured by a rotameter[36] (not shown) and a linear mass flowmeter.[37] The buffer gas pressure is measured at the center of the reaction tube by a capacitance manometer.[38] Electrons produced in the active discharge are rapidly thermalized in the high pressure environment (1 to 4 Torr) and flow past the reactant gas injection port, where a gas such as fluorine may be introduced into the afterglow. The reactant gas flow is monitored by a linear mass flowmeter capable of measuring argon flows over the range 1 to 225 atm-microliters/sec.[39] Negative ions formed in the reaction tube (19.6 cm in length) are sampled through a 0.23 mm orifice, 0.076 mm in length, located on the tip of a stainless steel

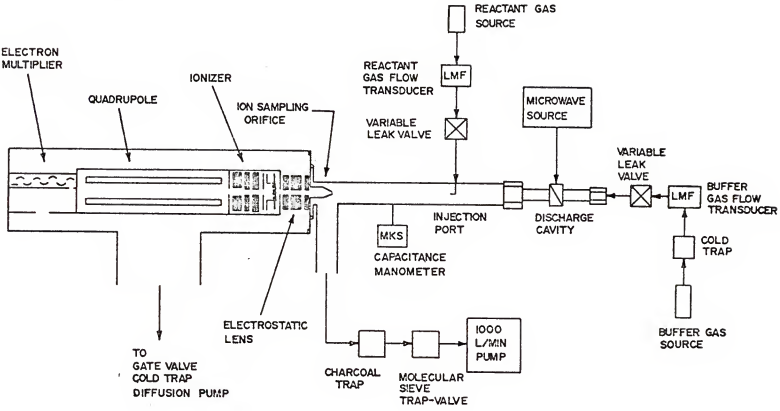

Figure 8. Flowing Afterglow Apparatus in the Microwave Discharge Source Configuration

cone. The cone is maintained at +4 to +13 volts with respect to ground in order to extract negative ions from the flowing afterglow at the end of the reaction tube. The ions extracted are focused by a cylindrical electrostatic lens system into the lens elements of an ionizer. These elements then focus the ions into a voltage-scanned quadrupole mass spectrometer.[40] The ions are then mass resolved by the quadrupole filter and detected by an electron multiplier. A preamp-electrometer (not shown) amplifies the resulting signal and provides analog outputs for computer and oscilloscope inputs. The flow tube is pumped by a 1000 liter/minute rotary pump.[41] A charcoal trap in the pump line converts fluorine to carbon tetrafluoride in order to prevent mechanical pump degradation. A molecular sieve trap in the pump line prevents back diffusion of hydrocarbons from the mechanical pump.

The flowing afterglow apparatus in the filament source configuration is shown in Figure 9. The basic difference between this configuration and that shown in Figure 8 is the removal of the microwave source and the substitution of a filament electron source. In addition, a sintered glass disc was installed upstream of the source in order to smooth the buffer gas flow through the flow tube. Also, at this point an automatic flow control system[42] was installed so that the reactant gas flow rate could be controlled by a computer during an experiment. The filament source is shown in detail in Figure 10. The filament is a thoriated-iridium ribbon[43] which is spot-welded to hermetic feedthroughs mounted in the

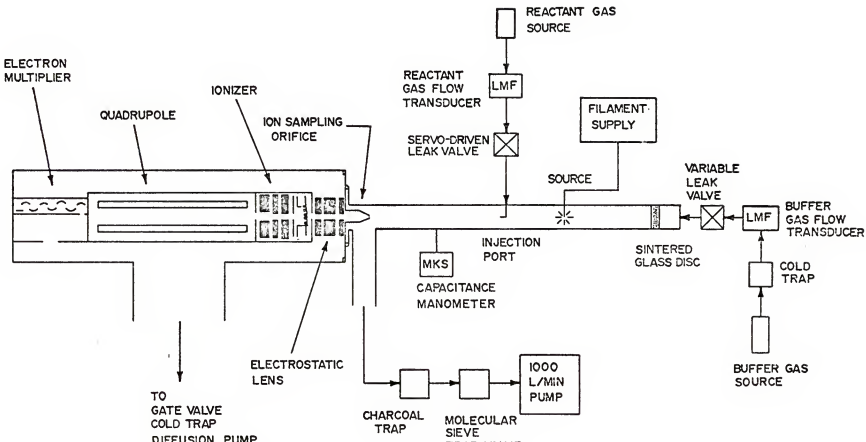

Figure 9. Flowing Afterglow Apparatus in the Filament Source Configuration

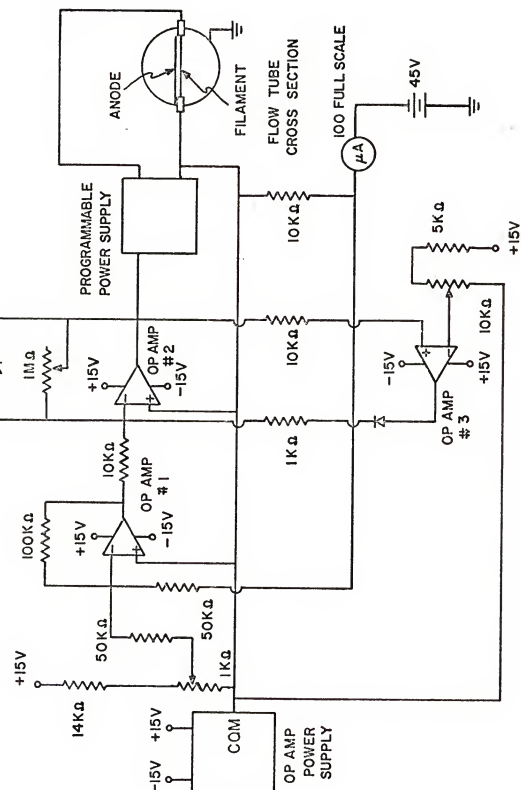

Figure 10. Filament Emission Regulator Circuit

flow tube walls. The anode is at ground potential and mounted approximately 1.3 mm from the filament. Filament current is supplied by a remotely programmable power supply.[44] Electrons emitted by thermionic emission from the filament are accelerated to the anode by the -45-volt negative bias applied to the filament. These electrons produce secondary electrons by ionization of the buffer gas in the flow tube. The secondary electrons are then swept down the flow tube by the axial velocity of the buffer gas and thermalized by elastic collisions in the high pressure environment. Filament emission is monitored by a microammeter.

The filament emission control circuit contains operational amplifiers #1 and #2 which provide the necessary voltage to the input of the programmable power supply. The emission current causes a voltage drop across a 10 kΩ resistor. This voltage drop is applied through a 50 kΩ resistor to the inverting input of operational amplifier #1. This technique provides feedback stabilization of the emission current. Operational amplifier #3 acts as a comparator to prevent the voltage input to the programmable power supply from exceeding the limit set by the 10 kΩ potentiometer. This prevents the passage of excess current through the filament (that is, prevents filament destruction).

The buffer gas generally used in these experiments was argon, the flow rate typically being 10-25 atm-cm^3/sec. Two methods were employed to monitor the buffer gas flow in these

studies. Initially, the buffer flow was measured with a rotameter, using both sapphire and stainless steel floats. Calibration curves at 20 psig (regulator gauge pressure) for the rotameter are shown in Figure 11. These curves were obtained using a bubble meter calibration method. Use of the rotameter for measuring flow rates has several disadvantages which severely limit its accuracy and utility. These include the dependence of the calibration on temperature and gas pressure, the poor dynamic range, the difficulty in accurately reading the meter, and the lack of an electrical signal output, which is needed for automated readout devices. Therefore, a linear mass flowmeter was used to measure flow rates for all experiments presented in this report. The flowmeter used to measure buffer flow permits monitoring of flow rates up to 155 atm-cm^3/sec with an accuracy of approximately ±0.1% of full scale. The calibration of this meter remains constant over a pressure range 1 psia (absolute pressure) to 150 psig. In addition, the meter provides a 5-volt output signal at full scale for use with a readout device. The buffer gas linear mass flowmeter was not calibrated in this laboratory but was calibrated by the manufacturer.[37]

Figure 12 is a plot of buffer gas flow versus pressure in the flow tube. The buffer gas flow was calculated from the relation

$$F = f(T/273.15)(760/P) \qquad (15)$$

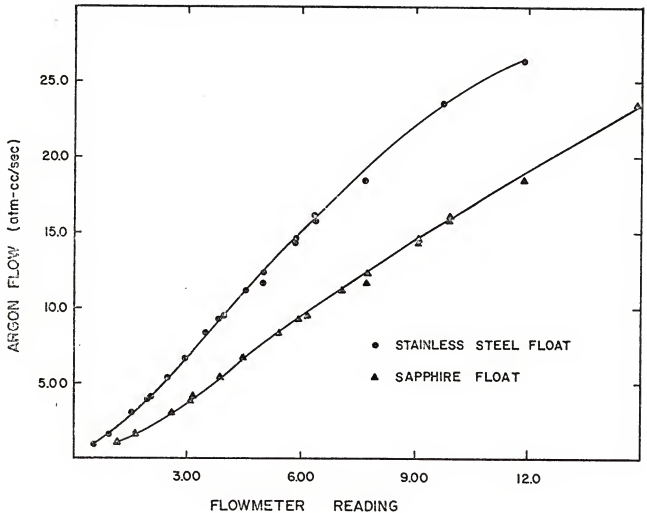

Figure 11. Buffer Gas Rotameter Calibration Curves

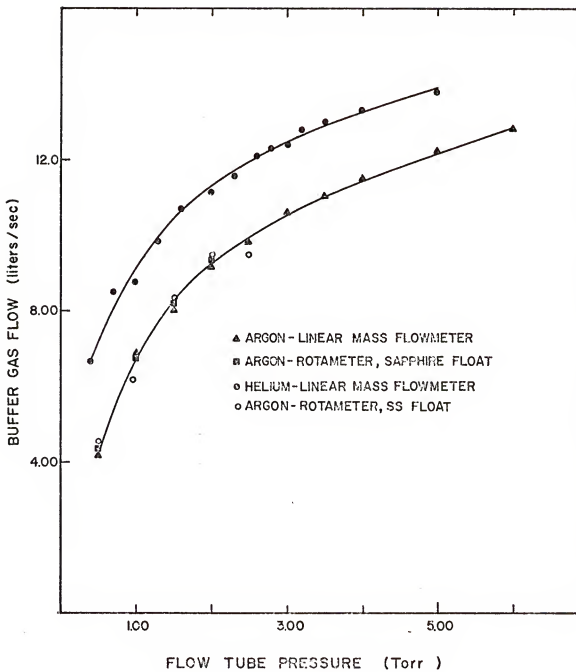

Figure 12. Buffer Gas Volume Flow Rate Versus Flow Tube Pressure

where f is the buffer gas flow rate in atm-cm^3/sec, T is the gas temperature (°K), and P is the gas pressure (Torr) at the center of the reaction tube. The agreement between the data obtained using the rotameter with sapphire float and that obtained with the linear mass flowmeter is obvious. The buffer gas flow measured by the rotameter with stainless steel float and the linear mass flowmeter exhibit poorer agreement.

The buffer gas flow rate is maintained constant by regulating the backing pressure behind a fixed leak. The stability of the buffer gas flow has been checked by monitoring the linear mass flowmeter output as a function of time. The observed drift in the voltage output at a given flow rate was approximately 0.007 volt/hour. This corresponds to approximately 0.1% of full scale per hour and is negligible during a typical experiment.

The derivation of the expression relating the linear mass flowmeter signal output to the buffer gas axial velocity (bulk flow velocity) is given below. The buffer gas flow in atm-cm^3/sec is given by

$$f = V_b(10000/5)(273.15/294.26)(M_b/60) \qquad (16)$$

where V_b is the voltage output of the linear mass flowmeter (5-volt output, full scale, corresponds to 10000 standard cm^3/sec (SCCM) of air) and M_b is a factor specific for the buffer gas in use. Therefore, the expression relating the buffer gas flow in cm^3/sec to the bulk flow axial velocity may be written

$$v_o = F/\pi a^2 = 2.583 \times 10^4 \, M_b V_b / P\pi a^2 \qquad (17)$$

where P is the pressure in Torr at the center of the reaction tube and a is the flow tube radius in centimeters. If argon or helium is the buffer gas, then

$$v_o = 7.15 \times 10^3 \, V_b / P \qquad (18)$$

since a = 1.283 cm for the flow tube used in the current experiments and M_b = 1.43 for argon or helium.

The reactant gas flow rate was monitored with a linear mass flowmeter for which full scale deflection corresponds to 5 SCCM of air. A monel transducer was used with this flowmeter in order to permit monitoring of corrosive gases. In the experiments reported here, the flowmeter was calibrated for argon since most reactant gas mixtures used consisted of at least 99.8% argon, and thus, the thermal conductivity of the mixture is essentially that of argon. Conversion factors supplied by the manufacturer allow the calculation of gas flow for other gases or mixtures of gases. A typical calibration plot is shown in Figure 13 (data points and solid line). Calibration curves measured over a six-month period were found to differ by less than 2% (slope difference). The full scale flow measured for argon agrees to better than 2% with that calculated by use of a conversion factor given in the flowmeter manual. The dashed line shown in Figure 13 is the manufacturer's calibration. It is concluded, therefore, that the reactant gas flow rates

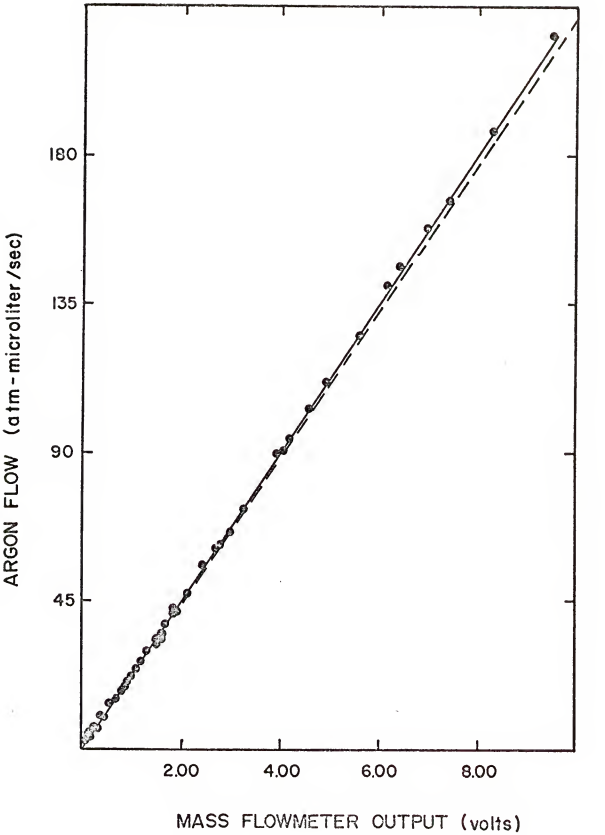

Figure 13. Reactant Gas Linear Mass Flowmeter Calibration

are accurate to within 2%. The mass flowmeter has been found to be linear over the flow regime from 1 to 225 atm-microliters/sec, which corresponds to a 10-volt output from the flowmeter. Since the flowmeter operation depends on the mass flow of the gas to change the temperature along a heated conduit (which in turn is dependent upon the heat capacity of the gas), the flowmeter calibration is independent of pressure over a wide range. The calibration curve shown in Figure 13 was obtained over the range 2 to 20 psig, and no variations with pressure were observed.

From the measured reactant gas flow, the number density of the reacting species in the reaction tube can be calculated. If argon is the diluent and buffer gas, then the number density of the reactant in the flow tube, calculated from measured reactant and buffer gas flows, is given by

$$n_{LMF} = 1.61 \times 10^{13} V_r C_f P / V_b \qquad (19)$$

where C_f is the fractional concentration of the reactant gas and V_r is the voltage output of the linear mass flowmeter used to monitor the reactant gas. As a check against this method of determining the reactant gas number density, the change in pressure in the reaction tube may be monitored as the reactant gas flow is varied, and the number density can then be calculated independently of the linear mass flowmeter signal. Thus, from the ideal gas law

$$n_{\Delta P} = \Delta P(N_A/RT) \tag{20}$$

or

$$n_{\Delta P} = 3.22 \times 10^{13} \Delta P \tag{21}$$

if argon is used for these comparisons where N_A is Avogadro's number, R is the international gas constant and T is the gas temperature (assumed to be 300°K). The pressure change, ΔP, is measured in units of millitorr. Figure 14 gives a comparison of the number density of the reactant gas in the flow tube at 3 Torr buffer gas pressure (corresponding to 0.87 volts output from the buffer gas linear mass flowmeter) as calculated by the two methods noted above. The agreement is within at least 9% over the full range of reactant gas flow, thus indicating that the use of the linear mass flowmeter technique to determine reactant number density is satisfactory. The measurement of the partial pressure of the reactant gas mixture during an actual experiment is not feasible, since this corresponds to only about 14 millitorr for full scale flow and thus a small drift in reaction tube pressure during the experiment would introduce considerable error. Such drift probably accounts for the difference observed in the two number density measurement techniques compared above, especially since the deviations observed correspond to a pressure of about one millitorr on a buffer gas total pressure background of 3000 millitorr.

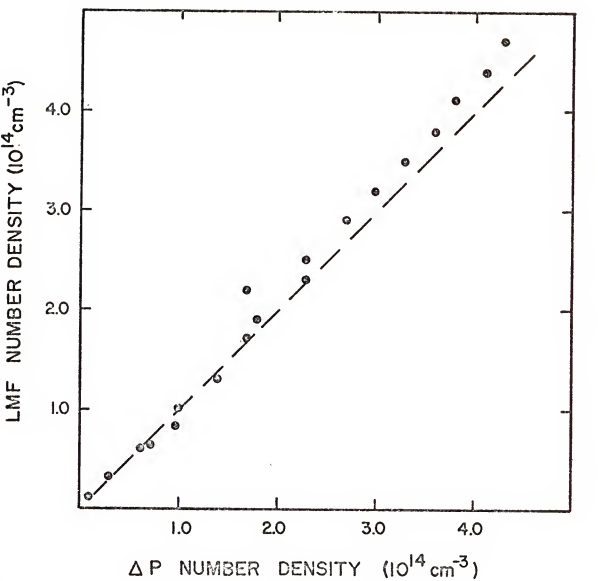

Figure 14. Comparison of Two Techniques Used to Measure the Reactant Gas Number Density

B. Data Acquisition

The data acquisition system ultimately developed during the course of this research is shown in Figure 15. The system was designed around a 24K, 16-bit minicomputer and its peripheral devices.[45] Analog signals proportional to experimental parameters such as reactant and buffer gas flows, reaction tube pressure, ion signal and ion mass were converted to digital signals by a 14-bit analog-to-digital converter. A relay register was used to advance the mass programmer-peak switching hardware. A 12-bit digital-to-analog converter provided the remote programmed input signal necessary to control the automatic flow system hardware. A cathode ray terminal was used to give the operator input/output capabilities. A storage oscilloscope allowed the operator to display ion signal versus reactant gas flow data at the end of an experiment. The raw data for each experiment were stored on a magnetic disc system to be reduced at a later time.

Once the flowing afterglow system is in the operational mode (traps filled, buffer gas flow set, the desired filament emission current obtained and so forth), a single experiment consists of little more than running the program AFGLO whose outline and listing are at the end of this chapter. Program AFGLO is loaded into the core of the minicomputer from the magnetic disc, where all data acquisition, reduction and storage files are located, by entering a directive at the teletype keyboard. At this point the operator moves to the cathode ray terminal

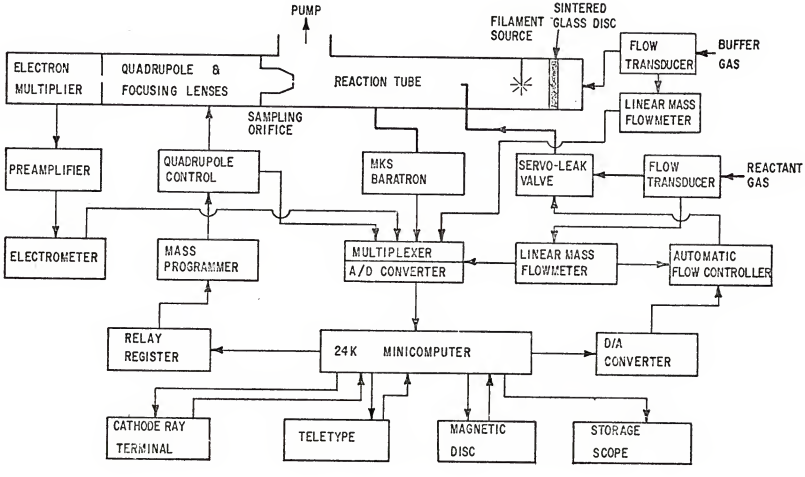

Figure 15. Computer-Interfaced Data Acquisition System

and inputs experimental parameters (sampling orifice potential, reactant gas concentration, reactant gas linear mass flowmeter multiplier, the capacitance manometer full scale pressure, the electrometer input resistor value, the number of mass programmer channels used and the A/D converter rate), operating limits (the reactant gas flow stability time, the reactant gas upper flow limit, the number of data points desired and the number of runs desired) and the data file name. Program AFGLO then reads sector zero of the data file to determine three pieces of information: the next sector available in the file for the storage of experimental data and two calibration constants (slope and intercept) necessary for the operation of the automatic flow control system. The D/A converter voltage necessary to obtain the reactant gas upper flow limit is then applied to the programmable input of the automatic flow controller. The reactant gas flow is then monitored until it has been within ±0.1 volts of the desired flow for a period of time greater than the reactant gas flow stability time (generally 15 or 20 seconds). At this point the ion intensity of peak #1 is obtained and then the quadrupole is switched through the remaining peaks measuring the ion signal intensity of each. The reactant gas flow, buffer gas flow and buffer gas pressure are also measured at this point. The reactant gas flow is then decremented by an amount determined by the number of data points desired and the upper reactant gas flow limit (the lower limit is always 0.05 volts for

decrement purposes). If the desired reactant gas flow is greater than 0.02 volts at this point, then the D/A converter output is decremented and the data point acquisition cycle repeated. If the desired reactant gas flow is less than 0.02 volts, then the data acquisition process is complete. The average values for the buffer gas flow and the buffer gas pressure during the experiment are then determined and the experimental data and input parameters are stored on a magnetic disc in the data file specified above. A plot of the ion signal of primary interest versus reactant gas flow for the experiment is also displayed on a storage oscilloscope.

The configuration of a magnetic disc data file is shown in Figure 16. The number preceding each stored parameter is the word number within a specific sector. Each data file consists of 501 fixed point sectors; each sector consists of 128 fixed point words. Sector 0 of the data file is used to store parameters needed for each experiment such as the next sector available for data storage, the number of experiments stored in the data file and the slope and intercept calibration constants relating the 12-bit D/A converter output voltage to the reactant gas flow obtained. Sectors 1 through 500 allow the storage of 100 sets of experimental data, 5 sectors per experiment. The first 80 words of each block of 5 sectors (one experiment) are reserved for the storage of experimental parameters such as the reactant gas concentration, orifice potential and so forth. Words 81 through 640 of each

SECTOR 0

1. next sector available	2. number of experiments	3. AFC slope calibration	4. AFC intercept calibration

.
.
.

SECTOR 1

1. measured transit time	2. react gas conc, mant	3. react gas conc, char	4. react gas multiplier
5. manometer full scale	6. electrometer resistor	7. # mass channels	8. A/D rate
9. stability time for AFC	10. # data points	11. buffer gas flow	12. . . .
13. . . .	14. buffer gas pressure	15. . . .	16. . . .
17. experiment #	18. mass of peak 1	19. mass of peak 2	20. mass of peak 3
21. mass of peak 4	22. mass of peak 5	23. mass of peak 6	24. orifice potential

.
.
.

81. react flow data pt 1	82. intensity peak 1 pt 1	83. intensity peak 2 pt 1	84. intensity peak 3 pt 1
85. intensity peak 4 pt 1	86. intensity peak 5 pt 1	87. intensity peak 6 pt 1	88. react flow data pt 2
89. intensity peak 1 pt 2	90. intensity peak 2 pt 2	91. intensity peak 3 pt 2	. . .

.
.
.

SECTOR 2

.
.
.

SECTOR 5

. . .	122. react flow data pt 80	123. intensity peak 1 pt 80	124. intensity peak 2 pt 80
125. intensity peak 3 pt 80	126. intensity peak 4 pt 80	127. intensity peak 5 pt 80	128. intensity peak 6 pt 80

SECTOR 6

.
.
.

SECTOR 500

Figure 16. Magnetic Disc Data File Organization

experimental 5-sector block are used to store reactant gas flow versus ion signal data points (up to 80 per experiment). Since this data file is fixed point, some floating point parameters (for example, reactant gas per cent concentration) must be converted to digital form in such a way as to preserve all significant figures.

OUTLINE OF PROGRAM AFGLO

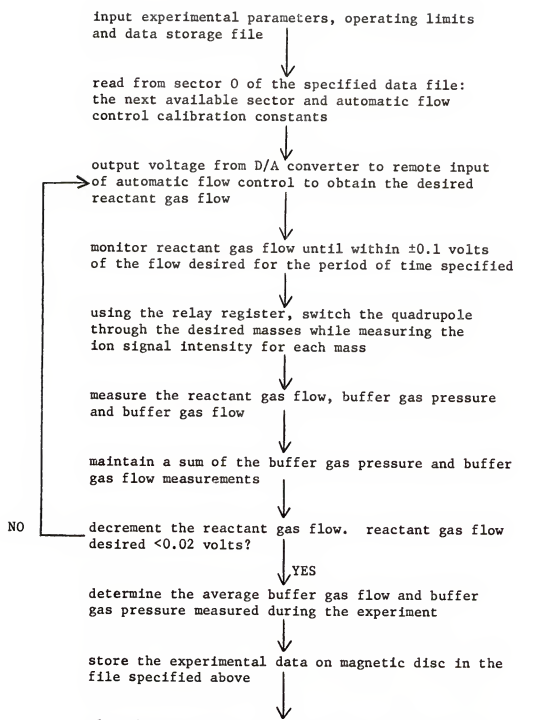
input experimental parameters, operating limits and data storage file
read from sector 0 of the specified data file: the next available sector and automatic flow control calibration constants
output voltage from D/A converter to remote input of automatic flow control to obtain the desired reactant gas flow
monitor reactant gas flow until within ±0.1 volts of the flow desired for the period of time specified
using the relay register, switch the quadrupole through the desired masses while measuring the ion signal intensity for each mass
measure the reactant gas flow, buffer gas pressure and buffer gas flow
maintain a sum of the buffer gas pressure and buffer gas flow measurements
NO
decrement the reactant gas flow. reactant gas flow desired <0.02 volts?
YES
determine the average buffer gas flow and buffer gas pressure measured during the experiment
store the experimental data on magnetic disc in the file specified above
plot the ion signal versus reactant gas flow data of primary interest on the storage oscilloscope

```
C001  FTN,L
C002        PROGRAM AFGLC
C003  C*************************************************************
C004  C*                                                           *
C005  C*  SOURCE PROGRAM IS GSFAC.  WHEN LOADING, ATTACH THE       *
C006  C*  FILES BADRV, CONCB AND DAQR FOR THE CALLS ADCCN,         *
C007  C*  RELAY AND DAQ, RESPECTIVELY.  WHEN LOADING, ATTACH       *
C008  C*  THE FILES CDPTR AND CDPLR FOR THE CALL PLOTR.            *
C009  C*                                                           *
0010  C*     PARAMETER              CHANNEL          MULTIPLIER     *
0011  C*  REACTANT FLOW               0                1          *
0012  C*  ION SIGNAL                  1                1          *
0013  C*  ION SIGNAL                  2               10          *
0014  C*  PRESSURE                    3              100          *
0015  C*  BUFFER FLOW                 4               10          *
0016  C*  MASS                        5               10          *
0017  C*  PEAK SWITCHING             10            (RELAY)        *
0018  C*                                                           *
0019  C*************************************************************
0020        DIMENSION NX(80),NY(80)
0021        COMMON IRRAY(640),IFILE(3),JRRAY(10),ION(6)
0022        ICNWD=1C2B
0023        CALL RELAY(10,0)
0024        DO 25 I=1,64C
0025  25    IRRAY(I)=0
0026  C*************************************************************
0027  C*                                                           *
0028  C*  LINES 32 THROUGH 110 REQUIRE THE OPERATOR TO INPUT       *
0029  C*  EXPERIMENTAL CONDITIONS AND LIMITS.                      *
0030  C*                                                           *
0031  C*************************************************************
0032        WRITE(7,60)
0033  60    FORMAT(1X, INPUT ORIFICE POTENTIAL (VOLTS) )
0034        READ(7,*)POTEN
0035        IRRAY(24)=IFIX(POTEN*10.)
0036        WRITE(7,70)
0037  70    FORMAT(1X, INPUT REACTANT GAS CONCENTRATION ( ) )
0038        READ(7,*)RCONC
0039  75    IF(RCONC-100.)80,100
0040  80    RCONC=RCONC*10.
0041        IRRAY(3)=IRRAY(3)+1
0042        GOTO 75
0043  100   IRRAY(2)=IFIX(RCONC)
0044        WRITE(7,125)
0045  125   FORMAT(1X, INPUT REACTANT GAS LMF MULTIPLIER )
0046        READ(7,*)RGMUL
0047        IRRAY(4)=IFIX(RGMUL*100.)
0048        WRITE(7,150)
0049  C*************************************************************
0050  C*                                                           *
0051  C*  EXPERIMENTAL DATA IS STORED ON DISC IN THE FILE          *
0052  C*  GIVEN HERE.                                              *
```

```
0053  C*                                                              *
0054  C*****************************************************************
0055  150   FORMAT(1X, INPUT DATA FILE NAME )
0056        READ(7,175)(IFILE(I),I=1,3)
0057  175   FORMAT(3A2)
0058        WRITE(7,200)
0059  200   FORMAT(1X, INPUT BARATRON FULL SCALE (MICRONS) )
0060        READ(7,*)IRRAY(5)
0061        WRITE(7,225)
0062  225   FORMAT(1X, INPUT ELECTROMETER RESISTOR (5,7 OR 9) )
0063        READ(7,*)IRRAY(6)
0064        WRITE(7,235)
0065  235   FORMAT(1X, INPUT NUMBER OF MASS PROGRAMMER CHANNELS
0066       1 USED )
0067        WRITE(7,240)
0068  240   FORMAT(1X, INPUT ACC RATE (CPS) )
0069        READ(7,*)IRRAY(8)
0070        WRITE(7,245)
0071  245   FORMAT(1X, INPUT REFLO APC STABILITY TIME (SEC) )
0072  C*****************************************************************
0073  C*                                                              *
0074  C*  APC STABILITY TIME IS THE TIME WITHIN WHICH THE             *
0075  C*  REACTANT GAS FLOW MUST BE BETWEEN THE PRESCRIBED            *
0076  C*  LIMITS BEFORE A DATA POINT IS TAKEN.                        *
0077  C*                                                              *
0078  C*****************************************************************
0079        READ(7,*)IRRAY(9)
0080        NOSEC=IRRAY(8)*IRRAY(9)
0081  265   WRITE(7,275)
0082  275   FORMAT(1X, INPUT REACTANT GAS UPPER FLOW LIMIT
0083       1 (VOLTS) )
0084        IRCD=14
0085        CALL EXEC(IRCD,ICNWC,JRRAY,10,IFILE,0)
0086  C*****************************************************************
0087  C*                                                              *
0088  C*   SLOPE  AND  YINTC  ARE CALIBRATION CONSTANTS FOR           *
0089  C*  THE AUTOMATIC REACTANT GAS FLOW CONTROL SYSTEM.             *
0090  C*                                                              *
0091  C*****************************************************************
0092        SLOPE=FLOAT(JRRAY(3))/10000.
0093        YINTC=FLOAT(JRRAY(4))/100.
0094        V=UFLIM*SLOPE+YINTC
0095        CALL DAC(V)
0096  C*****************************************************************
0097  C*                                                              *
0098  C*  AT THIS POINT THE D/A CONVERTER SETS THE REACTANT            *
0099  C*  GAS FLOW AT THE DESIRED UPPER LIMIT BY APPLYING  V          *
0100  C*  VOLTS TO THE REMOTE PROGRAMMING INPUT OF THE                *
0101  C*  AUTOMATIC FLOW SYSTEM.                                      *
0102  C*                                                              *
0103  C*****************************************************************
0104        WRITE(7,300)
```

```
0105  300   FORMAT(1X, INPUT NUMBER DATA POINTS DESIRED (80 MAX
0106       1) )
0107        READ(7,*)IRRAY(10)
0108        WRITE(7,325)
0109  325   FORMAT(1X, INPUT NUMBER OF RUNS DESIRED )
0110        READ(7,*)NRUNS
0111  C*************************************************************
0112  C*                                                           *
0113  C*  AT THIS POINT THE AUTOMATIC DATA ACQUISITION             *
0114  C*  SYSTEM TAKES OVER.                                       *
0115  C*                                                           *
0116  C*************************************************************
0117        DO 900 NN=1,NRUNS
0118        BFSUM=0.0
0119        PRSUM=0.0
0120        DO 350 KK=1,6
0121  350   ICN(KK)=0
0122        DO 375 KK=81,640
0123  375   IRRAY(KK)=0
0124        V=UFLIM*SLOPE+YINTC
0125        CALL DAC(V)
0126        DESFL=UFLIM
0127        CALL STAPC(NCSEC,DESFL)
0128        K=81
0129  400   CALL DATA(BUFLO,IRFLO,PRESS,K)
0130        IRRAY(K)=IRFLO
0131        IRRAY(K+1)=ICN(1)
0132        IRRAY(K+2)=ICN(2)
0133        IRRAY(K+3)=ICN(3)
0134        IRRAY(K+4)=ICN(4)
0135        IRRAY(K+5)=ICN(5)
0136        IRRAY(K+6)=ICN(6)
0137        BFSUM=BFSUM+BUFLO
0138        PRSUM=PRSUM+PRESS
0139        K=K+7
0140        DESFL=DESFL-(UFLIM-0.05)/FLOAT(IRRAY(10)-1)
0141        IF(DESFL-0.02)500,450
0142  450   V=DESFL*SLOPE+YINTC
0143        CALL DAC(V)
0144        CALL STAPC(NCSEC,DESFL)
0145        GOTO 400
0146  500   IRRAY(11)=IFIX(BFSUM/FLOAT(IRRAY(10)))
0147        IRRAY(14)=IFIX(PRSUM/FLOAT(IRRAY(10)))
0148        N=JRRAY(1)
0149        JRRAY(2)=JRRAY(2)+1
0150        JRRAY(1)=JRRAY(1)+5
0151        IRRAY(17)=JRRAY(2)
0152        IRCD=15
0153  C*************************************************************
0154  C*                                                           *
0155  C*  AT THIS POINT THE DATA FOR ONE EXPERIMENT IS             *
0156  C*  TRANSFERRED TO THE MAGNETIC DISC SYSTEM AND STORED       *
```

```
C*  IN THE DATA FILE SPECIFIED ABOVE.                              *
C*                                                                 *
C*****************************************************************
      CALL EXEC(IRCD,ICNWD,IRRAY,640,IFILE,N)
      CALL EXEC(IRCD,ICNWD,JRRAY,10,IFILE,0)
C*****************************************************************
C*                                                                 *
C*  LINES 169 THROUGH 180 NORMALIZE THE ION SIGNAL OF              *
C*  CN A STORAGE CSCILLOSCOPE.                                     *
C*                                                                 *
C*****************************************************************
      MAX=0
      N=81+(IRRAY(10)-1)*7
      DO 600 I=81,N,7
      IF(IRRAY(I+2)-MAX)600,550
550   MAX=IRRAY(I+2)
600   CONTINUE
      DO 700 I=81,N,7
      J=(I-74)/7
      NX(J)=IFIX(4095.*FLOAT(IRRAY(I))/32764.)
700   NY(J)=IFIX(4095.*0.9*FLOAT(IRRAY(I+2))/FLOAT(MAX))
      N=IRRAY(10)
900   CALL PLOTR(NX,NY,N)
      GOTO 265
      END
C*****************************************************************
C*                                                                 *
C*  SUBROUTINE STAPCO  THIS SUBROUTINE DETERMINES WHEN             *
C*  THE REACTANT GAS FLOW HAS BEEN WITHIN THE DESIRED              *
C*  LIMITS FOR THE PERIOD OF TIME PRESCRIBED ABOVE BY              *
C*  THE INPUT  REFLO STABILITY TIME .  CONTROL IS THEN             *
C*  RETURNED TO THE MAIN PROGRAM.                                  *
C*                                                                 *
C*****************************************************************
      SUBROUTINE STAPC(NCSEC,DESFL)
1000  N=0
1050  CALL ADCCN(IFLOW,0)
      REFLC=FLOAT(IFLOW)/3276.4
      IF(REFLC-DESFL+0.10)1000,1100
1100  IF(REFLC-DESFL-0.10)1200,1000
1200  N=N+1
      IF(N-NCSEC)1050,1300
1300  RETURN
      END
C*****************************************************************
C*                                                                 *
C*  SUBROUTINE DATAQ  THIS SUBROUTINE MEASURES THE                 *
C*  BASELINE AND ION SIGNALS FOR UP TO FIVE MASSES, THE            *
C*  BUFFER GAS FLOW AND THE REACTION CHANNEL PRESSURE              *
C*  FOR A GIVEN REACTANT FLOW, WHICH IS ALSO MEASURED.             *
C*                                                                 *
```

```
0209  C*************************************************************
0210        SUBROUTINE DATA(BUFLC,IRFLO,PRESS)
0211        COMMON IRRAY(640),IFILE(3),JRRAY(10),ION(6)
0212        COMMON ITIME(5)
0213        SBFLC=0.0
0214        SPRES=0.0
0215        SFLOW=0.0
0216        NCHAN=IRRAY(7)
0217        DO 2000 J=1,NCHAN
0218        IF(K-82)1350,1400
0219  1350  CALL ADCCN(IRRAY(J+17),5)
0220  1400  SIGNS=0.0
0221        CALL ADCCN(ICNS,1)
0222        IF(ICNS-3113)1800,1500
0223  1500  DO 1600 I=1,100
0224        CALL ADCCN(ICNS,1)
0225  1600  SIGNS=SIGNS+FLOAT(ICNS)
0226        SIGNS=SIGNS/100.
0227        GOTO 1950
0228  1800  DO 1900 I=1,100
0229        CALL ADCCN(ICNS,2)
0230  1900  SIGNS=SIGNS+FLOAT(ICNS)
0231        SIGNS=SIGNS/1000.
0232  1950  ION(J)=IFIX(SIGNS)
0233        CALL RELAY(10,1)
0234        CALL RELAY(10,0)
0235        IRCDE=11
0236        CALL EXEC(IRCDE,ITIME)
0237        I1=ITIME(1)
0238  1960  CALL EXEC(IRCDE,ITIME)
0239        I2=ITIME(1)
0240        IF(I2-I1)1975,1980
0241  1975  I2=I2+100
0242  1980  IF((I2-I1)-90)1960,2000
0243  2000  CONTINUE
0244        DO 2050 I=1,100
0245        CALL ADCCN(IFLOW,0)
0246        CALL ADCCN(IPRES,3)
0247        CALL ADCCN(IBFLC,4)
0248        SFLOW=SFLOW+FLOAT(IFLOW)
0249        SPRES=SPRES+FLOAT(IPRES)
0250  2050  SBFLC=SBFLC+FLOAT(IBFLC)
0251        BUFLC=SBFLC/100.
0252        IRFLC=IFIX(SFLOW/100.)
0253        PRESS=SPRES/100.
0254        RETURN
0255        END
0256        END$
****  LIST END ****
```

CHAPTER III

MATHEMATICAL MODEL

A. Basic Model

The simplest analysis of reaction kinetics for a flowing afterglow system may be accomplished by using a plug flow model. This model assumes that the buffer gas axial velocity, v_o (and the electron and ion axial velocities in the high pressure environment) is independent of radial or axial position in the reaction tube. In this simple model it is also assumed that the neutral reactant gas is injected uniformly throughout the flow tube cross-section at z=0, where the z-axis is the cylindrical axis of the flow tube. In addition, the diffusion of reactants and products in the reaction tube is not considered.

For net reactions of the type

$$e^- + X_2 \rightarrow X^- + X \qquad X_2 = F_2, Cl_2, Br_2 \qquad (22)$$

the rate equation becomes

$$d[X^-]/dt = k[e^-][X_2] \qquad (23)$$

where the symbols within brackets represent the number densities of reactants and product and k is the bimolecular rate constant. In order to determine $[X^-]$ as a function of time, $[e^-]$ and

$[X_2]$ must first be evaluated. The rate equation for the electrons is

$$d[e^-]/dt = -k[e^-][X_2] \tag{24}$$

If the assumption is made that $[X_2] >> [e^-]$ for all t, then $[X_2]$ may be treated as a constant. Integrating Equation 24 then yields

$$[e^-] = [e^-]_o \exp\{-k[X_2]t\} \tag{25}$$

where $[e^-]_o$ is the electron number density in the reaction tube at t=0 (that is, at the neutral reactant gas injection port). Substitution of this result into Equation 23 yields the differential equation

$$d[X^-]/dt = k[X_2][e^-]_o \exp\{-k[X_2]t\} \tag{26}$$

Integrating this equation gives the desired solution for the product ion number density

$$[X^-] = [e^-]_o\{1 - \exp(-k[X_2]t)\} \tag{27}$$

The reaction time, t, written in terms of the reaction tube length, L, and the axial flow velocity, v_o, is

$$t = L/v_o \tag{28}$$

for the plug flow model. Equation 27 then becomes

$$[X^-] = [e^-]_o\{1 - \exp(-k[X_2]L/v_o)\} \qquad (29)$$

Thus, the measurement of $[X^-]$ at the end of the reaction tube versus $[X_2]$ results in the determination of the rate constant k if the reaction tube length and the axial flow velocity are known. At this point it is useful to reiterate the assumptions made in the derivation of Equation 29:

1. the axial flow velocity, v_o, is constant throughout the reaction tube,
2. diffusion of reactants and products in the reaction tube is unimportant,
3. the neutral reactant gas is injected uniformly in a cross-section of the reaction tube at t=0 (that is, z=0) and
4. the neutral reactant number density is much greater than the electron number density for all t>0 in the reaction tube.

Each of these assumptions will now be examined and accepted or modified on the basis of experimental evidence. The derivation of the model for the experimental system will then be altered to include any changes made in the basic assumptions.

B. Axial Flow Velocity

Determination of the axial flow velocity in the flow tube is necessary in order to calculate the reaction time

$$t = L/v_o \qquad (28)$$

available to the electrons and halogen gas in the reaction tube. Two basic assumptions concerning the axial flow velocity

were made in the derivation of Equation 29

1. the axial flow velocity, v_o, is constant throughout the reaction tube and

2. in the high pressure environment present in the reaction tube, ions, electrons and buffer gas move down the tube with the same velocity profile.

If these assumptions are true, then the time required by any species to transit the reaction tube is given by

$$t = \pi a^2 L/F \tag{30}$$

where a is the flow tube radius, L is the reaction tube length and F is the buffer gas volume flow rate.

The method illustrated in Figure 17 was used to determine whether Equation 30 could be used to calculate reaction times for the flowing afterglow experimental configuration containing a microwave discharge electron source. During normal operation of the flowing afterglow system, the neutral reactant gas injected into the flow tube reacts with electrons produced by the microwave discharge and forms negative ions, which are sampled by the mass spectrometer system. If a platinum probe is inserted into the afterglow and a positive potential applied to this probe as shown in Figure 17, electrons will be removed from the afterglow as they reach the probe. Thus, negative ions will not be formed downstream after the electrons already beyond the probe at the time of the potential application are consumed. If the potential applied to the probe is used to simultaneously trigger an oscilloscope sweep, then the ion current (at the scope vertical input) as a function of time

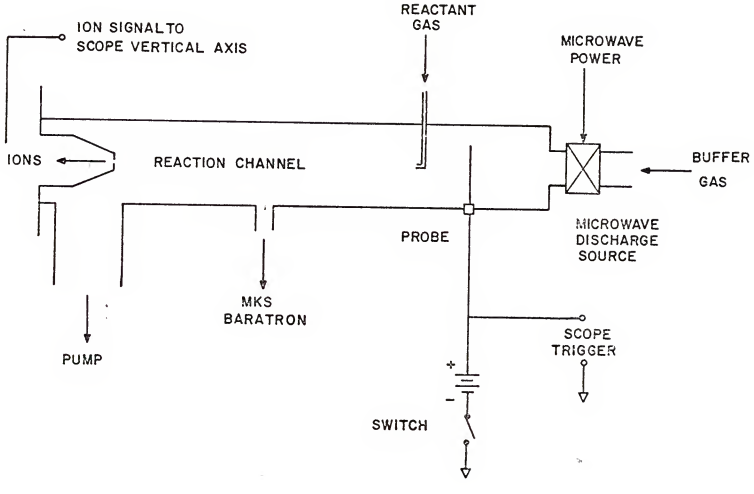

Figure 17. Experimental Configuration for the Measurement of Transit Times for Ions in the Flow Tube

is displayed on the oscilloscope. This scope trace can be photographed with a Polaroid camera. Neglecting axial diffusion, it is expected that the ion signal versus time trace obtained in the manner described above would be a step function if the assumptions previously made are correct. A sample experimental trace is shown in Figure 18. Since the trace is not a step function and axial diffusion is not expected to result in a tailing of the magnitude observed in this trace, it is apparent that the radial velocity profile (that is, the axial flow velocity as a function of radial distance, r, in the flow tube) is not planar and also that radial diffusion of species present in the reaction tube is important.

A literature search previously revealed that due to frictional forces at the walls, the radial velocity profile for the viscous flow of a gas in a cylindrical tube is not planar but parabolic. Neglecting the axial velocity gradient (near zero in the present experiment), the radial velocity profile is given by[46]

$$v(r) = wv_o(b - r^2/a^2) \tag{31}$$

where

$$w = 2/(1 + 5.52\lambda/Pa) \tag{32}$$

and

$$b = 1 + 2.76\lambda/Pa \tag{33}$$

λ is the mean free path (cm) at one Torr, P is the pressure (Torr)

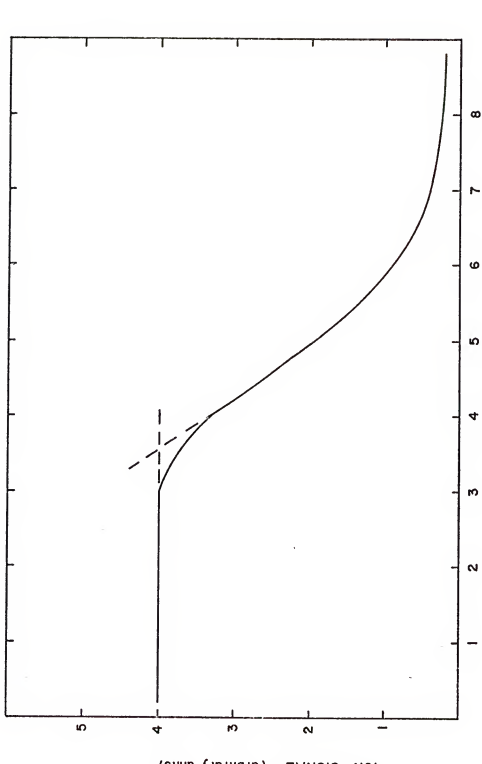

Figure 18. Sample Trace Obtained in the Measurement of Ion Transit Times in the Flow Tube

in the reaction tube and a is the flow tube radius (cm). In the present experiments $1 \leq P \leq 3$ Torr of argon buffer gas. This yields $1.97 \leq w \leq 1.99$ and $1.008 \geq b \geq 1.002$. Thus, the radial velocity profile is approximately given by

$$v(r) = 2v_o(1 - r^2/a^2) \tag{34}$$

where v_o is the plug flow linear velocity. The ion signal versus time trace shown in Figure 18 may now be explained in terms of this velocity profile.

When a potential is applied to the probe at t=0, any electrons downstream of the probe will continue to be carried down the tube in the flowing stream and will react with the reactant gas present in the reaction tube. The resulting ions are extracted through the orifice and detected by the quadrupole mass spectrometer system. Since the radial velocity profile of the buffer gas is of the form given in Equation 34, ions at the center of the flow tube will have the shortest reaction tube transit times while those nearer the walls will have the longest. As the ion density along the cylindrical axis of the reaction tube is depleted, ions diffuse from the areas where r>0. This accounts for the fact that the observed ion current as a function of time after the application of the blocking potential to the probe does not drop sharply to zero after the initial constant period and tailing occurs as shown in Figure 18.

Figure 19 shows the results of a series of measurements (closed circles) of negative ion reaction tube transit times (for r=0) as a function of the argon buffer gas pressure in the flow tube, using the technique just described, where the break in the ion signal versus time trace such as that shown in Figure 18 is taken as the transit time for ions from the probe to the sampling orifice. The upper solid line in Figure 19 represents the reaction tube transit times calculated from the measured buffer gas volume flow rate using the equation

$$t = L/v(r=0) = \pi a^2 L/2F \qquad (35)$$

where the factor of 1/2 arises because $v(r=0) = 2v_o$. The ion transit times measured by the probe technique are seen to be smaller than those calculated from the buffer gas volume flow rate. This may be attributed to the geometry of the present flow tube when in the microwave discharge source configuration. The microwave discharge produces ions and electrons in a quartz tube with an inner diameter less than 1.12 cm. Buffer gas is pumped through this tube into the flow tube, which has an inner diameter of 2.57 cm. Due to this arrangement the buffer gas tends to stream through the center of the flow tube at a rate higher than predicted by a parabolic velocity profile. In addition, the velocity outside this central filament is less than expected. Given sufficient distance (that is, time), the radial velocity profile will become parabolic as the gas moves through the flow tube.[47] This statement

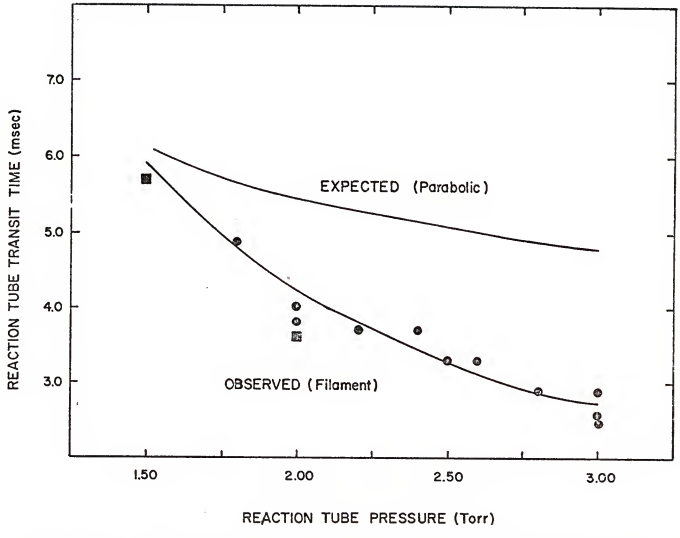

Figure 19. Measured Ion Transit Times in the Flow Tube Versus Pressure for the Microwave Discharge Source Configuration

is illustrated in Figure 19 by the fact that as the reaction tube transit time increases, the values measured by the probe technique and those calculated from the buffer gas volume flow rate merge. This indicates that given sufficient time, the velocity profile, even with the microwave discharge source, will develop its parabolic shape. The flow tube in the flowing afterglow apparatus, however, is not sufficiently long to permit the parabolic profile to become fully developed when using the microwave discharge source. Therefore, the filament flow phenomenon must be taken into account in analyzing the data obtained using the microwave discharge source. Thus, Equation 27 becomes

$$[X^-] = [e^-]_o\{1 - \exp(-k[X_2]t')\} \qquad (36)$$

where t' is the ion reaction tube transit time measured by the probe technique described above.

As a check of the probe technique used to measure ion reaction tube transit times, these parameters were also measured by an alternative probe technique. This procedure involved monitoring the current collected by a second probe (downstream from the blocking probe shown in Figure 17) as a function of time after application of the potential to the blocking probe. Two transit time measurements obtained in this manner are shown in Figure 19 as closed squares. The results of this double probe technique are seen to be in near agreement with the probe-ion signal technique discussed earlier.

In order to avoid the filament flow problem described above, previous researchers have found it necessary to make their flow tubes long enough to allow the parabolic velocity profile to develop[48] or to smooth the buffer gas flow with a sintered glass disc placed in the flow tube upstream of the reaction region.[46] In the present experiments the latter solution was employed. This necessitated the location of the electron source downstream of the sintered glass disc. Thus, at this point the apparatus was converted to the filament source previously described.

With the filament source installed in the flow tube, ion transit times could easily be measured using the technique previously described with the exception that the blanking potential was no longer applied to a probe but to the filament. The circuit used to accomplish this is shown in Figure 20. With the double-pole double-throw switch in the upper position, a negative bias is applied continuously to the filament and the source operates in a continuous mode. With the double-pole double-throw switch in the lower position, the source operates in a pulsed mode at a rate determined by the square wave input at the PNP transistor base. Ion transit times may be determined by triggering an oscilloscope sweep on the negative slope of the square wave input. This negative pulse results in zero volts filament bias; that is, the source is switched to the "off" position from the "on" position. Thus, the ion signal output of the mass spectrometer system,

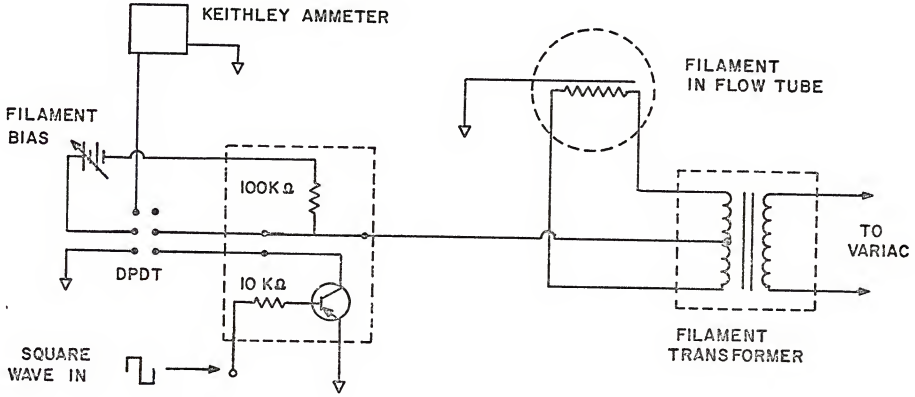

Figure 20. Filament Source Configuration for the Measurement of Ion Transit Times in the Flow Tube

applied to the vertical input of the oscilloscope, versus time trace is obtained similar to that shown in Figure 18. The oscilloscope sweep may also be triggered on the positive slope of the square wave input. This positive pulse results in a negative filament bias; that is, the source is switched to the "on" position from the "off" position. Ion transit times are then determined by the time required for the appearance of the ion signal after pulse application. Figure 21 shows the results of a series of transit time measurements (for r=0) with the filament source installed in the flowing afterglow system. The measurements were made on three different ions, triggering on both positive and negative square wave pulses as described above. Ion transit times calculated from the measured buffer gas volume flow rate assuming a parabolic velocity profile are also shown in Figure 21. The good agreement between transit times measured by the pulse technique and those calculated from the measured buffer gas volume flow rates indicates that the sintered glass disc installed in the flow tube is effective in smoothing the buffer gas flow, enabling a parabolic velocity profile to be established in the flow tube. The agreement also indicates that the ions and buffer gas move down the flow tube at the same velocity. For the moment it is also assumed that the electrons are at thermal energy. This assumption will be discussed later.

From the discussion above it is clear that for the flowing afterglow filament source configuration, Equation 29 must

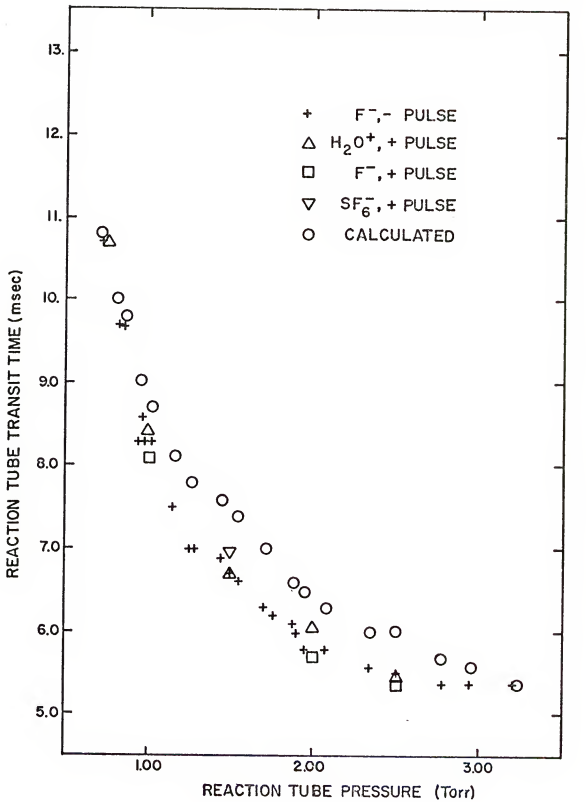

Figure 21. Measured Ion Transit Times in the Flow Tube Versus Pressure for the Filament Source Configuration

be modified to include the parabolic radial velocity profile. Thus, Equation 29 becomes

$$[X^-] = [e^-]_o\{1 - \exp(-k[X_2]L/2v_o)\} \quad (37)$$

Consideration of the axial flow velocity radial profile has led to a modification of the basic model, derived in Section A, to account for the filament flow phenomenon with the microwave discharge source and the parabolic profile with the filament source. The kinetic equations relating the ion density $[X^-]$ to the rate constant, k, are then

$$[X^-] = [e^-]_o\{1 - \exp(-k[X_2]t')\} \quad (36)$$

for the microwave source and

$$[X^-] = [e^-]_o\{1 - \exp(-k[X_2]L/2v_o)\} \quad (37)$$

for the filament source.

C. Radial Diffusion of Charged Species

The tailing observed in the ion signal versus time traces of the ion transit time measurements in the previous section indicates that radial diffusion is an important factor in the analysis of flowing afterglow reaction kinetics. Thus, the transport equation for negative ions produced by dissociative electron attachment in the flowing afterglow reaction tube becomes

$$2v_o(1 - r^2/a^2)\partial[X^-]/\partial z =$$

$$(D_-/r)\partial(r\partial[X^-]/\partial r)/\partial r + k[e^-][X_2] \qquad (38)$$

where the left side represents the time rate of change of the negative ion concentration, the first term on the right represents the negative ion radial diffusion loss rate and the second term, the negative ion production rate from the attachment reaction.[48] D_- is the negative ion radial diffusion coefficient. However, before a solution for this equation can be found, a similar transport equation for the electron density must be solved

$$2v_o(1 - r^2/a^2)\partial[e^-]/\partial z =$$

$$(D_e/r)\partial(r\partial[e^-]/\partial r)/\partial r - k[e^-][X_2] \qquad (39)$$

where the left side represents the time rate of change of the electron density, the first term on the right, the electron diffusion loss rate and the second, the electron reaction loss rate. D_e is the electron radial diffusion coefficient. Equation 39 has been solved by Cher and Hollingsworth[49] and its solution may be written

$$[e^-] = [e^-]_o R(r)Z(z) \qquad (40)$$

where

$$R(r) =$$

$$\exp(-\beta\lambda r^2/Za^2)\ {}_1F_1(1/2 - \lambda/4\beta,\ 1;\beta\lambda r^2/a^2) \qquad (41)$$

$$Z(z) = \exp(-D_e\lambda^2 z/2v_o a^2 - k[X_2]z/2v_o) \qquad (42)$$

$$\lambda^2 = \lambda_o^2 + \varepsilon_1 ka^2[X_2]/D_e - \varepsilon_2 k^2 a^4 [X_2]^2/D_e^2 \qquad (43)$$

$$\beta^2 = 1 + ka^2[X_2]/D_e\lambda^2 \qquad (44)$$

and $[e^-]_o$ is the electron density at r=0 and z=0, a is the flow tube radius and λ_o (=2.7098), ε_1 (=0.2372) and ε_2 (=0.00150) are empirical quantities determined from the solution of the equation

$${}_1F_1(1/2 - \lambda/4\beta,\ 1;\beta\lambda) = 0 \qquad (45)$$

a necessary condition in order for the density of the electrons to approach zero as r approaches a.[49] ${}_1F_1(1/2 - \lambda/4\beta,\ 1;\beta\lambda)$ represents a confluent hypergeometric function. Now that a solution has been obtained for the electron density in the flow tube this solution must be substituted into Equation 38 and an expression for $[X^-]$ found. It is obvious at this point that obtaining an exact analytical expression for the negative ion number density is impossible due to the intractability of Equation 38 upon substitution of the expression derived for the electron number density.

At this point the assumption is made that since the present experiments measure only the axial variation of the reactants/products, then only the solution of Equation 39 at r=0 is necessary. Therefore, Equation 40 becomes

$$[e^-] = [e^-]_o \exp\{-D_e z\lambda_o^2/2v_o a^2 - (1 + \varepsilon_1)k[X_2]z/2v_o - \varepsilon_2 k^2 a^2 [X_2]^2 z/2D_e v_o\} \quad (46)$$

where the first term in the exponential represents radial diffusion losses, the second reaction losses and the third coupling between reaction and diffusion. If we define $[e^-]_o$ as the electron density at r=0, z=L and $[X_2]$=0, then

$$[e^-]_o = [e^-]_o \exp\{-D_e L\lambda_o^2/2v_o a^2\} \quad (47)$$

and

$$[e^-] = [e^-]_o \exp\{-(1 + \varepsilon_1)k[X_2]L/2v_o - \varepsilon_2 k^2 a^2 [X_2]^2 L/2D_e v_o\} \quad (48)$$

where L is the reaction tube length. This equation applies only to the electron density at r=0, that is, on the flow tube axis. Therefore, substitution of Equation 48 into Equation 38 and the subsequent solution to yield an expression $[X^-] = f(r,z)$ is meaningless. At this point it is assumed that

$$[X^-] = [e^-]_o - [e^-] \quad (49)$$

that is, that the difference between the electron number density at r=0 and z=L with $[X_2]=0$ and the electron number density at r=0 and z=L with $[X_2]\neq 0$ is due to the formation of negative ions, which undergo negligible radial diffusion in their transit through the reaction tube. Substitution of Equation 49 into 48 then yields

$$[X^-] = [e^-]_o[1 - \exp\{-(1 + \varepsilon_1)k[X_2]L/2v_o - \varepsilon_2 k^2a^2[X_2]^2L/2D_e v_o\}] \quad (50)$$

The validity of this equation will be tested by measuring known reaction rates. Generally,

$$\varepsilon_2 k^2a^2[X_2]^2L/2D_e v_o << (1 + \varepsilon_1)k[X_2]L/2v_o \quad (51)$$

Thus, Equation 50 may be written

$$[X^-] = [e^-]_o\{1 - \exp(-0.619k[X_2]L/v_o)\} \quad (52)$$

Comparing this result (applicable to the filament source configuration) to Equation 29, it can be seen that correcting for a parabolic velocity profile and the radial diffusion of electrons yields a correction factor of 0.616, that is,

$$k = (1 + 0.616)k_s \quad (53)$$

where k is the actual rate constant and k_s is that derived from data using the model outlined in Section A. This result

expresses the assumption used by Ferguson et al.[48] in the reduction of experimental data where it is assumed

$$k = (1 + \sum_i a_i)k_s \tag{54}$$

where the a_i represent corrections to the rate constant obtained by the reduction of data with the simple model. These correction factors include the effects of a parabolic velocity profile, radial diffusion, non-uniform neutral reactant injection and axial diffusion. The largest correction factors by far are the corrections for the parabolic radial velocity profile and radial diffusion.[48] Axial diffusion corrections are usually negligible and will not be considered here.[48]

The inclusion of the radial diffusion of electrons in the mathematical model has yielded the equation

$$[X^-] = [e^-]_o\{1 - \exp(-0.619k[X_2]L/v_o)\} \tag{52}$$

for the filament source configuration.

Due to the lack of a parametric form for the radial velocity profile with the microwave discharge source configuration, no correction could be made to the model. In addition, the effect of the radial diffusion of electrons is expected to be less than that for the filament source configuration since the axial flow velocity at the center of the reaction tube, where the density of the charged species is highest, is much faster in the microwave source configuration; therefore, the electrons have less time to diffuse.

D. Inlet Effects

As pointed out by several authors, the effect of a point source reactant gas inlet in a flowing afterglow is to drastically deplete the electron density in the center of the reaction tube due to the large neutral reactant density at r=0 and z=0.[46,48] Given sufficient distance (that is, time), this perturbation will correct itself as the mixture flows down the reaction tube. This self correction is accomplished through diffusion of electrons from r>0 to r=0 and diffusion of the neutral species from r=0 to the region r>0. This problem has been studied thoroughly by Ferguson et al.[48] In their system this phenomenon results in a correction of about 30% ($a_i = -0.3$) in the simple rate constant for an order of magnitude decrease in the primary ion signal. Since the radial diffusion of the electrons in the flow tube results in an axial density profile proportional to

$$\exp\{-D_e\lambda_o^2 L/2v_o a^2\} \tag{55}$$

comparison of the exponent in both the present experiments and those of Ferguson et al. will indicate whether point source injection of the neutral reactant is more or less of a correction in the present experiments. Thus,

$$[(\lambda_o^2/2)(LD_e/v_o a^2)]_C \;/\; [(\lambda_o^2/2)(LD_e/v_o a^2)]_F =$$

$$[L/Pv_o a^2]_C \;/\; [L/Pv_o a^2]_F \tag{56}$$

since $D_e \propto P^{-1}$ where P is the flow tube pressure. The subcripts C and F refer to the current apparatus and that of Ferguson et al., respectively. Inserting typical numerical values yields

$$(20/2 \times 2.5 \times 10^3 \times 1.28^2)_C \; / \; (60/0.5 \times 8 \times 10^3 \times 4^2)_F \simeq 2.6 \qquad (57)$$

Therefore, radial diffusion in the current experiment should be faster and the perturbations produced by a point source should result in a smaller correction factor than in the experiments of Ferguson et al. For this reason no modification was made to the mathematical model for perturbations due to inlet effects.

E. Reactant/Electron Number Density Ratio

No actual determination of the electron density in the present experiments was made. However, previous researchers have found electron densities on the order of 10^7 to 10^{10} electrons/cm^3 for flowing afterglow systems.[48,50] Since one of the assumptions made in the derivation of models presented in the previous sections was that

$$[X_2] >> [e^-] \qquad (58)$$

for all t>0, it is important to determine whether this assumption is in fact true. An analysis of the models presented previously reveals that if the neutral density were not always greater

than the electron density, then the rate constants determined by the reduction of data using these models would be too small. The only experiments where this was expected to be a problem were those in which the attachment of electrons to sulfur hexafluoride was studied. In these experiments the sulfur hexafluoride number density was sometimes as low as 10^8 molecules/cm^3. However, reduction of the experimental data using a model which does not make the assumption expressed by Equation 58 above yields no significant difference in the rate constants obtained. Therefore, the assumption above was retained.

F. Ambipolar Diffusion

In an afterglow containing electron densities greater than the order of 10^7 electrons/cm^3, electrons diffuse to the walls of the flow tube at a rate several orders of magnitude slower than their free diffusion rate. This phenomenon, known as ambipolar diffusion, is due to the retarding potential exerted on the electrons by the positive ions present in the afterglow. When a gas, which attaches electrons to form negative ions, is injected into the afterglow, the electron diffusion rate is governed approximately by the equation[51]

$$D_a = 2D_+\{1 + [X^-]/[e^-]\} \tag{59}$$

where D_a is the ambipolar diffusion coefficient, D_+ is the positive ion free diffusion coefficient, $[X^-]$ is the number density of the negative ion formed and $[e^-]$ is the electron

number density. Substitution of this equation into the models derived previously, reveals that the rate constant calculated, assuming constant electron diffusion, will be smaller than the actual rate constant. This error is probably significant in electron attachment studies of the type presented here.

CHAPTER IV

DATA REDUCTION

The product ion number density at the end of the reaction tube may be related to the product signal by the expression

$$[X^-] = cI \tag{60}$$

where I is the product ion current and c is a coefficient which depends on the ion sampling efficiency, the transmission coefficient for the electrostatic lens system and quadrupole mass spectrometer and the gain of the electron multiplier used for ion detection. The coefficient c is a constant during a particular experiment. Equation 52 may now be written

$$I = \{[e^-]_o/c\}\{I - \exp(-0.619k[X_2]L/v_o)\} \tag{61}$$

As the neutral reactant number density, $[X_2]$, approaches infinity (or in reality, a number density large enough to attach essentially all of the electrons in the reaction tube within a short distance of the reactant gas injection port), the product ion number density approaches a maximum, which may be written

$$[X^-]_\infty = cI_\infty = [e^-]_o \tag{62}$$

Substitution of this result into Equation 61 yields the expression

$$I = I_\infty\{1 - \exp(-0.619k[X_2]L/v_o)\} \tag{63}$$

If the product ion signal, I, is measured as a function of the reactant gas number density, $[X_2]$, and the maximum product ion signal, I_∞, is determined, then a simple one parameter curve fit will yield the desired rate constant, k. In actual practice there are at least three complications:

1. the measured product ion signal includes a baseline, ΔI,
2. the determination of I_∞ is difficult due to noise in the ion signal and
3. there may be a significant error, ΔQ, in the determination of the factor $[X_2]/v_o$.

Substitution of these errors into Equation 63 yields

$$I_m = I_\infty + \Delta I - I_\infty\exp\{-0.619kL[X_2]_m/(v_o)_m + 0.619kL\Delta Q\} \tag{64}$$

where I_m is the measured product ion signal, $[X_2]_m$ is the measured reactant gas number density and $(v_o)_m$ is the measured buffer gas linear velocity (plug flow). Equation 64 may be written

$$y = P_1 - P_2\exp(-P_3x) \tag{65}$$

where

$$P_1 = I_\infty + \Delta I \tag{66}$$

$$P_2 = I_\infty\exp(0.619kL\Delta Q) \tag{67}$$

$$P_3 = 0.619kL/(v_o)_m \tag{68}$$

and where $y = I_m$ and $x = [X_2]_m$. Thus, a curve fit of measured ion signal versus reactant gas number density data yields the parameter P_3 from which the desired rate constant, k, can be determined. Generally, $\Delta Q \simeq 0$; therefore,

$$P_1 - P_2 \simeq \Delta I \tag{69}$$

and

$$P_2 \simeq I_\infty \tag{70}$$

Thus, the values obtained for the parameters P_1 and P_2 were checked by noting the approximate values of ΔI and I_∞. Typical values for the ion signal baseline, ΔI, and the maximum ion signal observed, $I_\infty + \Delta I$, may be obtained by looking at the data listed in Appendix IV.

A. Jacobian Matrix Technique

As indicated above, the mathematical models derived in Chapter III generally result in an equation of the form

$$y_i = P_1 - P_2 \exp(-P_3 x_i) \tag{71}$$

which relates the observed ion signal, y_i, to the reactant gas flow, x_i. In this equation the parameter P_3 must be determined in order to calculate the rate constant, k, from the experimental observations.

The method used to find the parameters P_1, P_2 and P_3 is an iterative least squares technique.[52] The set of observations, y_i (n in number), are thought to be a function of the set of parameters, P_j (3 in number in this case).

$$y_i = f_i(P_1,P_2,P_3,x_i) =$$

$$P_1 - P_2 \exp(-P_3 x_i) \qquad i=1,n \qquad (72)$$

However, due to experimental errors and/or model inadequacies, there will be deviations defined by

$$d_i = y_i - f_i(P_1,P_2,P_3,x_i) \qquad i=1,n \qquad (73)$$

The least squares technique involves finding the set of parameters, P_j, such that

$$S = \sum_{i=1}^{n} d_i^2 \qquad (74)$$

is minimized. At this point the observations are linearized with respect to the parameters, P_j, by assuming a set of initial values, P_j^o, for the parameters and expanding in a Taylor series about the initial values, keeping only the first two terms.

$$d_i = y_i - f_i(P_1^o,P_2^o,P_3^o,x_i) +$$

$$\sum_{j=1}^{3} (\partial f_i/\partial P_j)\Big|_{P_j^o} (P_j - P_j^o) \qquad (75)$$

Defining the vector d (length n) as above and the vectors a (length n) and δ (length m=3) by

$$a_i = y_i - f_i(P^o_1, P^o_2, P^o_3, x_i) \tag{76}$$

and

$$\delta_j = P_j - P^o_j \tag{77}$$

and the matrix A (n x 3)

$$A_{ij} = (\partial f_i/\partial P_j)\Big|_{P^o_j} \tag{78}$$

the deviation can be written in matrix notation as

$$d = a - A \tag{79}$$

and

$$S = d'd = (a' - A'\delta')(a - A\delta) \tag{80}$$

where d', a', A' and δ' are the transpose of d, a, A and δ, respectively. S is minimized if

$$\partial S/\partial \delta_j = 0 \qquad j=1,2,3 \tag{81}$$

This yields

$$B\delta = b \tag{82}$$

where $B = A'A$ and $b = A'a$.

$$\delta = B^{-1}b \tag{83}$$

then gives the change to be made in the initial parameters in order to minimize the sum of the squares of the deviation, that is, S. Thus, a new set of initial parameters is defined by

$$P^1 = P^o + \delta \tag{84}$$

and the Taylor series expansion made about the new points P_j^1. The entire process is then repeated until the iterations converge and parameters P_1, P_2 and P_3 are determined.

Figure 22 shows the result of the application of the Jacobian matrix curve fit technique to actual experimental data. The open squares represent data points obtained in an experiment in which the dissociative attachment of electrons to fluorine was studied. The solid line defines the least squares fit obtained by fitting the data to an equation of the form

$$y_i = P_1 - P_2 \exp(-P_3 x_i) \tag{71}$$

Following the sample curve fit result is a listing of a version of the Jacobian matrix technique which allows all of the selected peaks (F^- ion signal for instance) from a specific data file to be fit to the same parametric equation, such as that given above. The operator specifies the data file, whether or not to delete any experimental data points and selects the specific ion signal within that data file to be analyzed. The program then estimates the initial parameters P_1^o, P_2^o and P_3^o

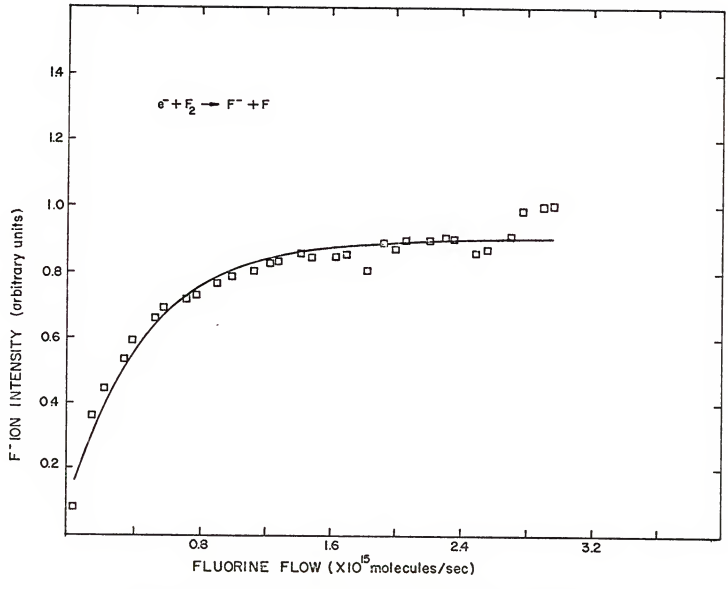

Figure 22. Dissociative Electron Attachment in Fluorine

```
0001  FTN,L
0002        PROGRAM AUTO
0003  C*************************************************************
0004  C*                                                           *
0005  C*  PROGRAM AUTOO  THIS PROGRAM FITS DATA, STORED IN         *
0006  C*  THE SPECIFIED DATA FILE, TO A RATE EQUATION OF THE       *
0007  C*  FORM GIVEN IN LINE 118 (IN THIS PROGRAM EITHER           *
0008  C*  EXPONENTIALLY DECREASING DATA OR ASYMPTOTIC              *
0009  C*  EXPONENTIALLY INCREASING DATA) USING A JACOBIAN          *
0010  C*  MATRIX LEAST SQUARES TECHNIQUE.  SOURCE IS STORED       *
0011  C*  ON DISC AS CTUA.                                        *
0012  C*                                                           *
0013  C*************************************************************
0014        DIMENSION ZVECT(4),BMTRX(4,4),XVECT(4),BINV(4,4)
0015       1,XOBS(100),YOBS(100),DELY(4),PARMT(4),IRRAY(640),
0016       2IFILE(3),NY(100),NX(100),ZY(100)
0017         ICNWD=10B
0018         IRCD=14
0019         WRITE(7,20)
0020  20     FORMAT(1X, INPUT FILE NAME )
0021         READ(7,30)(IFILE(I),I=1,3)
0022  30     FORMAT(3A2)
0023  C*************************************************************
0024  C*                                                           *
0025  C*  LINES 32 THROUGH 37 ALLOW THE OPERATOR TO DELETE         *
0026  C*  THE FIRST FEW DATA POINTS (IF THE EXPERIMENT             *
0027  C*  REQUIRES A PERIOD OF TIME TO ATTAIN STABILITY) AND       *
0028  C*  TO SELECT THE SPECIFIC ION SIGNAL DATA TO BE             *
0029  C*  REDUCED (CL-(35) INSTEAD OF CL-(37) FOR INSTANCE).       *
0030  C*                                                           *
0031  C*************************************************************
0032         WRITE(7,43)
0033  43     FORMAT(1X, INPUT NUMBER OF STARTING DATA POINT )
0034         READ(7,*)JJ
0035         WRITE(7,45)
0036  45     FORMAT(1X, INPUT PEAK   TO BE FIT )
0037         READ(7,*)JJJ
0038         CALL EXEC(IRCD,ICNWD,IRRAY,10,IFILE,0)
0039         NU=IRRAY(2)
0040         ICHAN=JJJ+1
0041         WRITE(6,48)(IFILE(I),I=1,3),ICHAN
0042  48     FORMAT(1X, DATA FILED   ,2X,3A2/1X, MASS CHANNEL  0  ,
0043       113/1X, Y=A-B*EXP(-C*X) CURVE FIT ///1X, RUN   ,7X,
0044       2 A ,14X, B ,14X, C ,8X, K (T MEAS.) ,2X, K (T CALC.
0045       3) //)
0046         DO 1200 MM=1,NU
0047         N=5*MM-4
0048         CALL EXEC(IRCD,ICNWD,IRRAY,640,IFILE,N)
0049         J=IRRAY(10)
0050         DO 50 I=JJ,J
0051         K=75+7*I+JJJ
0052         II=I+1-JJ
```

```
0053        YOBS(II)=FLOAT(IRRAY(K))*(10.**12)/(3276.4*(10.**
0054       1(IRRAY(6))))
0055        K=K-JJJ+1
0056  50    XOBS(II)=FLOAT(IRRAY(K-2))/3276.4
0057  C*************************************************************
0058  C*                                                           *
0059  C*  LINES 63 THROUGH 92 MAKE INITIAL ESTIMATES OF THE        *
0060  C*  PARAMETERS PARMT(1), PARMT(2) AND PARMT(3).              *
0061  C*                                                           *
0062  C*************************************************************
0063        YMIN=1.E+20
0064        DO 55 I=1,J
0065        IF(YMIN-YOBS(I))55,53
0066  53    YMIN=YOBS(I)
0067        XMIN=XOBS(I)
0068  55    CONTINUE
0069        DO 60 I=1,J
0070  60   ZY(I)=YOBS(I)-YMIN
0071        YMAX=-1.E+20
0072        DO 70 I=1,J
0073        IF(ZY(I)-YMAX)70,65
0074  65    YMAX=ZY(I)
0075        XMAX=XOBS(I)
0076  70    CONTINUE
0077        IF(XMAX-XMIN)75,100
0078  75    PARMT(1)=YMIN
0079        PARMT(2)=-YMAX
0080        I=1
0081  77    IF(ZY(I)-0.5*YMAX)80,90
0082  80    I=I+1
0083        GOTO 77
0084  90    PARMT(3)=ALOG(PARMT(2)/(PARMT(1)-YOBS(I)))/XOBS(I)
0085        GOTO 150
0086  100   PARMT(1)=YMAX+YMIN
0087        PARMT(2)=YMAX
0088        I=1
0089  110   IF(ZY(I)-.5*YMAX)120,115
0090  115   I=I+1
0091        GOTO 110
0092  120   PARMT(3)=ALOG(PARMT(2)/(PARMT(1)-YOBS(I)))/XOBS(I)
0093  150   M=IRRAY(10)
0094        N=3
0095        IL=0
0096  C*************************************************************
0097  C*                                                           *
0098  C*  LINES 107 THROUGH 193 USE AN ITERATIVE LEAST             *
0099  C*  SQUARES TECHNIQUE TO ARRIVE AT VALUES FOR THE            *
0100  C*  PARAMETERS PARMT(1), PARMT(2) AND PARMT(3).  IF THE      *
0101  C*  CURVE FIT DOES NOT CONVERGE AFTER 35 ITERATIONS,         *
0102  C*  THE PROCESS IS TERMINATED AND THE PROGRAM PROCEEDS       *
0103  C*  TO THE NEXT EXPERIMENT STORED IN THE SPECIFIED DATA      *
0104  C*  FILE.                                                    *
```

```
0105  C*                                                              *
0106  C****************************************************************
0107  175    DO 210 I=1,4
0108         ZVECT(I)=0.0
0109         DO 210 J=1,4
0110  210    BMTRX(I,J)=0.0
0111         DO 500 I=1,N
0112         IF(ABS(PARMT(3)*XOBS(I))-85.5)260,250
0113  250    WRITE(7,255)NN
0114         WRITE(6,255)NN
0115  255    FORMAT(1X, NO FIT POSSIBLE FOR RUN   ,I4)
0116         GOTO 1200
0117  260    CONTINUE
0118         YPREC=PARMT(1)-PARMT(2)*EXP(-PARMT(3)*XOBS(I))
0119         DELY(1)=1.0
0120         DELY(2)=-EXP(-PARMT(3)*XOBS(I))
0121         DELY(3)=PARMT(2)*XOBS(I)*EXP(-PARMT(3)*XOBS(I))
0122         DEV=YOBS(I)-YPREC
0123         DO 200 K=1,N
0124         ZVECT(K)=ZVECT(K)+DELY(K)*DEV
0125         DO 300 J=1,N
0126         BMTRX(K,J)=BMTRX(K,J)+DELY(K)*DELY(J)
0127  300    CONTINUE
0128  200    CONTINUE
0129  500    CONTINUE
0130         NN=N+1
0131         IF(NN-5)650,750
0132  650    DO 699 L=NN,4
0133  699    BMTRX(L,L)=1.0
0134  750    CONTINUE
0135         DTM1=BMTRX(3,3)*BMTRX(4,4)-BMTRX(3,4)**2
0136         DTM2=BMTRX(2,3)*BMTRX(4,4)-BMTRX(2,4)*BMTRX(3,4)
0137         DTM3=BMTRX(2,3)*BMTRX(3,4)-BMTRX(3,3)*BMTRX(2,4)
0138         DTM4=BMTRX(1,3)*BMTRX(4,4)-BMTRX(1,4)*BMTRX(3,4)
0139         DTM5=BMTRX(1,3)*BMTRX(3,4)-BMTRX(1,4)*BMTRX(3,3)
0140         DTM6=BMTRX(1,3)*BMTRX(2,4)-BMTRX(1,4)*BMTRX(2,3)
0141         DTMN1=BMTRX(1,1)*(BMTRX(2,2)*DTM1-BMTRX(2,3)*DTM2+
0142        1BMTRX(2,4)*DTM3)
0143         DTMN2=BMTRX(1,2)*(BMTRX(1,2)*DTM1-BMTRX(2,3)*DTM4+
0144        1BMTRX(2,4)*DTM5)
0145         DTMN3=BMTRX(1,3)*(BMTRX(1,2)*DTM2-BMTRX(2,2)*DTM4+
0146        1BMTRX(2,4)*DTM6)
0147         DTMN4=BMTRX(1,4)*(BMTRX(1,2)*DTM3-BMTRX(2,2)*DTM5+
0148        1BMTRX(2,3)*DTM6)
0149         DTMNT=DTMN1-DTMN2+DTMN3-DTMN4
0150         BINV(1,1)=BMTRX(2,2)*DTM1-BMTRX(2,3)*DTM2+BMTRX(2,4)
0151        1*DTM3
0152         BINV(1,2)=-BMTRX(1,2)*DTM1+BMTRX(2,3)*DTM4-
0153        1BMTRX(2,4)*DTM5
0154         BINV(1,3)=BMTRX(1,2)*DTM2-BMTRX(2,2)*DTM4+BMTRX(2,4)
0155        1*DTM6
0156         BINV(1,4)=-BMTRX(1,2)*DTM3+BMTRX(2,2)*DTM5-
```

```
      1BMTRX(2,3)*DTM6
       BINV(2,2)=BMTRX(1,1)*DTM1-BMTRX(1,3)*DTM4+
      1BMTRX(1,4)*DTM5
       BINV(2,3)=-BMTRX(1,1)*DTM2+BMTRX(1,2)*DTM4-
      1BMTRX(1,4)*DTM6
       BINV(2,4)=BMTRX(1,1)*DTM3-BMTRX(1,2)*DTM5+BMTRX(1,3)
      1*DTM6
       BINV(3,3)=BMTRX(1,1)*(BMTRX(2,2)*BMTRX(4,4)-
      1BMTRX(2,4)**2)-BMTRX(1,2)*(BMTRX(1,2)*BMTRX(4,4)-
      2BMTRX(2,4)*BMTRX(1,4))+BMTRX(1,4)*(BMTRX(1,2)*
      3BMTRX(2,4)-BMTRX(1,4)*BMTRX(2,2))
       BINV(3,4)=-BMTRX(1,1)*(BMTRX(2,2)*BMTRX(3,4)-
      1BMTRX(2,4)*BMTRX(2,3))+BMTRX(1,2)*(BMTRX(1,2)*
      2BMTRX(3,4)-BMTRX(1,4)*BMTRX(2,3))-BMTRX(1,3)*
      3(BMTRX(1,2)*BMTRX(2,4)-BMTRX(1,4)*BMTRX(2,2))
       BINV(4,4)=BMTRX(1,1)*(BMTRX(2,2)*BMTRX(3,3)-
      1BMTRX(2,3)**2)-BMTRX(1,2)*(BMTRX(1,2)*BMTRX(3,3)-
      2BMTRX(1,3)*BMTRX(2,3))+BMTRX(1,3)*(BMTRX(1,2)*
      3BMTRX(2,3)-BMTRX(1,3)*BMTRX(2,2))
       BINV(2,1)=BINV(1,2)
       BINV(3,1)=BINV(1,3)
       BINV(3,2)=BINV(2,3)
       BINV(4,1)=BINV(1,4)
       BINV(4,2)=BINV(2,4)
       BINV(4,3)=BINV(3,4)
       DO 800 I=1,N
       XVECT(I)=0.0
       DO 800 J=1,N
800    XVECT(I)=XVECT(I)+(BINV(I,J)*ZVECT(J)/DTMNT)
       DO 850 I=1,N
850    PARMT(I)=PARMT(I)+XVECT(I)
       IF(ABS(XVECT(1))-0.01)920,950
920    IF(ABS(XVECT(2))-0.01)930,950
930    IF(ABS(XVECT(3))-0.0001)1000,950
950    IL=IL+1
       IF(IL-35)975,250
975    GOTO 175
C*****************************************************
C*                                                   *
C*  LINES 201 THROUGH 220 CALCULATE A REACTION RATE  *
C*  CONSTANT FROM THE RESULT OF THE CURVE FIT DONE   *
C*  ABOVE AND OUTPUT THE RESULTS.                    *
C*                                                   *
C*****************************************************
1000   VSUBB=FLOAT(IRRAY(11))/32764.
       EMSBR=FLOAT(IRRAY(4))/100.
       PRESS=FLOAT(IRRAY(14))*FLOAT(IRRAY(5))/(3276400.)
       CONCF=(FLOAT(IRRAY(2))*10.**(-IRRAY(3)))/100.
       TMEAS=FLOAT(IRRAY(1))/10000.
       RLENT=19.61
       XK1=(7.17*10.**(-14))*PARMT(3)*VSUBB/(TMEAS*CONCF*
      1EMSBR*PRESS)
```

```
0209          XK2=((1.026*10.**(-9))*PARMT(3)*VSUBB**2)/(EMSBR*
0210         1CONCF*RLENT*PRESS**2)
0211          IF(TMEAS)1010,1010,1020
0212   1010   XK1=0.0
0213   1020   WRITE(7,1015)MM,PARMT(1),PARMT(2),PARMT(3),XK1,XK2
0214          WRITE(6,1015)MM,PARMT(1),PARMT(2),PARMT(3),XK1,XK2
0215   1015   FORMAT(I4,3X,E12.5,3X,E12.5,3X,E12.5,3X,E10.3,3X,
0216         1E10.3)
0217          GOTO 1200
0218          WRITE(7,1050)XK1,XK2
0219   1050   FORMAT(2E20.4)
0220   1200   CONTINUE
0221          END
0222          END$
**** LIST END ****
```

and fits the specified ion signal of experiment 1 to the parametric form given in line 118. When convergence of the fit is obtained, the results are then combined with other experimental parameters stored in the data file and a reaction rate constant is calculated. The program then curve fits the remaining data and calculates corresponding rate constants for each experiment.

B. Grid Search Technique

The Jacobian matrix technique described in the previous section has one major disadvantage. Since it uses a Taylor series expansion to linearize the parametric equation with respect to the parameters P_1, P_2 and P_3, it is possible for the iterations performed in the program to diverge if the initial guesses for the parameters are too unreasonable. A more powerful technique (albeit slower), which avoids this difficulty, is a direct grid search procedure.[53] Using this technique the equation

$$y_i = P_1 - P_2 \exp(-P_3 x_i) \tag{71}$$

may be written

$$y_i = Af(C,x_i) + B \tag{85}$$

where $A = -P_2$, $B = P_1$, $C = P_3$ and

$$f(C,x) = \exp(-Cx) \tag{86}$$

In this form A and B are linear parameters and C is a non-linear

parameter. An estimate is then made of the initial value of the parameter C and a one-dimensional grid of step size ΔC constructed around this initial guess, C_o. Once the initial estimate C_o is made, initial estimates for the parameters A and B may be found by a linear least squares curve fit of the experimental data to the equation

$$y_i = A_o f(C_o, x_i) + B_o \tag{87}$$

The sum of the squares of the deviations for each grid point can then be calculated. If a minimum does not fall within the grid, then it is increased in size until a minimum is captured. The grid is then shifted to center on the minimum and reduced in size until the location (that is, values of A, B and C) of the minimum sum of the squares of the deviations is known. Each manipulation of the grid (expansion, contraction or shift) is accompanied by a new estimate of the linear parameters and the calculation of the sum of the squares of the deviations at each grid point.

This technique may be easily extended to fit data with more than one non-linear parameter. When a metastable quenchant is added to the argon afterglow, the bromine system reduces to the equations

$$Br_2 + e^- \rightleftarrows (Br^-)^* \rightarrow Br^- + Br \tag{13}$$

$$Br^- + Br_2 + Ar \rightarrow Br_3^- + Ar \tag{14}$$

The kinetics equation describing the Br^- ion behavior is then

$$[Br^-] = \{k_1/(k_2' - k_1)\}[e^-]_o\{\exp(-k_1[Br_2]t) - \exp(-k_2'[Br_2]t)\} \quad (88)$$

where $k_2' = k_2[Ar]$. In parametric form this may be written

$$I^- = A\{\exp(-ax) - \exp(-bx)\} + B \quad (89)$$

where B is the baseline and I^- is the Br^- ion signal. Listed on the following pages is a version of the direct grid search technique used to fit the Br^- signal to Equation 89 above. A sample curve fit result is shown in Figure 23. The open squares represent experimental data obtained in the study of the two reaction sequence listed above. The solid line is the curve fit result obtained by fitting the Br^- ion signal to Equation 89.

```
0001  FTN4,L
0002        PROGRAM BRFIT
0003  C*************************************************************
0004  C*                                                           *
0005  C*  PROGRAM BRFITC  THIS PROGRAM USES THE DIRECT GRID        *
0006  C*  SEARCH TECHNIQUE TO FIT THE BR- ION SIGNAL TO AN         *
0007  C*  EQUATION OF THE FORM Y=A*(EXP(-AA*X)-EXP(-BB*X))+B.      *
0008  C*  RATE CONSTANTS FOR THE REACTIONS BR2 + E- = BR- +        *
0009  C*  BR AND BR- + BR2 + M = BR3- + M ARE THUS OBTAINED.       *
0010  C*  SOURCE IS STORED AS TIFRB.   ATTACH GRIDA WHEN          *
0011  C*  LOADING.                                                 *
0012  C*                                                           *
0013  C*************************************************************
0014        DIMENSION IRRAY(640),IFILE(3)
0015        COMMON N,XOBS(100),YOBS(100)
0016        COMMON A,B
0017        EXTERNAL SUMDE
0018  C*************************************************************
0019  C*                                                           *
0020  C*  STATEMENTS 27 THROUGH 46 ALLOW THE OPERATOR TO           *
0021  C*  CHOOSE THE DATA FILE, RUN NUMBER, PEAK NUMBER AND        *
0022  C*  TO DECIDE WHETHER TO DELETE THE FIRST FEW DATA           *
0023  C*  POINTS.                                                  *
0024  C*                                                           *
0025  C*************************************************************
0026        ICNWD=1C2B
0027        WRITE(7,20)
0028  20    FORMAT(1X, INPUT FILE NAME )
0029        READ(7,30)(IFILE(I),I=1,3)
0030  30    FORMAT(3A2)
0031  35    WRITE(7,40)
0032  40    FORMAT(1X, ENTER RUN NUMBER )
0033        READ(7,*)M
0034        WRITE(7,42)
0035  42    FORMAT(1X, INPUT   PTS AT LOW VOLT. END OF EXPT TO
0036       1DELETE )
0037        READ(7,*)IDLTE
0038        N=5*M-4
0039        IRCD=14
0040        CALL EXEC(IRCD,ICNWD,IRRAY,640,IFILE,N)
0041        WRITE(7,43)
0042  43    FORMAT(1X, INPUT NUMBER OF STARTING DATA POINT )
0043        READ(7,*)JJ
0044        WRITE(7,45)
0045  45    FORMAT(1X, INPUT PEAK   TO BE FIT )
0046        READ(7,*)JJJ
0047        IRRAY(10)=IRRAY(10)-IDLTE
0048        J=IRRAY(10)
0049        DO 50 I=JJ,J
0050        K=75+7*I+JJJ
0051        II=I+1-JJ
0052        YOBS(II)=FLOAT(IRRAY(K))*(10.**12)/(3276.4*(10.**
```

```
0053        1(IRRAY(6))))
0054          K=K-JJJ+1
0055     50   XOBS(II)=FLOAT(IRRAY(K-2))/3276.4
0056          IRRAY(10)=IRRAY(10)+1-JJ
0057          WRITE(7,60)
0058     60   FORMAT(1X, INPUT ESTIMATES FOR AA AND BB )
0059          READ(7,*)AA,BB
0060          WRITE(7,65)
0061     65   FORMAT(1X, INPUT AASTP AND BBSTP )
0062          READ(7,*)AASTP,BBSTP
0063          N=IRRAY(10)
0064     C*************************************************************
0065     C*                                                           *
0066     C*  SUBROUTINE SERCH CONTROLS THE GRID CONSTRUCTED           *
0067     C*  AROUND THE NON-LINEAR PARAMETERS AA AND BB ( THAT        *
0068     C*  IS, CONTROLS THE EXPANSION, CONTRACTION AND SHIFT        *
0069     C*  OF THIS GRID.)                                           *
0070     C*                                                           *
0071     C*************************************************************
0072          CALL SERCH(SUMDE,1.E-13,AASTP,BBSTP,0.,AA,BB,0.,S)
0073          WRITE(6,3)A,B,AA,BB,S
0074          WRITE(7,3)A,B,AA,BB,S
0075     3    FORMAT(5E14.4)
0076     C*************************************************************
0077     C*                                                           *
0078     C*  LINES 83 THROUGH 90 COMPUTE THE RATE CONSTANTS FROM      *
0079     C*  THE CURVE FIT PARAMETERS AA AND BB OBTAINED ABOVE        *
0080     C*  AND EXPERIMENTAL PARAMETERS STORED IN THE DATA FILE.     *
0081     C*                                                           *
0082     C*************************************************************
0083     1000 VSUBB=FLOAT(IRRAY(11))/32764.
0084          EMSBR=FLOAT(IRRAY(4))/100.
0085          PRESS=FLOAT(IRRAY(14))*FLOAT(IRRAY(5))/(32764000.)
0086          CONCF=(FLOAT(IRRAY(2))*10.**(-IRRAY(3)))/100.
0087          RLENT=19.61
0088          XK1=((1.01*10.**(-9))*AA*VSUBB**2)/(EMSBR*CONCF*
0089         1RLENT*PRESS**2)
0090          XK2=BB*XK1/AA
0091          WRITE(6,1050)XK1,XK2
0092          WRITE(7,1050)XK1,XK2
0093     1050 FORMAT(2E20.4)
0094          GOTO 35
0095          END
0096     C*************************************************************
0097     C*                                                           *
0098     C*  FUNCTION SUMDE USES A LINEAR LEAST SQUARES               *
0099     C*  TECHNIQUE TO CALCULATE THE LINEAR PARAMETERS A AND       *
0100     C*  B AND THE SUM OF THE SQUARES OF THE DEVIATIONS AT        *
0101     C*  EACH GRID POINT.                                         *
0102     C*                                                           *
0103     C*************************************************************
0104          FUNCTION SUMDE(AA,BB,DUMY)
```

```
0105          DIMENSION FX(100)
0106          COMMON N,XOBS(100),YOBS(100)
0107          COMMON A,B
0108          FN=N
0109          SUMX=0.
0110          SUMXY=0.
0111          SUMX2=0.
0112          SUMY=0.
0113          DO 100 J=1,N
0114          FX(J)=EXP(-AA*XOBS(J))-EXP(-BB*XOBS(J))
0115          SUMX=SUMX+FX(J)
0116          SUMXY=SUMXY+FX(J)*YOBS(J)
0117          SUMX2=SUMX2+FX(J)**2
0118   100    SUMY=SUMY+YOBS(J)
0119          DET=FN*SUMX2-SUMX**2
0120          A=(FN*SUMXY-SUMX*SUMY)/DET
0121          B=(SUMX2*SUMY-SUMXY*SUMX)/DET
0122          SUMDE=0.
0123          DO 101 J=1,N
0124          CALC=A*FX(J)+B
0125   101    SUMDE=SUMDE+(YOBS(J)-CALC)**2
0126          RETURN
0127          END
0128          END$
****   LIST END  ****
```

```
0001  FTN4,L
0002        SUBROUTINE SERCH(FUNCM,STEPLI,XSTEP,YSTEP,ZSTEP,X,
0003       1Y,Z,VALUMI)
0004  C*************************************************************
0005  C*                                                           *
0006  C*  FUNCM IS THE USER CODED FUNCTION SUBROUTINE.  MUST       *
0007  C*  BE DECLARED EXTERNAL IN THE MAIN PROGRAM.  FUNCM         *
0008  C*  MUST HAVE THREE ARGUMENTS.  IF THE FUNCTION HAS          *
0009  C*  LESS THAN THREE VARIABLES, DUMMY ARGUMENTS MUST          *
0010  C*  REPLACE THE INACTIVE ARGUMENTS.  STEPLI IS A             *
0011  C*  PRE-DETERMINED LOWER LIMIT FOR THE DESIRED ACCURACY      *
0012  C*  IN THE VARIABLES ON RETURN.  XSTEP, YSTEP AND ZSTEP      *
0013  C*  ARE INITIAL STEP INCREMENTS OF THE VARIABLES.  THE       *
0014  C*  MINIMUM SEARCH BECOMES INACTIVE IN A PARTICULAR          *
0015  C*  DIRECTION IF THE CORRESPONDING STEP INCREMENT IS         *
0016  C*  MADE EQUAL TO ZERO IN THE CALL STATEMENT.  THESE         *
0017  C*  QUANTITIES ON RETURN BECOME THE FINAL ACCURACIES OF      *
0018  C*  THE VARIABLES.  X, Y AND Z ARE THE INITIAL GUESS         *
0019  C*  VALUES FOR THE INDEPENDENT VARIABLES.  IN RETURN         *
0020  C*  X, Y AND Z ARE THE VALUES OF THE VARIABLES AT THE        *
0021  C*  MINIMUM AND VALUMI IS THE VALUE OF THE FUNCTION AT       *
0022  C*  THE MINIMUM.  F1 IS THE FIRST FUNCTION VALUE ON          *
0023  C*  RETURN, ITERA IS THE TOTAL NUMBER OF ITERATIONS ON       *
0024  C*  RETURN, KFLAT IS RETURNED 1 IF AFTER 10 CONSECUTIVE     *
0025  C*  ITERATIONS THE FUNCTION DID NOT CHANGE, MINE IS          *
0026  C*  RETURNED 1 IF TRUE MINIMUM WAS FOUND AND IF KSTOP       *
0027  C*  IS SET TO 1 OUTSIDE THE PROGRAM, THE MINIMIZATION       *
0028  C*  STOPS.                                                   *
0029  C*                                                           *
0030  C*************************************************************
0031        DIMENSION XD(7),YD(7),ZD(7),VALUED(7,7,7)
0032        ITERA=0
0033        KSTOP=0
0034        NCEND=0
0035        KP1=0
0036        KP2=0
0037        KP3=0
0038        KFLAT=0
0039        MINI=0
0040        MINPER=0
0041        KREP=0
0042        JXF1=0
0043        JYF1=0
0044        JZF1=0
0045        JXFU=0
0046        JYFU=0
0047        JZFU=0
0048        XSTEPF=0.
0049        YSTEPF=0.
0050        ZSTEPF=0.
0051  1000  CONTINUE
0052        ABSX=ABS(X)
```

```
0053          ABSY=ABS(Y)
0054          ABSZ=ABS(Z)
0055          JXM=4
0056          JYM=4
0057          JZM=4
0058          IF(XSTEP+ABSX.NE.ABSX)XSTEPF=XSTEP
0059          IF(YSTEP+ABSY.NE.ABSY)YSTEPF=YSTEP
0060          IF(ZSTEP+ABSZ.NE.ABSZ)ZSTEPF=ZSTEP
0061          IF(KP1.NE.0)XSTEPF=XSTEPK
0062          IF(KP2.NE.0)YSTEPF=YSTEPK
0063          IF(KP3.NE.0)ZSTEPF=ZSTEPK
0064          IF(XSTEP+ABSX.EQ.ABSX.AND.YSTEP+ABSY.EQ.ABSY.AND.
0065         1ZSTEP+ABSZ.EQ.ABSZ)GOTO 1017
0066          ITERA=ITERA+1
0067          IF(XSTEP+ABSX.EQ.ABSX)GO TO 201
0068          IF(YSTEP+ABSY.EQ.ABSY)GO TO 202
0069          IF(ZSTEP+ABSZ.EQ.ABSZ)GO TO 203
0070          DO 301 J=1,7
0071          XD(J)=X+FLOAT(J-4)*XSTEP
0072          YD(J)=Y+FLOAT(J-4)*YSTEP
0073   301    ZD(J)=Z+FLOAT(J-4)*ZSTEP
0074          DO 302 JX=1,7
0075          X=XD(JX)
0076          DO 302 JY=1,7
0077          Y=YD(JY)
0078          DO 302 JZ=1,7
0079          Z=ZD(JZ)
0080   302    VALUED(JX,JY,JZ)=FUNCM(X,Y,Z)
0081          VALUEC=VALUED(4,4,4)
0082          VALUMI=VALUED(1,1,1)
0083          IFLAT=0
0084          DO 304 JX=1,7
0085          DO 304 JY=1,7
0086          DO 304 JZ=1,7
0087          IF(VALUMI.LT.VALUED(JX,JY,JZ))GO TO 304
0088          JXM=JX
0089          JYM=JY
0090          JZM=JZ
0091          IF(VALUMI.GT.VALUED(JX,JY,JZ))IFLAT=0
0092          IFLAT=IFLAT+1
0093          IF(IFLAT.GT.1)GO TO 303
0094          JXF1=JXM
0095          JYF1=JYM
0096          JZF1=JZM
0097          X1=XD(JXM)
0098          Y1=YD(JYM)
0099          Z1=ZD(JZM)
0100   303    JXFU=JXM
0101          JYFU=JYM
0102          JZFU=JZM
0103          XU=XD(JXM)
0104          YU=YD(JYM)
```

```
0105          ZU=ZC(JZM)
0106          VALUMI=VALUEC(JX,JY,JZ)
0107    304   CONTINUE
0108          X=XD(JXM)
0109          Y=YD(JYM)
0110          Z=ZD(JZM)
0111          IF(IFLAT.EQ.1)GO TO 1001
0112          X=.5*(X1+XU)
0113          Y=.5*(Y1+YU)
0114          Z=.5*(Z1+ZU)
0115          GO TO 1001
0116    201   JJ=1
0117          A=Y
0118          B=Z
0119          ABSA=ABSY
0120          ABSB=ABSZ
0121          ASTEP=YSTEP
0122          BSTEP=ZSTEP
0123          GO TO 204
0124    202   JJ=2
0125          A=X
0126          B=Z
0127          ABSA=ABSX
0128          ABSB=ABSZ
0129          ASTEP=XSTEP
0130          BSTEP=ZSTEP
0131          GO TO 204
0132    203   JJ=3
0133          A=X
0134          B=Y
0135          ABSA=ABSX
0136          ABSB=ABSY
0137          ASTEP=XSTEP
0138          BSTEP=YSTEP
0139    204   IF(ASTEP+ABSA.EQ.ABSA)GO TO 104
0140          IF(BSTEP+ABSB.EQ.ABSB)GO TO 101
0141          DO 205 J=1,7
0142          XD(J)=A+FLOAT(J-4)*ASTEP
0143    205   YD(J)=B+FLOAT(J-4)*BSTEP
0144          DO 206 JX=1,7
0145          A=XD(JX)
0146          DO 206 JY=1,7
0147          B=YD(JY)
0148          IF(JJ.EQ.1)VALUEC(JX,JY,1)=FUNCM(X,A,B)
0149          IF(JJ.EQ.2)VALUEC(JX,JY,1)=FUNCM(A,Y,B)
0150    206   IF(JJ.EQ.3)VALUEC(JX,JY,1)=FUNCM(A,B,Z)
0151          VALUEC=VALUEC(4,4,1)
0152          VALUMI=VALUEC(1,1,1)
0153          IFLAT=0
0154          DO 208 JX=1,7
0155          DO 208 JY=1,7
0156          IF(VALUMI.LT.VALUEC(JX,JY,1))GO TO 208
```

```
0157          JAM=JX
0158          JBM=JY
0159          IF(VALUMI.GT.VALUED(JX,JY,1))IFLAT=0
0160          IFLAT=IFLAT+1
0161          IF(IFLAT.GT.1)GC TO 207
0162          JAF1=JAM
0163          JBF1=JBM
0164          A1=XD(JAM)
0165          B1=YD(JBM)
0166    207   JAFU=JAM
0167          JBFU=JBM
0168          AU=XD(JAM)
0169          BU=YD(JBM)
0170          VALUMI=VALUED(JX,JY,1)
0171    208   CCNTINUE
0172          GC TC (209,210,211),JJ
0173    209   JYM=JAM
0174          JZM=JBM
0175          Y=XD(JYM)
0176          Z=YD(JZM)
0177          YSTEP=ASTEP
0178          ZSTEP=BSTEP
0179          XSTEP=0.
0180          JYF1=JAF1
0181          JZF1=JBF1
0182          JYFU=JAFU
0183          JZFU=JBFU
0184          IF(IFLAT.EQ.1)GC TO 1001
0185          Y=.5*(A1+AU)
0186          Z=.5*(B1+BU)
0187          GC TC 1C01
0188    210   JXM=JAM
0189          JZM=JBM
0190          X=XD(JXM)
0191          Z=YD(JZM)
0192          XSTEP=ASTEP
0193          ZSTEP=BSTEP
0194          YSTEP=0.
0195          JXF1=JAF1
0196          JZF1=JBF1
0197          JXFU=JAFU
0198          JZFU=JBFU
0199          IF(IFLAT.EQ.1)GC TO 1001
0200          X=.5*(A1+AU)
0201          Z=.5*(B1+BU)
0202          GC TC 1C01
0203    211   JXM=JAM
0204          JYM=JBM
0205          X=XD(JXM)
0206          Y=YD(JYM)
0207          XSTEP=ASTEP
0208          YSTEP=BSTEP
```

```
0209          ZSTEP=0.
0210          JXF1=JAF1
0211          JYF1=JBF1
0212          JXFU=JAFU
0213          JYFU=JBFU
0214          IF(IFLAT.EQ.1)GO TO 1001
0215          X=.5*(A1+AU)
0216          Y=.5*(B1+BU)
0217          GO TO 1001
0218    101   GO TO (103,102,102),JJ
0219    102   A=X
0220          ABSA=ABSX
0221          ASTEP=XSTEP
0222          JJJ=1
0223          GO TO 106
0224    103   A=Y
0225          ABSA=ABSY
0226          ASTEP=YSTEP
0227          JJJ=2
0228          GO TO 106
0229    104   GO TO (105,105,103),JJ
0230    105   A=Z
0231          ABSA=ABSZ
0232          ASTEP=ZSTEP
0233          JJJ=3
0234    106   DO 107 J=1,7
0235    107   XD(J)=A+FLOAT(J-4)*ASTEP
0236          DO 108 JX=1,7
0237          A=XD(JX)
0238          IF(JJJ.EQ.1)VALUED(JX,1,1)=FUNCM(A,Y,Z)
0239          IF(JJJ.EQ.2)VALUED(JX,1,1)=FUNCM(X,A,Z)
0240    108   IF(JJJ.EQ.3)VALUED(JX,1,1)=FUNCM(X,Y,A)
0241          VALUEC=VALUED(4,1,1)
0242          VALUMI=VALUED(1,1,1)
0243          IFLAT=0
0244          DO 110 JX=1,7
0245          IF(VALUMI.LT.VALUED(JX,1,1))GO TO 110
0246          JAM=JX
0247          IF(VALUMI.GT.VALUED(JX,1,1))IFLAT=0
0248          IFLAT=IFLAT+1
0249          IF(IFLAT.GT.1)GO TO 109
0250          JAF1=JAM
0251          A1=XD(JAM)
0252    109   JAFU=JAM
0253          AU=XD(JAM)
0254          VALUMI=VALUED(JX,1,1)
0255    110   CONTINUE
0256          GO TO (111,112,113),JJJ
0257    111   JXM=JAM
0258          X=XD(JXM)
0259          XSTEP=ASTEP
0260          YSTEP=0.
```

```
0261          ZSTEP=0.
0262          JXF1=JAF1
0263          JXFU=JAFU
0264          IF(IFLAT.EQ.1)GO TO 1001
0265          X=.5*(A1+AU)
0266          GO TO 1001
0267   112    JYM=JAM
0268          Y=XD(JYM)
0269          YSTEP=ASTEP
0270          XSTEP=0.
0271          ZSTEP=0.
0272          JYF1=JAF1
0273          JYFU=JAFU
0274          IF(IFLAT.EQ.1)GO TO 1001
0275          Y=.5*(A1+AU)
0276          GO TO 1001
0277   113    JZM=JAM
0278          Z=XD(JZM)
0279          ZSTEP=ASTEP
0280          XSTEP=0.
0281          YSTEP=0.
0282          JZF1=JAF1
0283          JZFU=JAFU
0284          IF(IFLAT.EQ.1)GO TO 1001
0285          Z=.5*(A1+AU)
0286          GO TO 1001
0287   1001   IF(ITERA.EQ.1)F1=VALUEC
0288          IF(VALUMI.LT.VALUEC)GO TO 1003
0289          IF(IFLAT.GT.1)GO TO 1006
0290          IF(KSTOP.EQ.1)GO TO 1017
0291   1002   XSTEP=.5*XSTEP
0292          YSTEP=.5*YSTEP
0293          ZSTEP=.5*ZSTEP
0294          MINI=1
0295          KPREP=0
0296          IF(XSTEP.GT.STEPLI.OR.YSTEP.GT.STEPLI.OR.ZSTEP.GT.
0297         1STEPLI)GOTO 1016
0298          GO TO 1017
0299   1003   KP1=0
0300          KP2=0
0301          KP3=0
0302          IF(JXM.EQ.1.OR.JXM.EQ.7.OR.JYM.EQ.1.OR.JYM.EQ.7.OR.
0303         1JZM.EQ.1.OR.JZM.EQ.7)GOTO 1004
0304          GO TO 1016
0305   1004   MINPER=1
0306          KREP=KREP+1
0307          IF(KREP.GT.1)GO TO 1005
0308          JXM1=JXM
0309          JYM1=JYM
0310          JZM1=JZM
0311          GO TO 1016
0312   1005   IF(JXM1.EQ.JXM.AND.JYM1.EQ.JYM.AND.JZM1.EQ.JZM)GOTO
```

```
0313        11008
0314         KREP=0
0315         GO TO 1016
0316   1006  IF(MINI.EQ.1)GO TO 1010
0317         IF(MINPER.EQ.1)GO TO 1007
0318         XSTEPF=XSTEP
0319         YSTEPF=YSTEP
0320         ZSTEPF=ZSTEP
0321         KFLAT=KFLAT+1
0322         IF(KFLAT.EQ.10)GO TO 1017
0323   1007  KREP=KREP+1
0324   1008  IF(JXF1.EQ.1.OR.JXFU.EQ.7.OR.JYF1.EQ.1.OR.JYFU.EQ.
0325        17.OR.JZF1.EQ.1.OR.JZFU.EQ.7)GOTO 1009
0326         MINI=1
0327         GO TO 1016
0328   1009  FKREP=KREP
0329         IF(JXF1.EQ.1.OR.JXFU.EQ.7)XSTEP=XSTEP*FKREP
0330         IF(JYF1.EQ.1.OR.JYFU.EQ.7)YSTEP=FSTEP*FKREP
0331         IF(JZF1.EQ.1.OR.JZFU.EQ.7)ZSTEP=ZSTEP*FKREP
0332         GO TO 1016
0333   1010  IF(JXF1.EQ.1.AND.JXFU.EQ.7)GO TO 1013
0334   1011  IF(JYF1.EQ.1.AND.JYFU.EQ.7)GO TO 1014
0335   1012  IF(JZF1.EQ.1.AND.JZFU.EQ.7)GO TO 1015
0336         GO TO 1002
0337   1013  KP1=KP1+1
0338         IF(KP1.EQ.1)XSTEPK=XSTEP
0339         IF(KP1.EQ.3)XSTEP=0.
0340         GO TO 1011
0341   1014  KP2=KP2+1
0342         IF(KP2.EQ.1)YSTEPK=YSTEP
0343         IF(KP2.EQ.3)YSTEP=0.
0344         GO TO 1012
0345   1015  KP3=KP3+1
0346         IF(KP3.EQ.1)ZSTEPK=ZSTEP
0347         IF(KP3.EQ.3)ZSTEP=0.
0348         GO TO 1002
0349   1016  GO TO 1000
0350   1017  IF(XSTEPF.GT.0.)XSTEP=XSTEPF
0351         IF(YSTEPF.GT.0.)YSTEP=YSTEPF
0352         IF(ZSTEPF.GT.0.)ZSTEP=ZSTEPF
0353         RETURN
****   LIST END ****
```

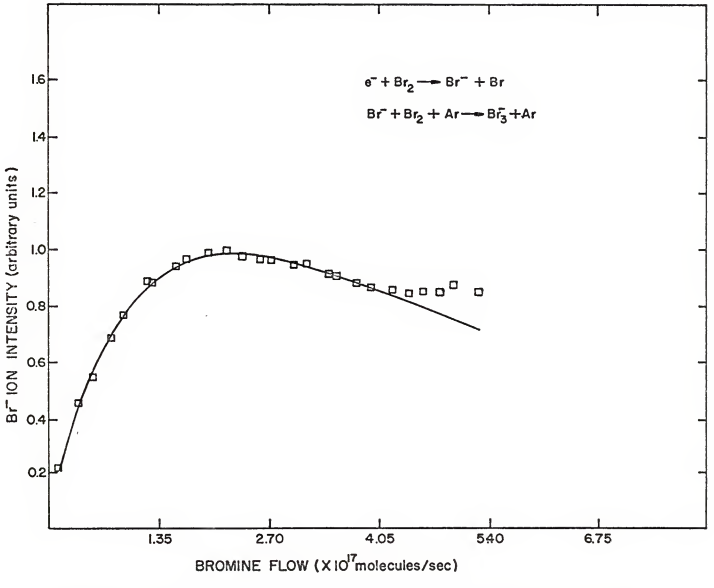

Figure 23. Dissociative Electron Attachment and Br_3^- Formation in Bromine

CHAPTER V

EXPERIMENTAL RESULTS

As previously mentioned, experiments using the flowing afterglow apparatus with both a microwave discharge source and a filament source have been carried out. Thus, the experimental results will be presented under these two headings. The rate constants measured in the present experiments are summarized in Table 5 at the end of this chapter.

A. Microwave Discharge Source

1. Electron Energy

Several authors have shown that electrons are rapidly thermalized in a flowing afterglow environment.[2,5] An approach to the problem, given in Appendix III, indicates that the electrons should indeed be rapidly thermalized, under the present experimental conditions, by the time (1-3 msec) they reach the reactant gas injection port from their source in the microwave discharge. The only experimental procedure used to actually estimate electron temperatures in the flowing afterglow was based on the measurement of the ratio of SF_5^- to SF_6^- ion currents when SF_6 was injected at the neutral reactant port. This ratio has been shown by other investigators to

be strongly dependent on electron energy.[2,3,5] The results of the present measurements are illustrated by Figure 24. Since the ratio, SF_5^-/SF_6^-, is known to be independent of pressure in the pressure regime of Figure 24, the variable ratio observed must reflect changes in electron energy in the reaction tube as the pressure is varied. The energy variation observed is probably a result of the change in experimental conditions influenced by flow tube pressure. These conditions include electron collision frequency, electron diffusion losses, buffer gas axial velocity and the microwave discharge coupling efficiency. In any event the SF_5^-/SF_6^- ratios measured here indicate an average electron temperature of approximately 400°K or 600°K depending on whether the ratios are compared to the data of Chen and Chantry[5] or Fehsenfeld,[2] respectively.

2. Electron Attachment in Sulfur Hexafluoride

In order to determine whether attachment rates measured with the flowing afterglow system in the microwave source configuration are reliable, the total attachment rate of electrons to sulfur hexafluoride was measured. This reaction has previously been studied by several investigators,[27-30] including Fehsenfeld[2] who reported an attachment rate constant of 2.1×10^{-7} cm^3/molecule-sec measured in a flowing afterglow with helium buffer gas at a temperature of 289°K. The total attachment rate for this reaction was found by Fehsenfeld to be constant over a range of several hundred degrees.

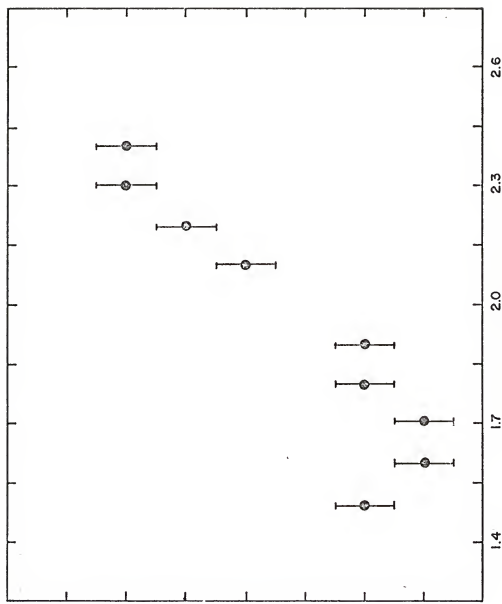

Figure 24. SF_5^-/SF_6^- Ratio in the Microwave Discharge Source Configuration

The rate for the attachment reaction is so large that 100% SF_6 cannot be injected into the afterglow without quenching it, that is, immediately attaching all free electrons. Thus, mixtures of SF_6 with argon, which were in the concentration range 0.1 to 0.001% SF_6, were used in these experiments.

In the experiments utilizing the microwave discharge source the total product ion signal (the sum of SF_6^- and SF_5^-) was monitored as a function of the sulfur hexafluoride flow into the afterglow. The resulting data, listed in Appendix IV, were reduced using the filament flow model derived in Chapter III Section B. The average value obtained for the total attachment rate constant for SF_6 was $4.2 \pm 1.1 \times 10^{-8}$ cm^3/molecule-sec.

In order to make accurate kinetic measurements in a flowing afterglow system, downstream sources of electrons must be removed in order to ensure that all electrons in the flow tube have the same time to react with the injected gas; that is, no electrons should be produced downstream of the reactant gas injection port. One possible source of electrons in the reaction tube is Penning ionization which can occur with rare gas metastable atoms. In the case of argon metastables, this reaction

$$Ar^m + X \rightarrow Ar + X^+ + e^- \qquad (90)$$

is possible if the ionization potential of X is less than the energy of the argon metastable. This is not a problem in the $SF_6 + e^-$ reaction studies since the energies of the argon metastables, 11.54 and 11.72 eV,[54] are less than the ionization potential of sulfur hexafluoride, 16.15 eV.[55]

Another possible mechanism for the production of electrons by metastables has been suggested by Biondi.[56,57] The reaction

$$Ar^m + Ar^m \rightarrow Ar + Ar^+ + e^- \qquad (91)$$

is energetically possible since $IP(Ar) < 2E(Ar^m)$. Because of the possibility of this metastable-metastable reaction, experiments were conducted in which nitrogen was injected into the afterglow, upstream of the reaction tube. The added nitrogen removes metastables by the reaction

$$Ar(^3P_2) + N_2(X^1\Sigma_g) \rightarrow N_2(C^3\pi_u) + Ar(^1S_o) \qquad (92)$$

followed by radiative emission of the excited nitrogen product ($C^3\pi_u \rightarrow B^3\pi_g$). The rate of this quenching reaction has been measured and found to be high (0.3×10^{-10} cm^3/molecule-sec).[54] Thus, the injection of even a few millitorr of nitrogen into the afterglow should deplete the metastable concentration by several orders of magnitude before the reactant gas is injected. The data listed in Appendix IV include experiments in which nitrogen was injected as a metastable quenchant. Considering the scatter in the data, there is no significant difference in the average electron attachment rate constant calculated from experiments using the quenchant ($k = 4.6 \pm 1.3 \times 10^{-8}$ cm^3/molecule-sec) and that obtained from experiments not using the quenchant ($k = 3.9 \pm 0.9 \times 10^{-8}$ cm^3/molecule-sec). Thus, it does not appear that the metastable-metastable reaction is an important source of electrons in the present experiments.

3. Electron Attachment in Fluorine

As previously stated, fluorine and electrons undergo a dissociative attachment reaction to form a negative ion and an atom

$$e^- + F_2 \rightleftarrows (F_2^-)^* \rightarrow F^- + F \qquad (4)$$

The experimental data obtained in the study of this reaction are listed in Appendix IV. The data were reduced to rate constants using the filament flow model derived in Chapter III Section B. The average value obtained for the bimolecular rate constant for the dissociative attachment of electrons to fluorine in a series of seven measurements is $4.6 \pm 1.2 \times 10^{-9}$ cm^3/molecule-sec.

A 0.065% fluorine in argon gas mixture was injected into the afterglow in order to determine the dissociative electron attachment reaction rate for fluorine. The mixture was specified to be nominally 0.1% fluorine by the manufacturer. An analysis to determine more accurately the fluorine concentration was carried out as described in Appendix I.

Since the ionization potential of fluorine, 16.6 eV,[9] is greater than the energy of the argon metastable, Penning ionization is not expected to be a downstream source of electrons. In order to show that metastables were not interfering with the measurement of the fluorine electron attachment rate through some other mechanism, the following simple experiment was

devised. A constant flow of fluorine was injected into the reaction tube and the resulting F^- ion signal was continuously monitored as a function of the partial pressure of the metastable quenchant, nitrogen, injected upstream into the afterglow. If the metastables constitute an important downstream source of electrons, then the injection of nitrogen upstream from the reaction tube should drastically reduce the F^- ion signal by removing metastables at a rate $k = 0.3 \times 10^{-10}$ cm^3/molecule-sec as discussed previously. Figure 25 is a log plot of the resulting F^- ion signal versus the partial pressure of nitrogen. It is seen that the F^- ion signal decreases at a rate corresponding to $k \simeq 10^{-14}$ cm^3/molecule-sec, approximately four orders of magnitude smaller than the quenching rate of the metastables by nitrogen. Thus, it does not appear that argon metastables interfere with the measurement of the fluorine electron attachment rate.

4. Sulfur Hexafluoride - Oxygen Negative Ion Charge Transfer

In the process of checking out the flowing afterglow system, the rate of the charge transfer reaction

$$SF_6 + O_2^- \rightarrow SF_6^- + O_2 \qquad (10)$$

was measured. The rate coefficient for this reaction was determined by Fehsenfeld[26] in a flowing afterglow system to be 7×10^{-11} cm^3/molecule-sec. This charge transfer reaction is particularly suitable for checking out a flowing afterglow system since the rate is so slow that pure sulfur hexafluoride

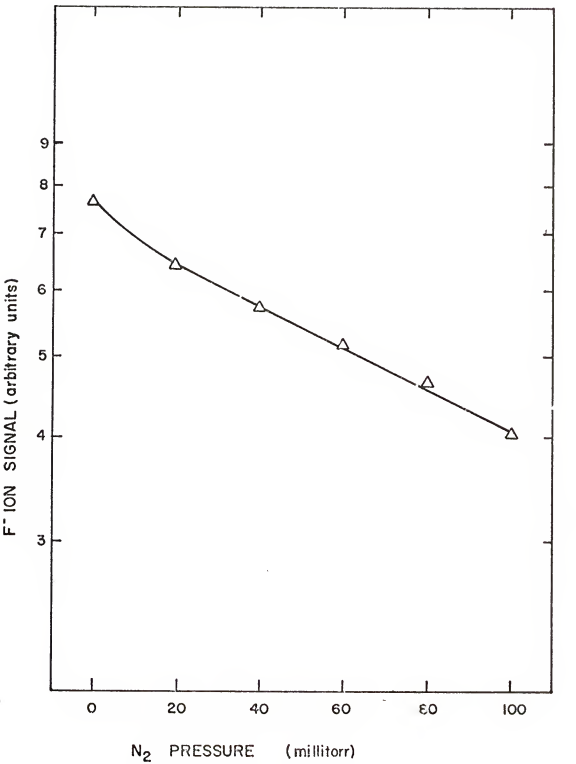

Figure 25. F^- Ion Signal Versus the Partial Pressure of an Argon Metastable Atom Quenchant, Nitrogen, Injected into the Afterglow

may be injected into the afterglow in order to study the reaction. Thus, this eliminates errors in making reactant/diluent mixtures. In addition, the reaction rate has been previously measured in a similar flowing afterglow system.

In making these measurements, helium was used as the buffer gas and oxygen was injected into the afterglow both to remove helium metastables and to produce O_2^- ions. The helium metastables were removed by Penning ionization

$$He^m + O_2 \rightarrow He + O_2^+ + e^- \qquad (93)$$

O_2^- ions were then formed by the attachment of electrons to oxygen

$$O_2 + e^- \rightleftarrows (O_2^-)^* \xrightarrow{O_2} O_2^- \qquad (11)$$

Sulfur hexafluoride was injected into the afterglow downstream from the oxygen inlet port and the decay of the O_2^- ion signal was monitored as a function of the SF_6 flow rate as determined by a linear mass flowmeter. The data obtained are listed in Appendix IV. Using the filament flow model derived in Chapter III Section B, the data listed in Appendix IV yield an average rate constant of $3.7 \pm 0.4 \times 10^{-11}$ cm^3/molecule-sec, indicating better than a factor of two agreement with the Fehsenfeld result. In one experiment, illustrated in Figure 26, both the O_2^- and SF_6^- ion signals were monitored as the SF_6 flow rate was varied. The solid lines are the least squares curve fit results. The rate constants obtained from the SF_6^- and O_2^-

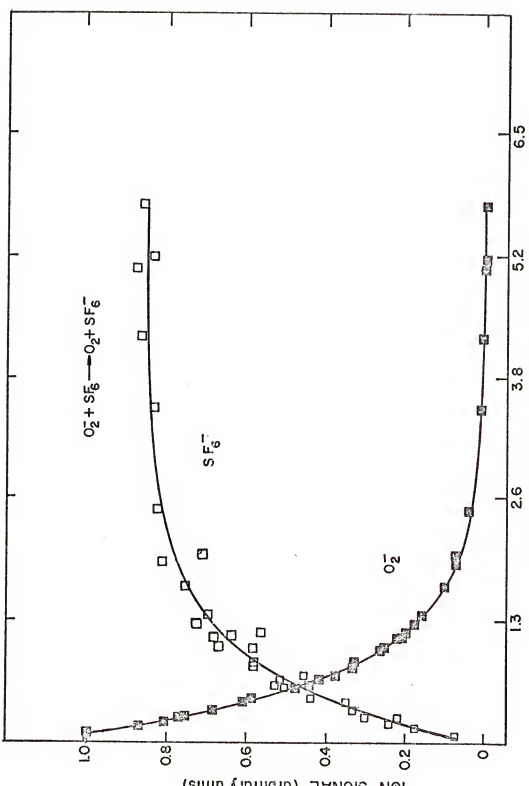

Figure 26. Charge Transfer Between SF_6 and O_2^-

ion signals were 3.1×10^{-11} cm^3/molecule-sec and 3.8×10^{-11} cm^3/molecule-sec, respectively. The agreement between the two values indicates the feasibility of obtaining rate constants from the appearance of ion signals.

A Cl^- ion signal was observed in the afterglow in the charge transfer experiments. The Cl^- originates from a residual impurity in the afterglow. Since Cl^- has a higher electron affinity than SF_6, it should not undergo charge transfer with the molecule and the Cl^- signal should remain constant throughout the experiment provided that sampling conditions are constant. This is precisely what was observed as shown in the data listed in Appendix IV.

B. Filament Source

1. Electron Energy

When sulfur hexafluoride was injected into the flowing afterglow apparatus in the filament source configuration, the SF_5^- signal levels were so low that they could not be extracted from the noise (~5 mV). Even for experiments in which the system sensitivity was fairly high (~5 volts SF_6^- signal), no SF_5^- signal could be observed. Therefore, it is assumed that the SF_5^-/SF_6^- ratio is on the order of 10^{-3}. This corresponds to an average electron energy of 300°K or 350°K depending on whether this ratio is compared to the data of Chen and Chantry[5] or Fehsenfeld,[2] respectively. Since the flow time between the filament source and the reactant gas injection

port is on the order of 1-3 msec, the calculations in Appendix III are still applicable. These calculations indicate a rapid thermalization of electrons in a high pressure flowing afterglow. The lower electron energy estimate for the filament source configuration compared to the microwave source configuration is not unreasonable since a microwave discharge results in a greater heating of the buffer gas with which the electrons are in thermodynamic equilibrium.[48] In addition, the incidence of superelastic collisions between electrons and metastable atoms, which tend to increase the average electron energy, is greater in a microwave discharge afterglow due to the higher metastable atom densities.[58]

2. Electron Attachment in Sulfur Hexafluoride

A series of nineteen determinations of the rate of attachment of thermal electrons to sulfur hexafluoride were made using the flowing afterglow system in the filament source configuration. These data are summarized in Appendix IV. The average value obtained for the rate constant, k, was $3.8 \pm 1.8 \times 10^{-8}$ cm^3/molecule-sec using the reaction tube transit times calculated from the measured buffer gas flows assuming a parabolic radial velocity profile and $3.5 \pm 1.7 \times 10^{-8}$ cm^3/molecule-sec using the reaction tube transit times measured by the probe technique described in Chapter III Section B. It has been shown that flowing afterglows with a filament source have a lower metastable atom density than those with a microwave discharge source.

Therefore, no experiments were done in which a metastable quenchant was injected into the afterglow since the experiments with a microwave discharge source configuration indicated that argon metastable atoms were not a significant downstream source of electrons.

3. Electron Attachment in Fluorine

The study of dissociative electron attachment in fluorine, using the filament source, yielded a rate constant, k, of $3.1 \pm 1.2 \times 10^{-9}$ cm^3/molecule-sec using the reaction tube transit times calculated from the measured buffer gas flows assuming a parabolic radial velocity profile and $3.1 \pm 1.2 \times 10^{-9}$ cm^3/molecule-sec using reaction tube transit times measured by the probe technique discussed in Chapter III Section B. The experimental data obtained in the study of this reaction are listed in Appendix IV. A sample of the data obtained in the study of electron attachment in fluorine with the flowing afterglow system in the filament source configuration is shown in Figure 22.

4. Electron Attachment in Chlorine

The dissociative attachment rate of electrons in chlorine was measured in the flowing afterglow using the filament source. Both the Cl^- (m/e = 35) and the Cl^- (m/e = 37) isotopes were monitored in these experiments. The rate constants obtained for the dissociative attachment of electrons in chlorine were

$3.7 \pm 1.8 \times 10^{-9}$ cm^3/molecule-sec for the Cl^- (m/e = 35) isotope and $3.7 \pm 1.7 \times 10^{-9}$ cm^3/molecule-sec for the Cl^- (m/e = 37) isotope. The data obtained are listed in Appendix IV. Figure 27 illustrates the results of a typical chlorine experiment. The solid lines are least squares fits for this experiment.

5. Electron Attachment in Oxygen

Upon the injection of oxygen into the flowing afterglow reaction tube, O_2^- was formed by the attachment process

$$O_2 + e^- \rightleftarrows (O_2^-)^* \xrightarrow{O_2} O_2^- \qquad (11)$$

A plot of the O_2^- ion signal versus the oxygen partial pressure in the reaction tube is shown in Figure 28. The solid line represents a hand drawn curve fit. Reduction of these data to a rate constant yields $k = 2.2 \times 10^{-29}$ cm^6/molecule^2-sec.

The reaction

$$O_2 + e^- \rightarrow O^- + O \qquad (94)$$

has a threshold of approximately 3 eV.[59] Since only a very small O^- signal (two orders of magnitude less than the O_2^- signal) was observed when oxygen was injected into the reaction tube in the present experiments, it is assumed that the electron energy distribution contains no significant high energy tail. The O^- signal observed may be due to the diffusion of very small amounts of oxygen upstream to the filament region where electron energies greater than 3 eV occur.

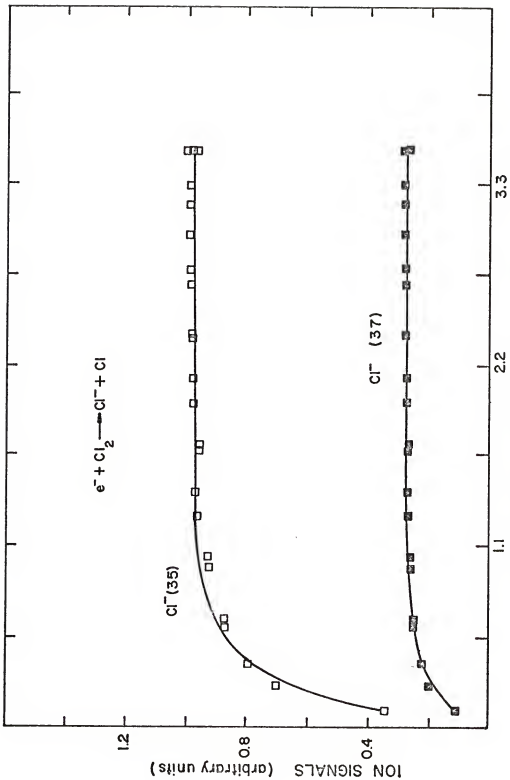

Figure 27. Dissociative Electron Attachment in Chlorine

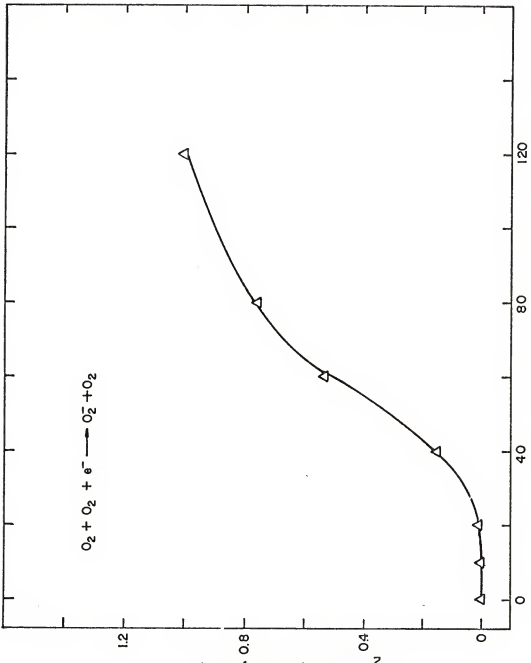

Figure 28. Electron Attachment in Oxygen

6. Electron Attachment in Bromine

The study of electron attachment in bromine is complicated by the occurence of three reactions when bromine is injected into the afterglow

$$e^- + Br_2 \rightleftarrows (Br_2^-)^* \rightarrow Br^- + Br \qquad (13)$$

$$Ar^m + Br_2 \rightarrow Br_2^+ + Ar + e^- \qquad (95)$$

$$Br^- + Br_2 + Ar \rightarrow Br_3^- + Ar \qquad (14)$$

The injection of a metastable quenchant, such as nitrogen, into the afterglow eliminates the need to consider the Penning ionization process. The data observed in experiments then depend on the two reactions shown as Equations 13 and 14.

The study of the bromine-electron reaction system, shown above as Equations 13 and 14, was performed in three steps

1. the injection of high concentrations of bromine so that only the second reaction need be considered in the reduction of data,
2. the injection of dilute bromine such that only the electron attachment reaction is important and
3. the injection of intermediate concentrations of bromine and reducing the data assuming both reactions to be important.

The techniques above apply to the case where k_1, the attachment rate constant, is on the order of $k_2[Ar]$, the pseudo second-order rate constant for Equation 14 (hereafter known as k_2').

Figure 29 illustrates the data obtained using the technique of step 1. The solid line represents the least squares curve fit obtained for the Br^- signal. The rate of bromine injection was so rapid that only the reaction

$$Br^- + Br_2 + Ar \rightarrow Br_3^- + Ar \qquad (14)$$

was observed. The average rate constant k_2', determined from the observation of the Br^- signal, is $1.2 \pm 0.3 \times 10^{-11}$ cm^3/molecule-sec. The observation of Br_3^- in one experiment yielded a rate constant k_2' equal to 0.48×10^{-11} cm^3/molecule-sec. The Br_3^- ion was at the upper mass limit for the mass spectrometer used in the present experiments. Observation of this signal was difficult and inaccurate.

Figure 30 illustrates the technique for which the bromine injection rate was so small that only the reaction

$$Br_2 + e^- \rightleftarrows (Br_2^-)^* \rightarrow Br^- + Br \qquad (13)$$

need be considered. The solid line represents the least squares curve fit obtained for the Br^- signal. The average rate constant, k_1, obtained for these experiments is $1.0 \pm 0.9 \times 10^{-11}$ cm^3/molecule-sec.

Figure 23 illustrates the data obtained for which both the electron attachment reaction and the Br_3^- formation reaction were important. In these experiments the average rate constants obtained were $1.5 \pm 1.2 \times 10^{-11}$ cm^3/molecule-sec for k_1 and

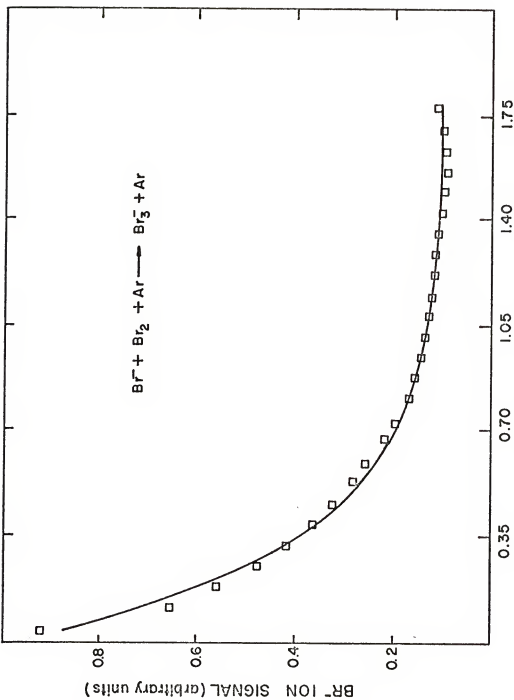

Figure 29. Formation of Br_3^- in Bromine

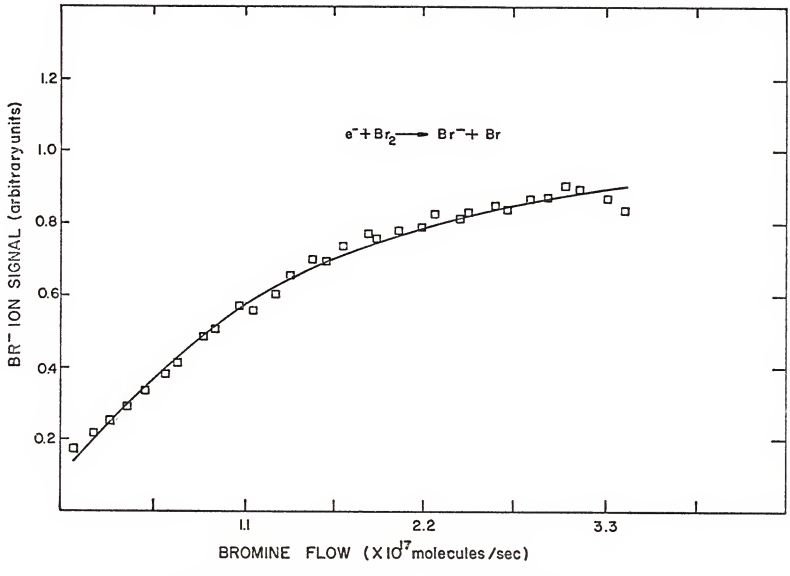

Figure 30. Dissociative Electron Attachment in Bromine

$1.4 \pm 0.8 \times 10^{-11}$ cm^3/molecule-sec for k_2'. The solid line is the least squares curve fit obtained for the Br^- signal.

The average value obtained for k_1 in all of the experiments was $1.1 \pm 0.9 \times 10^{-11}$ cm^3/molecule-sec. The average value for k_2' was found to be $1.2 \pm 0.6 \times 10^{-11}$ cm^3/molecule-sec. Since all of the experiments were done with the buffer gas pressure at approximately 2 Torr, the average rate constant, k_2', when converted to a third order rate constant, k_2, yields a value for k_2 of $1.9 \pm 1.0 \times 10^{-28}$ cm^6/molecule^2-sec.

Table 5

Rate Constants Determined in the Present Experiments

Net Reaction	Rate Constant[a]	Source[b]	Comments
$e^- + SF_6 \rightarrow SF_6^-, SF_5^-$	$4.6 \pm 1.3 \times 10^{-8}$	microwave	with metastable quenchant
	$3.9 \pm 0.9 \times 10^{-8}$	microwave	without metastable quenchant
	$4.2 \pm 1.1 \times 10^{-8}$	microwave	average value (all experiments)
	$3.8 \pm 1.8 \times 10^{-8}$	filament	buffer flow transit times
	$3.5 \pm 1.7 \times 10^{-8}$	filament	probe transit times
	$3.6 \pm 1.8 \times 10^{-8}$	filament	average value
$SF_6 + O_2^- \rightarrow SF_6^- + O_2$	3.1×10^{-11}	microwave	SF_6^- monitored } 1 experiment
	3.8×10^{-11}	microwave	O_2^- monitored
	$3.7 \pm 0.4 \times 10^{-11}$	microwave	average value (all experiments)
$e^- + 2O_2 \rightarrow O_2^- + O_2$	2.2×10^{-29}	filament	1 experiment
$e^- + F_2 \rightarrow F^- + F$	$4.6 \pm 1.2 \times 10^{-9}$	microwave	
	$3.1 \pm 1.2 \times 10^{-9}$	filament	buffer flow transit times
	$3.1 \pm 1.2 \times 10^{-9}$	filament	probe transit times
$e^- + Cl_2 \rightarrow Cl^- + Cl$	$3.7 \pm 1.8 \times 10^{-9}$	filament	$^{35}Cl^-$ isotope monitored
	$3.7 \pm 1.7 \times 10^{-9}$	filament	$^{37}Cl^-$ isotope monitored

$e^- + Br_2 \rightarrow Br^- + Br$	$1.0 \pm 0.9 \times 10^{-11}$	filament	low bromine concentrations
	$1.5 \pm 1.2 \times 10^{-11}$	filament	intermediate bromine concentrations
	$1.1 \pm 0.9 \times 10^{-11}$	filament	average value (all experiments)
$Br^- + Br_2 + Ar \rightarrow Br_3^- + Ar$	$1.9 \pm 0.5 \times 10^{-28}$	filament	high bromine concentration, Br^- monitored
	0.75×10^{-29}	filament	high bromine concentration, Br_3^- monitored
	$2.2 \pm 1.2 \times 10^{-28}$	filament	intermediate bromine concentration, Br^- monitored
	$1.9 \pm 1.0 \times 10^{-28}$	filament	average value (all experiments)

[a]All rate constants are in units of cm^3/molecule-sec except those for the three-body electron attachment to oxygen and the three-body Br_3^- formation which are in units of cm^6/molecule^2-sec.

[b]The electron temperature is 400-600°K for all experiments in which the microwave source was used and 300-350°K for all experiments in which the filament source was used.

CHAPTER VI

DISCUSSION OF RESULTS

A. Comparison with Published Data

Table 6 compares the average rate constants obtained for reactions studied in the present research with those published or extrapolated (EXT) from data published in chemical literature. The rate constants presented in Table 6 are in units of cm^3/molecule-sec except those for three-body electron attachment to oxygen and the three-body Br_3^- formation, the rates for which are in units of cm^6/$molecule^2$-sec. The electron temperature in the flowing afterglow was estimated in Chapter V to be in the range 300-600°K.

The first three reactions listed were investigated in order to determine whether rate constants measured in the present flowing afterglow apparatus are reliable. The rate constant measured for the attachment of electrons in sulfur hexafluoride is approximately a factor of six smaller than the rate constant measured by Fehsenfeld in a flowing afterglow apparatus and by other researchers using various techniques. Thus, it appears that rate constants for electron attachment measured in the present experiments may be low by this factor of six. As discussed in Chapter III Section F, the major reason for

Table 6

Comparison of the Present Results with Published Data

Net Reaction	k(measured)	k(published)	Author(s)
$e^- + SF_6 \rightarrow SF_6^-, SF_5^-$	$3.9 \pm 1.4 \times 10^{-8}$	2.21×10^{-7}	Fehsenfeld[2]
		3.1×10^{-7}	Mahan and Young[27]
		2.7×10^{-7}	Young[28]
		2.42×10^{-7}	Chen et al.[29]
		2.14×10^{-7}	Davis and Nelson[30]
$e^- + 2O_2 \rightarrow O_2^- + O_2$	2.2×10^{-29}	2.2×10^{-29}	Pack and Phelps[32]
		0.3×10^{-29}	Chanin et al.[31]
$SF_6 + O_2^- \rightarrow SF_6^- + O_2$	$3.7 \pm 0.4 \times 10^{-11}$	7×10^{-11}	Fehsenfeld[26]
$e^- + F_2 \rightarrow F^- + F$	$3.8 \pm 1.2 \times 10^{-9}$	—	—
$e^- + Cl_2 \rightarrow Cl^- + Cl$	$3.7 \pm 1.7 \times 10^{-9}$	$1.2\text{-}300 \times 10^{-12}$	Bradbury (EXT)[11]
		$<6 \times 10^{-12}$	Bailey and Healey (EXT)[12]
		large	Dunkin et al.[15]
$e^- + Br_2 \rightarrow Br^- + Br$	$1.1 \pm 0.9 \times 10^{-11}$	1.5×10^{-11}	Bailey et al. (EXT)[23]
		0.82×10^{-12}	Truby[24]

$Br^- + Br_2 + Ar \rightarrow Br_3^- + Ar$	$1.9 \pm 1.0 \times 10^{-28}$	——	——
$Br^- + 2Br_2 \rightarrow Br_3^- + Br_2$	——	2.9×10^{-29}	Truby[60]

this low rate constant is probably the change in the electron diffusion rate as negative ions are formed in the afterglow. The measurement of the three-body attachment of electrons to oxygen yielded a rate constant in agreement with the data published by Pack and Phelps.[32] The SF_6/O_2^- charge transfer reaction studied yielded a rate constant within a factor of two of the Fehsenfeld[26] result. Thus, it appears that the flowing afterglow apparatus used in the present experiments yields electron attachment rate constants within a factor of six and charge transfer rates within a factor of two.

As was discussed in Chapter I Section B no electron attachment rate data have been published for fluorine. The present results represent the first measurement of this rate constant.

Attachment to chlorine for thermal electrons has been qualitatively observed by Dunkin et al.[15] to be large. The present experiments certainly agree with that observation. The rate constant measured is larger than the estimates extrapolated from the data of Bradbury[11] and Bailey and Healey.[12] This is probably due to poor estimates of the mean free path at thermal energies of electrons in the gases used in their experiments. The value of the mean free path is necessary in order to convert measured attachment probabilities to rate constants.

The thermal electron attachment rate measured for bromine agrees well with the value extrapolated from the data of Bailey et al.[23] The rate constant obtained in the present experiments is a factor of thirteen larger than that obtained by Truby[24] in a static afterglow experiment.

The rate of the three-body formation of Br_3^- in which argon is the third body has not been reported. This rate may be compared to that measured by Truby[60] for Br_3^- formation in which bromine is the third body.

B. Significance of the Results

Dissociative electron attachment is currently being investigated due to the application of this technique to the development of chemical laser systems. For example, in the HF chemical laser F atoms react with hydrogen to yield vibrationally excited HF

$$F + H_2 \rightarrow H + HF(v \simeq 2,3) \qquad (96)$$

which produces the population inversion necessary for lasing.[61] Current research has focused on efficient mechanisms for the production of F atoms necessary to initiate this reaction. Electron beam techniques are currently being used to dissociate fluorine (and other fluorine atom containing compounds) in order to produce the required F atom concentrations. In the process some of the fluorine is ionized, producing electrons, and those electrons and electrons from the primary beam may be thermalized in the relatively high pressures used in the laser systems. These electrons can then rapidly attach to fluorine to produce F atoms at a rate measured in the current research. Thus, it is now possible for laser engineers to estimate the importance of dissociative electron attachment in fluorine in the operation of an HF chemical laser system.

In addition, the importance of the dissociative attachment of thermal electrons in chlorine in the HCl chemical laser system may be estimated.[62] No previous data for the thermal attachment of electrons to chlorine have been reported.

The measurement of the rate of dissociative attachment of thermal electrons in bromine confirms the previously reported fact that the rate of this reaction is much slower than that for chlorine, fluorine or iodine. Thus, the application of this technique as a source of bromine atoms in an HBr laser is not expected to be feasible.

C. Assumptions Made in the Derivation of the Mathematical Model

Several assumptions were made in the derivation of the mathematical models used to reduce the experimental data, obtained in this research, to rate constants. Further comment concerning the accuracy of these assumptions is certainly in order.

It was assumed that electrons, ions and buffer gas should move down the reaction tube at the same rate in the high pressures present in the flow tube. Figure 21 shows this assumption to be true for ions and buffer gas in the flow tube. The determination of the electron temperature in the reaction tube yielded values on the order of 300-600°K which indicates that the electrons are not being accelerated down the flow tube by small electric fields present in the tube. In addition,

in the high pressure environment in the reaction tube the electrons should suffer many collisions with the buffer gas and move down the flow tube at the same rate.

In view of the standard deviations (30-90%) obtained for rate constant measurements presented in this research, the neglect of inlet effects is probably justified since corrections for this effect would change the rate constants obtained by only about 20% ($1.62k_s \rightarrow 1.32k_s$) at most.[48] Thus, no corrections for inlet effects were made.

The change in the electron diffusion rate as negative ions are formed in the afterglow is probably the major reason for the low rate constant obtained in the present research for the attachment of electrons in sulfur hexafluoride. The only way to correct for this effect is to include this phenomenon in the transport equation for electrons in the reaction tube and to reduce the experimental data using numerical techniques.

D. Suggestions for Modifications of the Flowing Afterglow Apparatus and Further Research

There are several modifications of the flowing afterglow apparatus which could be made in order to improve the performance of the system. In the present design, fluctuations in the ion signals obtained may in part be due to the charging of surfaces in the flow tube, particularly the cone on which the ion sampling orifice is located. The present system configuration does not allow the cone to be easily removed

for cleaning since both the electrostatic lens system and the flow tube are attached to the same flange as the cone. In addition, in the present experimental configuration the buffer gas is not pumped smoothly over the cone but at a somewhat oblique angle to the orifice axis. This may prevent the sampling from being viscous and make the ion signal behavior versus reactant gas flow somewhat dependent on potentials applied to the sampling orifice. The flow tube should be redesigned such that the ion sampling is truly a viscous process. Another source of signal fluctuations in the present experiments may be charged surfaces present on the lens elements between the sampling orifice and the quadrupole. Most of these lens elements could be eliminated and the distance between the sampling orifice and the quadrupole shortened considerably. This would eliminate many unnecessary lens elements and should improve the transmission of the lens system. One problem also noted in the present research was the diffusion of reactant gas from the dead volume between the injection port and the reactant gas leak valve. This appeared to be significant at small reactant gas flow rates and probably caused the relatively large baseline observed in the chlorine and bromine experiments. One solution to the problem would be to maintain a constant carrier gas flow through the dead volume. This would constantly flush the reactant gas line.

There are many interesting research topics which can be pursued with the flowing afterglow apparatus. There is at

present a continuing interest in the measurement of the rate of thermal electron attachment to molecules containing halogen atoms and the possible applications of these measurements in the development of chemical lasers. In addition, during the course of the present research halogen-negative ion reactions such as

$$O_2^- + Br_2 \rightarrow Br^- + \text{products} \qquad (97)$$

were observed. Many reactions of this type are energetically possible and represent an area of halogen negative ion chemistry still unexplored.

APPENDIX I

ANALYSIS OF THE FLUORINE/ARGON MIXTURE

The fluorine/argon mixture obtained from Matheson Gas Products was specified to contain approximately 0.1% fluorine. In order to minimize errors in the determination of the rate of dissociative electron attachment, an analysis of the fluorine/argon mixture was made. The technique employed to determine fluorine was a wet chemical procedure in which fluorine is precipitated as triphenyltin fluoride.[63]

The fluorine/argon mixture was bubbled through a 0.025 M solution of sodium hydroxide at the rate of about 0.8 atm-cm^3/sec (1 bubble/sec) for a total of 64 hours. The fluorine reacts with water to form HF and ozone. The HF is then neutralized by the NaOH, resulting in a sodium fluoride solution. The flow of the mixture was monitored continuously with the reactant gas linear mass flowmeter and the flow rate versus time was recorded on a strip chart recorder. Integration of the resulting data indicated that the fluorine content was extracted from 3.743×10^4 atm-cm^3 of the mixture. The resulting sodium fluoride solution was then diluted to 200 ml. in a volumetric flask, and 25 ml. aliquots of this solution were analyzed by precipitating the fluorine as triphenyltin fluoride. The precipitate was

then filtered with a 0.45 micron millipore filter and weighed. The basis for this technique is that triphenyltin fluoride is highly insoluble in ethanol and water. Triphenyltin chloride is the precipitating reagent and is soluble in a 60-70% ethanol/water solution. Thus, a solution of triphenyltin chloride is added to a solution of sodium fluoride to precipitate triphenyltin fluoride, which can be filtered, dried at 110°C, and weighed.

The average weight of triphenyltin fluoride obtained from the aliquots analyzed was 0.1002 ± 0.0045 gram. Upon application of the appropriate factor (0.05153) to convert from triphenyltin fluoride to fluoride, the average per cent fluorine by volume in the fluorine/argon mixture was found to be 0.065 ± 0.003%. Therefore, the assumption that the nominal value given by Matheson (0.1%) was correct would have resulted in an error of about 50% in the attachment rate coefficient determined.

APPENDIX II

ELECTROSTATIC LENS SYSTEM

The electrostatic lens system used to focus ions from the flowing afterglow reaction tube into the quadrupole mass spectrometer system is shown in Figure 31. The lens system was designed from published guidelines for electron optics.[64] Cylindrical lens elements are mounted on sapphire rods, and potentials are applied to them to produce fields (labeled lens #1, lens #2 and lens #3), between the lens elements, which focus the ions. Figure 31 illustrates that there are four cylindrical lens elements (separated by spacers) at different potentials. The actual lenses are the electrostatic fields between these lens elements. The eight-inch flange on which three of the lens elements are mounted is also a cylindrical lens elements. The sampling cone is also mounted on the eight-inch flange. Since the flange and cone form one lens element in the system, they are isolated from the vacuum housing by using a Teflon ring seal and nylon bolts. One of the cylindrical elements is primarily wire mesh, which facilitates pumping of the gas from that region. Electrical potentials are applied to the lens elements through a hermetic seal mounted on the flange. Figure 8 shows the location of the electrostatic lens system in the flowing afterglow apparatus.

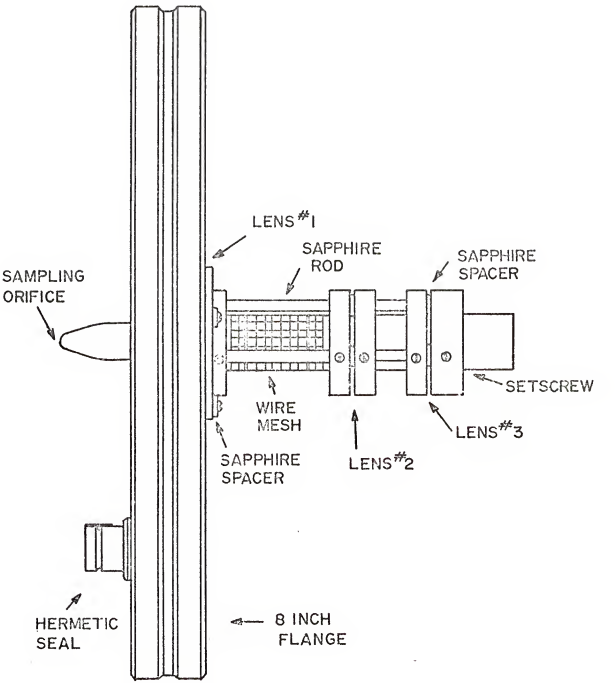

Figure 31. Electrostatic Lens System

Figure 32 illustrates the electrostatic lens control circuit. This is basically a voltage divider allowing positive or negative potentials to be applied to the lens elements. A digital panel meter is used to monitor the potentials applied to the lens elements.[65] Switches A through F are part of a six-pole quadrupole-throw function switch. In position 1 the digital panel meter displays the potential applied to the lens element selected by switch G. Positions 2 and 3, respectively, allow the digital panel meter to be used as either a 200-volt or a 2-volt voltmeter. Position 4 disconnects the panel meter from the voltage divider circuit. The power supply[66] output is grounded at center potential, allowing ±75 volts to be applied to the lens elements. The 8 mfd capacitors provide an AC ground for the circuit, decreasing the ripple superimposed on the DC output of the circuit due to AC pickup. In general, the potentials on the lens elements are adjusted for maximum ion signal. Typical potentials are +10, +20, +45 and +20 volts for the sampling cone, lens element #1, lens element #2 and lens element #3, respectively, when sampling negative ions from the afterglow. Figure 33 illustrates the response of the observed ion signal (F^- in this case) to variations in the potentials (up to 25 volts) applied to the lens elements. Each curve was obtained by initially adjusting all lens elements for maximum ion signal and then varying the potential for a given element. An important fact to note here is that no ion signal is obtained until the sampling cone potential is at least +4 volts. This is due to the fact that

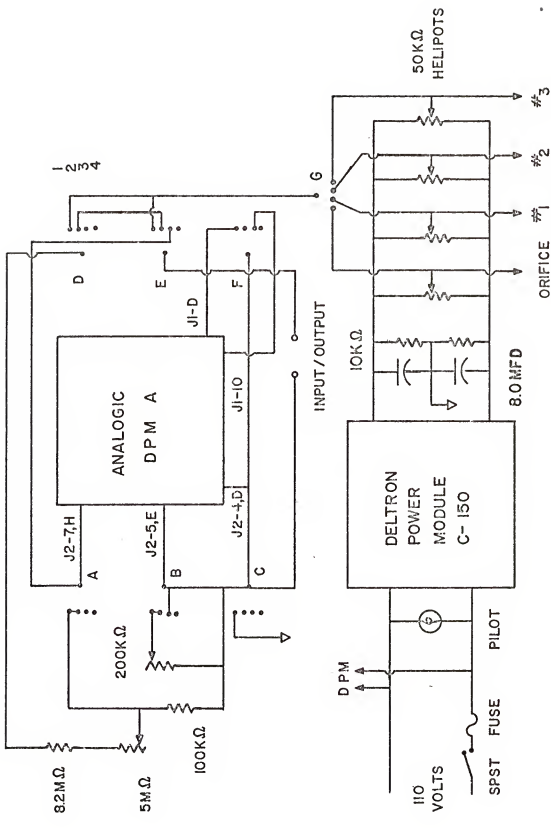

Figure 32. Electrostatic Lens Control Circuit

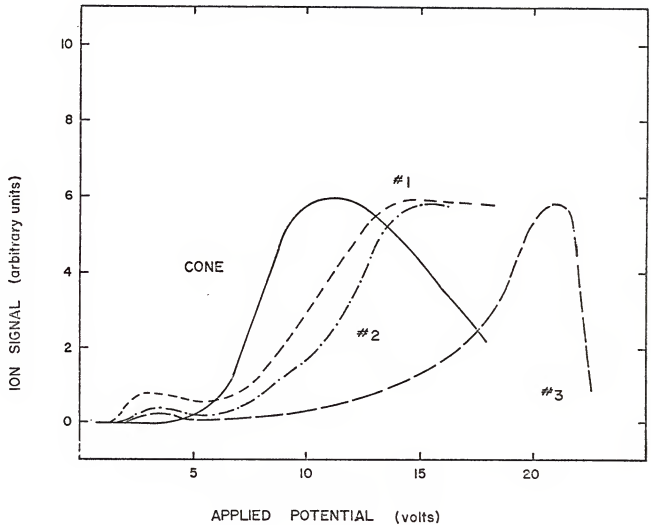

Figure 33. Electrostatic Lens Performance

the plasma is positive with respect to ground and the negative ions must be extracted by a positive potential. The small potentials applied to the sampling orifice should have no accelerating effect on the electrons in the high pressure environment of the reaction tube.

APPENDIX III

THERMALIZATION OF ELECTRONS BY ELASTIC COLLISIONS IN AN ARGON AFTERGLOW

Calculations were made to ascertain whether electrons in an active microwave discharge can be assumed to have been reduced to thermal energies (that is, to approximately the average energy of the buffer gas) within the period between their removal from the active discharge and their arrival at the point at which the neutral reactant gas is injected into the reaction tube (1 to 3 msec). These calculations were based on the following assumptions:

1. The electron energy in the active discharge was assumed to conform to a Maxwell-Boltzmann distribution with a temperature corresponding to an energy of 10 electron volts (approximately 175 volts/cm-Torr[67] for argon).

2. The argon buffer gas energy distribution was assumed to be Maxwell-Boltzmann, with a temperature of 300°K at all times.

3. The fraction of the energy lost per elastic collision with an argon atom by an electron was given by the relation[68]

$$f(E) = (8/3)[mM/(m + M)^2][1 - T/T_m] \qquad (98)$$

where m and M are the masses of the electron and atom, respectively, and T and T_m represent the temperature of the atoms and electrons, respectively.

4. Inelastic electron-atom collisions were not considered.

The history of an electron with energy E_o at t=0 in an argon buffer gas can be derived as follows. The changes in the energy of the electron upon suffering elastic collisions with argon are given by

$$E_1 = [1 - f(E)]E_o$$

$$E_2 = [1 - f(E)]^2 E_o$$

$$E_3 = [1 - f(E)]^3 E_o$$

$$\vdots$$

$$E_{n(t)} = [1 - f(E)]^{n(t)} E_o \qquad (99)$$

or

$$\ln[E_{n(t)}/E_o] = n(t)\ln[1 - f(E)] \qquad (100)$$

where n(t) is the total number of elastic collisions suffered by the electron. Using the approximation

$$\ln[1 - f(E)] = -f(E) + 1/2f(E)^2 - 1/3f(E)^3 - \ldots (-1)^i t^{-1} f(E)^i \qquad (101)$$

and dropping all but the first term, since $f(E) \ll 1$, reduces Equation 100 to

$$\ln[E_{n(t)}/E_o] = -n(t)f(E) \qquad (102)$$

The total number of collisions may be calculated from the expression

$$n(t) = \int_o^t \nu(t)dt \tag{103}$$

where $\nu(t)$ is the electron-atom collision frequency, which changes with respect to time by virtue of the fact that the electron energy, and thus the velocity, changes with respect to time. This assumes that the mean free path for an electron undergoing elastic collisions in argon is independent of electron energy. The mean free path used in these calculations was $\lambda_e=10^{-3}$ meters for an argon pressure of 2.5 Torr.[19] We can now write

$$v(t) = (2E/m)^{1/2} \tag{104}$$

$$\nu(t) = v(t)/\lambda_e = (2E/m)^{1/2}/\lambda_e \tag{105}$$

$$n(t) = \int_o^t [(2E/m)^{1/2}/\lambda_e]dt \tag{106}$$

$$\ln[E/E_o] = f(E)/\lambda_e \int_o^t (2E/m)^{1/2}dt \tag{107}$$

where $v(t)$ is the electron velocity and E is a function of time. The value $f(E)$ may be written

$$f(E) = (8/3)[mM/(m + M)^2][1 - kT/E] \tag{108}$$

where k is the Boltzmann constant and kT is the average energy of the argon atoms at 300°K (0.026 eV). We then have

$$\ln[E_o/E] = (8/3)[mM/(m + M)^2][1 - kT/E]$$

$$[1/\lambda_e] \int_o^t (2E/m)^{1/2} dt \qquad (109)$$

or

$$\ln[E_o/E] = (8/3)[mM/(m + M)^2][1/\lambda_e][2/m]^{1/2}$$

$$[1 - kT/E] \int_o^t E^{1/2} dt \qquad (110)$$

The integral may be approximated and the equation written in the form

$$\ln[E_o/E] = (8/3)[mM/(m + M)^2][1/\lambda_e][2/m]^{1/2}$$

$$[1 - kT/E]E^{1/2}t \qquad (111)$$

This equation gives a correct value for E at time t only if t is sufficiently small that the fraction kT/E and the term $E^{1/2}$ do not change appreciably during that interval. To extend the useful interval to which this equation may be applied, it can be written in the form

$$\ln[E_o/E] = (8/3)[mM/(m + M)^2][1/\lambda_e][2/m]^{1/2}$$

$$\sum_{j=1}^{t/\Delta t} [1 - kT/E_{j-1}]E_{j-1}^{1/2} \Delta t \qquad (112)$$

where Δt is a time increment which is small, such that the change in the fraction of energy transferred per collision

and the collision frequency can be considered constant during this interval. A Hewlett-Packard 2116C computer was used to calculate energy versus time data based on Equation 112. These data are shown in Table 7.

Table 7

Electron Energy Versus Time Calculations for an Afterglow

E(eV)	t(msec)
10	0
5.6	0.01
0.52	0.1
0.029	1
0.026	2
0.026	3

Therefore, the electrons are reduced to thermal energy by elastic collisions in an argon afterglow in a period of the order of 1-2 msec.

APPENDIX IV

EXPERIMENTAL DATA LISTINGS

The experimental data obtained in the present experiments are tabulated at the end of this appendix. Data obtained for which the resulting rate constants are greater than two standard deviations from the mean are not included in the listings. Table 8 provides a key to the data listings at the end of this appendix.

Table 8

Data Listings Key

Reaction Studied	Electron Source	Number of Experiments	Page
Electron Attachment in SF_6	microwave	22	153
$SF_6 - O_2^-$ Charge Transfer	microwave	4	154
Electron Attachment in F_2	microwave	7	155
Electron Attachment in SF_6	filament	19	156
Electron Attachment in F_2	filament	21	157
Electron Attachment in Cl_2	filament	16	158
Electron Attachment in Br_2	filament	20	159

In order to present the experimental data on a reasonable number of pages, the ion signal versus reactant flow results

were fitted to an equation of the form

$$y = a + bx + cx^2 + dx^3 + ex^4 + fx^5 + gx^6 \qquad (113)$$

using an orthogonal polynomial technique.[69] In this equation y represents the observed ion signal in picoamps and x represents the reactant gas flow in molecules/sec. Thus, by substituting the coefficients presented in the data listings for a given experiment into Equation 113 and knowing the maximum reactant gas flow during that particular experiment, the experimental data may be regenerated.

All of the experimental data listings follow the same format. The type of electron source used and the reaction studied are given at the top of each page. Each experiment is summarized in two lines. The first line, reading from left to right, contains seven pieces of information: the experiment number, the buffer gas flow in atm/cm^3-sec, the buffer gas pressure in Torr, the measured reaction tube transit time in msec, the sampling cone potential in volts, the metastable atom quenchant pressure in Torr and the maximum reactant gas flow in molecules/sec. The metastable atom quenchant used in the present experiments was nitrogen except in the $SF_6 - O_2^-$ charge transfer experiments in which oxygen was used. Three dashes appearing within the first line indicate that the measurement corresponding to the location of the dashes was not performed. The second line, reading left to right, lists the coefficients (a through g) obtained using the

orthogonal polynomial curve fit technique. Dashes appearing in the second line indicate a less than sixth order curve fit. The coefficients presented in the listings reproduce the data very well except for three experiments noted by asteriks beside the experiment numbers. The ions monitored in the present experiments are the product ions shown at the top of each page of the data listings.

In the $SF_6 - O_2^-$ charge transfer experiments the O_2^- ion was monitored. In experiment 3 the coefficients tabulated in the second and third lines correspond to the SF_6^- and O_2^- ion signals, respectively. In experiment 4 the coefficients tabulated in the second and third lines correspond to the O_2^- and Cl^- ion signals, respectively. In the chlorine data listings the coefficients tabulated in the second and third lines of each experiment correspond to the Cl^- (m/e = 35) and Cl^- (m/e = 37) ion signals, respectively. In the bromine data listings the coefficients tabulated in the third line of experiment 2 correspond to a Br_3^- ion signal.

MICROWAVE SOURCED SF6 + E- = SF6-

1	25.1	2.14	---	3.9	.C00	512E+12
747E+01	355E-11	-382E-25	235E-39	-820E-54	147E-68	-103E-83
2	25.0	2.15	---	4.2	.C00	385E+12
664E+01	549E-11	-634E-25	435E-39	-171E-53	348E-68	-281E-83
3	25.2	2.12	---	5.2	.C00	354E+12
736E+00	454E-11	-600E-25	433E-39	-167E-53	325E-68	-245E-83
4	25.0	2.16	---	5.2	.050	367E+12
282E+01	306E-11	-406E-25	291E-39	-112E-53	217E-68	-165E-83
5	24.8	2.15	---	5.2	.050	386E+12
375E+01	295E-11	-378E-25	256E-39	-882E-54	145E-68	-873E-84
6	24.8	2.10	---	5.2	.C00	186E+12
694E+01	136E-11	970E-25	-265E-38	269E-52	-123E-66	210E-81
7	23.9	2.06	---	3.9	.C00	290E+13
335E+02	993E-12	-264E-26	319E-41	-188E-56	535E-72	-583E-88
8	23.8	2.09	---	3.9	.020	279E+13
196E+02	832E-12	-228E-26	291E-41	-182E-56	551E-72	-636E-88
9	24.3	2.08	---	4.5	.C00	187E+13
263E+02	210E-11	-854E-26	160E-40	-149E-55	672E-71	-115E-86
10	24.6	2.13	---	5.1	.020	183E+13
311E+02	165E-11	-682E-26	131E-40	-126E-55	586E-71	-104E-86
11	24.5	2.12	---	5.4	.C00	349E+12
101E+02	608E-11	-740E-25	468E-39	-154E-53	245E-68	-141E-83
12	24.4	2.13	---	5.4	.020	296E+12
972E+01	470E-11	-613E-25	406E-39	-132E-53	182E-68	-507E-84
13	24.1	2.11	---	4.3	.C00	268E+12
102E+02	361E-11	-390E-25	188E-39	-808E-55	-200E-68	427E-83
14	24.2	2.14	---	4.3	.020	547E+12
118E+02	332E-11	-406E-25	266E-39	-909E-54	151E-68	-965E-84
15	23.9	2.08	---	4.6	.C00	222E+12
264E+01	228E-11	480E-25	-184E-38	219E-52	-110E-66	200E-81
16	24.1	2.11	---	4.6	.020	225E+12
109E+02	308E-11	-916E-27	-918E-39	130E-52	-685E-67	124E-81
17	25.0	2.16	---	4.7	.C00	640E+11
223E+01	304E-11	805E-25	275E-38	-436E-51	115E-64	-897E-79
18	25.0	2.17	---	4.7	.020	640E+11
478E+01	-149E-11	100E-23	-707E-37	232E-50	-362E-64	212E-78
19	24.8	2.11	---	5.2	.C00	360E+12
138E+02	398E-11	-448E-25	294E-39	-109E-53	211E-68	-165E-83
20	24.7	2.11	---	5.2	.C00	459E+12
160E+02	408E-11	-469E-25	307E-39	-109E-53	197E-68	-139E-83
21	24.6	2.08	---	5.5	.C00	934E+11
820E+00	688E-12	216E-24	-891E-38	163E-51	-143E-65	484E-80
22	24.4	2.07	---	5.5	.C00	108E+12
251E+00	695E-12	157E-24	-567E-38	889E-52	-661E-66	189E-80

MICROWAVE SOURCED SF6 + O2- = SF6- + O2

1	27.0	2.35	---	13.5	.320	215E+15
106E+02	-249E-15	457E-32	-496E-49	251E-66	-461E-84	---
2	27.0	2.35	---	13.5	.320	315E+15
941E-01	-112E-17	527E-35	-107E-52	739E-71	---	---
3	26.3	2.31	---	13.1	.310	572E+15
347E+00	281E-16	-122E-33	237E-51	-166E-69	---	---
912E-01	-109E-17	490E-35	-941E-53	648E-71	---	---
4	27.7	2.30	---	11.7	.300	582E+15
771E-01	-982E-18	520E-35	-132E-52	133E-70	---	---
469E+01	-867E-17	843E-34	-275E-51	265E-69	---	---

MICROWAVE SOURCE0 F2 + E- = F- + F

1	26.5	2.30	4.0	8.9	.C00	155E+13
118E+02	267E-12	-353E-27	-157E-42	842E-57	-726E-72	196E-87
2	26.5	2.30	4.0	8.9	.C00	155E+13
822E+01	116E-12	394E-27	-188E-41	284E-56	-184E-71	437E-87
3	26.5	2.30	4.0	8.9	.C00	155E+13
702E+01	-146E-12	128E-26	-278E-41	278E-56	-134E-71	253E-87
4	29.6	2.50	4.0	10.2	.C00	102E+13
781E+01	641E-12	-973E-27	-156E-41	645E-56	-676E-71	234E-86
5	29.6	2.50	4.0	10.2	.C00	698E+12
133E+01	213E-12	706E-26	-558E-40	169E-54	-229E-69	114E-84
6	29.6	2.50	4.0	10.2	.C00	606E+12
387E+01	-193E-12	798E-26	-523E-40	151E-54	-206E-69	106E-84
7	29.6	2.50	4.0	10.2	.C00	594E+12
105E+01	116E-12	799E-26	-624E-40	195E-54	-277E-69	147E-84

FILAMENT SOURCED SF6 + E- = SF6-

1	13.7	1.47	6.5	8.9	.000	165E+12
146E+00	428E-13	-137E-26	243E-40	-230E-54	108E-68	-199E-83
2*	13.6	1.48	6.5	9.0	.000	106E+12
124E-01	100E-12	-766E-26	310E-39	-590E-53	513E-67	-165E-81
3	20.2	1.92	6.1	8.9	.000	147E+12
328E+00	465E-13	-137E-26	225E-40	-201E-54	916E-69	-164E-83
4	6.8	.97	8.3	9.9	.000	214E+12
213E+00	848E-13	-236E-26	349E-40	-270E-54	104E-68	-158E-83
5	6.7	.96	8.3	9.9	.000	258E+12
415E+00	275E-13	-401E-27	416E-41	-272E-55	927E-70	-122E-84
6	13.0	1.48	6.6	9.9	.000	129E+12
319E+00	232E-12	-664E-26	963E-40	-653E-54	138E-68	203E-83
7*	13.1	1.45	6.6	---	.000	247E+12
175E+01	-745E-13	293E-26	-383E-40	226E-54	-616E-69	619E-84
8	13.2	1.43	6.5	---	.000	146E+12
107E+01	969E-13	433E-27	-734E-40	130E-53	-905E-68	222E-82
9	12.1	1.39	6.4	---	.000	235E+12
159E+01	128E-12	-227E-26	206E-40	-906E-55	171E-69	-853E-85
10	19.9	1.89	5.7	---	.000	231E+12
166E+01	125E-12	-312E-26	399E-40	-267E-54	892E-69	-117E-83
11	6.1	.88	8.6	---	.000	228E+12
125E+01	145E-12	-316E-26	343E-40	-198E-54	584E-69	-690E-84
12	10.9	1.27	7.0	---	.000	109E+12
951E+00	340E-12	-152E-25	422E-39	-682E-53	562E-67	-179E-81
13	10.9	1.26	7.0	---	.000	109E+12
808E+00	281E-12	-108E-25	242E-39	-321E-53	236E-67	-741E-82
14	10.8	1.26	7.0	---	.000	110E+12
768E+00	280E-12	-115E-25	261E-39	-339E-53	234E-67	-664E-82
15	11.4	1.30	7.0	---	.000	946E+11
454E+00	491E-12	-327E-25	117E-38	-215E-52	192E-66	-659E-81
16	11.3	1.30	7.0	---	.000	955E+11
633E+00	303E-12	-148E-25	390E-39	-540E-53	373E-67	-104E-81
17	17.3	1.32	4.9	---	.000	366E+11
416E+00	257E-13	146E-24	-218E-37	128E-50	-333E-64	321E-78
18	18.6	1.75	---	10.7	.000	294E+12
198E+00	258E-13	-263E-27	109E-41	-110E-56	-364E-71	657E-86
19	17.1	1.67	---	10.7	.000	148E+12
603E-01	661E-13	-162E-26	204E-40	-116E-54	171E-69	445E-84

* POOR CURVE FIT

FILAMENT SOURCE0 F2 + E- = F- + F

1	11.0	1.28	7.4	---	.C00	327E+13
450E+C0	246E-13	-519E-28	542E-43	-289E-58	75CE-74	-750E-90
2	22.1	2.C0	5.7	---	.C00	316E+13
228E-01	92CE-14	-192E-28	2C7E-43	-113E-58	3C1E-74	-307E-90
3	12.8	1.46	6.4	---	.C00	349E+13
503E+00	218E-13	-442E-28	429E-43	-209E-58	492E-74	-447E-90
4	12.9	1.46	6.5	---	.C00	322E+13
595E+00	206E-13	-436E-28	453E-43	-238E-58	6C8E-74	-599E-90
5	13.1	1.48	6.8	12.7	.C00	193E+13
109E+00	429E-14	-104E-28	145E-43	-110E	424E-74	-647E-90
6	13.1	1.47	6.8	12.7	.C00	287E+13
693E-01	357E-14	-600E-29	551E-44	-271E-59	666E-75	-641E-91
7	13.2	1.48	6.8	12.8	.C00	383E+13
843E-02	273E-14	-391E-29	3C6E-44	-129E-59	272E-75	-223E-91
8	13.3	1.46	6.8	12.8	.C00	194E+13
318E-01	313E-14	-742E-29	1C1E-43	-748E-59	28CE-74	-417E-90
9	13.3	1.47	6.8	12.8	.C00	286E+13
176E-01	242E-14	-455E-29	439E-44	-219E-59	543E-75	-524E-91
10	13.3	1.49	6.8	12.0	.C00	290E+13
106E-01	213E-14	-213E-29	1C9E-44	-303E-60	488E-76	-433E-92
11	13.2	1.48	6.8	12.0	.C00	3C8E+13
107E-01	395E-14	-583E-29	463E-44	-194E-59	404E-75	-323E-91
12	13.0	1.47	6.8	12.0	.C00	288E+13
303E-01	438E-14	-727E-29	68CE-44	-342E-59	863E-75	-855E-91
13	12.6	1.42	7.2	18.1	.C00	286E+13
517E-02	271E-14	-518E-29	513E-44	-286E-59	7C2E-75	-721E-91
14	12.3	1.41	7.2	15.9	.C00	291E+13
154E-01	287E-14	-566E-29	571E-44	-3C2E-59	787E-75	-791E-91
15	12.0	1.41	7.2	18.2	.C00	287E+13
124E-01	301E-14	-608E-29	612E-44	-320E-59	834E-75	-852E-91
16	11.9	1.40	7.2	17.C	.C00	289E+13
174E-01	344E-14	-681E-29	678E-44	-356E-59	944E-75	-989E-91
17	12.1	1.40	7.2	15.8	.C00	192E+13
452E-01	452E-14	-120E-28	167E-43	-122E-58	452E-74	-667E-90
18	12.1	1.40	7.2	15.4	.C00	194E+13
517E-01	415E-14	-119E-28	181E-43	-143E-58	563E-74	-862E-90
19	13.4	1.48	7.2	17.0	.C00	115E+13
226E+00	821E-14	-599E-29	-335E-43	828E-58	-708E-73	211E-88
20	13.2	1.47	7.2	17.1	.C00	113E+13
226E+00	113E-13	-262E-28	251E-43	134E-59	-170E-73	758E-89
21	13.0	1.47	7.2	17.1	.C00	113E+13
112E+00	661E-14	812E-29	-763E-43	146E-57	-117E-72	341E-88

FILAMENT SOURCED CL2 + E- = CL- + CL

1	8.0	1.01	---	11.0	.000	603E+13
141E+01	176E-14	-142E-29	529E-45	-850E-61	403E-77	122E-93
434E+00	489E-15	-394E-30	146E-45	-241E-61	126E-77	233E-94
2	11.2	1.26	---	11.0	.000	353E+13
220E+01	471E-14	-692E-29	541E-44	-230E-59	500E-75	-430E-91
557E+00	113E-14	-162E-29	129E-44	-566E-60	127E-75	-112E-91
3	11.2	1.24	---	11.0	.000	296E+13
189E+01	718E-14	-140E-28	139E-43	-729E-59	188E-74	-190E-90
560E+00	179E-14	-315E-29	292E-44	-144E-59	358E-75	-351E-91
4	11.1	1.25	---	11.0	.000	358E+13
208E+01	468E-14	-588E-29	395E-44	-145E-59	273E-75	-204E-91
581E+00	153E-14	-213E-29	159E-44	-650E-60	134E-75	-109E-91
5	11.0	1.25	---	11.0	.000	354E+13
175E+01	829E-14	-138E-28	113E-43	-484E-59	101E-74	-836E-91
498E+00	220E-14	-344E-29	275E-44	-116E-59	246E-75	-205E-91
6	12.9	1.40	---	10.9	.000	370E+13
380E+00	166E-13	-271E-28	217E-43	-899E-59	184E-74	-149E-90
102E+00	433E-14	-697E-29	556E-44	-230E-59	472E-75	-381E-91
7*	12.8	1.39	---	10.9	.000	368E+13
616E+00	174E-13	-238E-28	160E-43	-571E-59	103E-74	-756E-91
153E+00	442E-14	-569E-29	363E-44	-124E-59	220E-75	-157E-91
8	12.7	1.38	---	10.9	.000	371E+13
456E+00	196E-13	-315E-28	246E-43	-996E-59	200E-74	-158E-90
113E+00	475E-14	-767E-29	599E-44	-241E-59	485E-75	-382E-91
9	19.6	1.87	---	11.0	.000	370E+13
441E+00	511E-14	210E-29	-604E-44	352E-59	-849E-75	747E-91
929E-01	110E-14	660E-30	-150E-44	842E-60	-198E-75	171E-91
10	19.6	1.86	---	11.0	.000	365E+13
395E+00	455E-14	166E-29	-587E-44	369E-59	-943E-75	866E-91
814E-01	104E-14	538E-30	-149E-44	923E-60	-236E-75	218E-91
11	27.5	2.35	---	11.0	.000	365E+13
601E-01	799E-15	428E-30	290E-45	-403E-60	124E-75	-124E-91
171E-01	210E-15	512E-31	872E-46	-891E-61	250E-76	-231E-92
12	13.2	1.40	---	11.0	.000	351E+13
450E+00	857E-14	-144E-28	118E-43	-506E-59	106E-74	-881E-91
111E+00	237E-14	-405E-29	337E-44	-144E-59	305E-75	-252E-91
13	13.4	1.41	---	11.0	.000	359E+13
557E+00	138E-13	-225E-28	180E-43	-746E-59	154E-74	-125E-90
158E+00	382E-14	-628E-29	508E-44	-214E-59	448E-75	-370E-91
14	13.3	1.41	---	11.0	.000	355E+13
426E+00	135E-13	-223E-28	182E-43	-773E-59	162E-74	-134E-90
121E+00	370E-14	-605E-29	491E-44	-208E-59	439E-75	-364E-91
15	13.3	1.41	---	11.0	.000	354E+13
379E+00	134E-13	-221E-28	181E-43	-770E-59	163E-74	-135E-90
112E+00	370E-14	-597E-29	483E-44	-204E-59	432E-75	-359E-91
16	20.2	1.88	---	11.0	.000	362E+13
200E+00	247E-14	279E-29	-475E-44	259E-59	-622E-75	554E-91
553E-01	660E-15	708E-30	-116E-44	619E-60	-145E-75	127E-91

* POOR CURVE FIT

FILAMENT SOURCED BR2 + E- = BR- + BR

1	33.6	2.01	---	10.1	.050	219E+16
106E+01	-125E-17	900E-36	-206E-54	---	---	---
2	33.0	2.00	---	10.1	.050	214E+16
822E+00	-725E-18	401E-36	-886E-55	---	---	---
217E-01	961E-19	-579E-37	127E-55	---	---	---
3	31.5	1.91	---	10.0	.050	181E+16
359E+00	-765E-18	592E-36	-152E-54	---	---	---
4	31.4	1.93	---	10.0	.050	341E+15
176E-02	177E-17	-785E-36	-967E-53	126E-70	---	---
5	32.3	1.93	---	10.0	.050	293E+15
609E-03	343E-18	463E-35	193E-52	-102E-69	---	---
6	32.0	1.94	---	10.0	.050	297E+15
101E-02	222E-18	875E-35	-289E-52	355E-70	---	---
7	31.9	1.94	---	10.0	.050	339E+15
117E-01	-502E-18	221E-34	-103E-51	149E-69	---	---
8	31.8	1.97	---	10.0	.100	214E+15
202E-02	186E-18	119E-34	-624E-52	108E-69	175E-89	---
9	31.0	1.86	---	10.0	.050	542E+15
826E-02	532E-17	-209E-34	319E-52	-165E-70	---	---
10	30.7	1.85	---	10.0	.050	533E+15
132E-01	530E-17	-289E-34	622E-52	-462E-70	---	---
11	31.3	1.89	---	10.0	.050	526E+15
433E-02	392E-20	245E-35	660E-53	437E-71	---	---
12	31.2	1.94	---	10.0	.100	578E+15
205E-02	528E-18	308E-35	-963E-53	721E-71	---	---
13	31.5	1.93	---	10.0	.100	582E+15
127E-03	906E-18	729E-36	-625E-53	597E-71	---	---
14	31.5	1.89	---	10.0	.050	424E+15
122E-01	916E-18	445E-35	-254E-52	290E-70	---	---
15	32.1	1.94	---	10.0	.050	527E+15
121E-02	829E-18	145E-37	-579E-53	664E-71	---	---
16	32.0	1.98	---	10.0	.100	523E+15
535E-02	467E-18	147E-35	-723E-53	686E-71	---	---
17	33.3	2.05	---	10.0	.150	309E+15
485E-02	872E-18	-140E-34	120E-51	-421E-69	518E-87	---
18	32.4	1.97	---	10.0	.100	524E+15
108E-02	718E-19	427E-36	-101E-54	-538E-72	---	---
19	32.1	1.97	---	10.0	.100	627E+15
179E-02	455E-19	123E-35	-263E-53	169E-71	---	---
20	25.1	1.61	---	10.0	.100	650E+15
174E-03	164E-18	265E-35	-840E-53	657E-71	---	---

LIST OF REFERENCES

1. H.S.W. Massey, E.H.S. Burhop and H.B. Gilbody, Electronic and Ionic Impact Phenomena, Vol. II, Clarendon Press, Oxford, 1969.

2. F.C. Fehsenfeld, Journal of Chemical Physics, 53, 2000 (1970).

3. W.M. Hickam and R.E. Fox, Journal of Chemical Physics, 25, 642 (1950).

4. Fehsenfeld (see reference 2) believes SF_5^- to be formed by the attachment of electrons to sulfur hexafluoride to yield SF_6^- in a repulsive state ~0.43 eV above the SF_6 ground state.

5. C.L. Chen and P.J. Chantry, Bulletin of the American Physical Society, 15, 418 (1970).

6. H.O. Pritchard, Chemical Reviews, 52, 529 (1953).

7. T.L. Cottrell, The Strength of Chemical Bonds, Butterworth's Scientific Publications, London, 1954.

8. J.F. Burns, Carbide and Carbon Chemicals Company, K-25 Plant, Report K-1147 (1954).

9. R. Thorburn, Proceedings of the Physical Society of London, 73, 122 (1959).

10. J.J. DeCorpo and J.L. Franklin, Journal of Chemical Physics, 54, 1885 (1971).

11. N.E. Bradbury, Journal of Chemical Physics, 2, 827 (1934).

12. V.A. Bailey and R.H. Healey, Philosophical Magazine, 19, 725 (1935).

13. D.C. Frost and C.A. McDowell, Canadian Journal of Chemistry, 38, 407 (1960).

14. H-K Moe, Dissertation Abstracts International, 30, 158-B (1969).

15. D.B. Dunkin, F.C. Fehsenfeld and E.E. Ferguson, Chemical Physics Letters, 15, 257 (1972).

16. H.B. Wahlin, Physical Review, 19, 173 (1922).

17. S.E. Bozin and C.C. Goodyear, British Journal of Applied Physics, 18, 49 (1967).

18. L.B. Loeb, Basic Processes of Gaseous Electronics, University of California Press, Los Angeles, 1960.

19. O.J. Orient, Canadian Journal of Physics, 43, 422 (1965).

20. E.W. McDaniel, Collision Phenomena in Ionized Gases, John Wiley and Sons, Inc., New York, 1964.

21. G. Herzberg, Atomic Spectra and Atomic Structure, Dover Publications, New York, 1944.

22. G. Herzberg, Spectra of Diatomic Molecules, D. Van Nostrand Company, Inc., New York, 1950.

23. J.E. Bailey, R.E.B. Makinson and J.M. Somerville, Philosophical Magazine, 24, 177 (1937).

24. F.K. Truby, Physical Review A, 4, 613 (1971).

25. S.A.A. Razzak and C.C. Goodyear, Journal of Physics D, 2, 1577 (1969).

26. F.C. Fehsenfeld, Journal of Chemical Physics, 54, 438 (1971).

27. B.H. Mahan and C.E. Young, Journal of Chemical Physics, 44, 2192 (1966).

28. C.E. Young, UCRL Report No. UCRL-17171, 1966.

29. E. Chen, R.O. George and W.E. Wentworth, Journal of Chemical Physics, 49, 1973 (1968).

30. F.J. Davis and D.R. Nelson, Chemical Physics Letters, 3, 461 (1969).

31. L.M. Chanin, A.V. Phelps and M.A. Biondi, Physical Review, 128, 219 (1962).

32. J.L. Pack and A.V. Phelps, Journal of Chemical Physics, 44, 1870 (1966).

33. Model PGM-10, Raytheon Company, Manchester, New Hampshire.

34. Evenson Cavity, Opthos Instrument Company, Rockville, Maryland.

35. Model 725.3, Opthos Instrument Company, Rockville, Maryland.

36. Model 1355, Brooks Instrument Division, Emerson Electric Company, Cincinnati, Ohio.

37. Model All-10000, Hastings-Raydist, Hampton, Virginia.

38. Model 77H-300, MKS Instruments, Inc., Burlington, Massachusetts.

39. Model All-5, Hastings-Raydist, Hampton, Virginia.

40. Model 162-8, Extranuclear Laboratories, Inc., Pittsburgh, Pennsylvania.

41. Model 1375B, Sargent-Welch Scientific Company, Springfield, New Jersey.

42. Series 216, Granville-Phillips Company, Boulder, Colorado.

43. Made to specifications by Electron Technology, Inc., Kearny, New Jersey.

44. Model LCS-CC-01, Lambda Electronics Corporation, Melville, New York.

45. Model 2116C, Hewlett-Packard, Palo Alto, California.

46. R.C. Bolden, R.S. Hemsworth, M.J. Shaw and N.D. Twiddy, Journal of Physics B, 2, 45 (1969).

47. S. Dushman and J.M. Lafferty, Scientific Foundations of Vacuum Technique, John Wiley and Sons, Inc., New York, 1962.

48. E.E. Ferguson, F.C. Fehsenfeld and A.L. Schmeltekopf, Advances in Atomic and Molecular Physics, 5, 1 (1969).

49. M. Cher and C.S. Hollingsworth, Advances in Chemistry Series, 80, 118 (1969).

50. A. Redfield and R.B. Holt, Physical Review, 82, 874 (1951).

51. F. Kaufman, Advances in Chemistry Series, 80, 29 (1969).

52. R.F. Curl, Jr., Journal of Computational Physics, 6, 367 (1970).

53. J.C. Becsey, L. Berke and J.R. Callan, Journal of Chemical Education, 45, 728 (1968).

54. M. Bourene and J. Le Calve, Journal of Chemical Physics, 58, 1452 (1973).

55. J.L. Franklin, J.G. Dillard, H.M. Rosenstock, K. Draxil and F.H. Field, National Standard Reference Data Series, 26, 1 (1969).

56. M.A. Biondi, Physical Review, 82, 453 (1951).

57. M.A. Biondi, Physical Review, 88, 660 (1952).

58. D. Smith, C.V. Goodall and M.J. Copsey, Journal of Physics B, 1, 660 (1968).

59. J.F. Paulson, Advances in Chemistry Series, 58, 28 (1966).

60. F.K. Truby, Physical Review A, 4, 114 (1971).

61. D.I. Rosen, R.N. Sileo and T.A. Cool, IEEE Journal of Quantum Electronics, QE-9, 163 (1973).

62. J.V.V. Kasper and G.C. Pimentel, Physical Review Letters, 14, 352 (1965).

63. N. Allen and N.H. Furman, Journal of the American Chemical Society, 54, 4625 (1932).

64. K.R. Spangenburg, Vacuum Tubes, McGraw-Hill, New York, 1948.

65. Model AN2510-1B, Analogic, Wakefield, Massachusetts.

66. Model C150-.08, Deltron, Inc., North Wales, Pennsylvania.

67. V.E. Golant, Soviet Physics-Technical Physics, 4, 680 (1959).

68. A.M. Cravath, Physical Review, 36, 248 (1930).

69. J.W. Bright and G.S. Dawkins, I and EC Fundamentals, 4, 93 (1965).

BIOGRAPHICAL SKETCH

Gary Donald Sides was born October 5, 1947, in Tuscaloosa, Alabama. He graduated from Holt High School in Holt, Alabama, in June, 1965. He received his Bachelor of Science in chemistry from the University of Alabama in June, 1969. He received his Master of Science in chemistry from the University of Florida in June, 1971. In July, 1971 he entered the United States Air Force as an officer and was stationed at Wright-Patterson Air Force Base where he has worked since that time as a research chemist at the Aerospace Research Laboratories. During this time he pursued his degree of Doctor of Philosophy from the University of Florida.

He was married to the former Sarah Ann Smith in May, 1968 and they have one son.

I certify that I have read this study and that in my opinion it conforms to acceptable standards of scholarly presentation and is fully adequate, in scope and quality, as a dissertation for the degree of Doctor of Philosophy.

Robert J. Hanrahan, Chairman
Professor of Chemistry

I certify that I have read this study and that in my opinion it conforms to acceptable standards of scholarly presentation and is fully adequate, in scope and quality, as a dissertation for the degree of Doctor of Philosophy.

Thomas O. Tiernan, Co-Chairman
Aerospace Research Laboratories

I certify that I have read this study and that in my opinion it conforms to acceptable standards of scholarly presentation and is fully adequate, in scope and quality, as a dissertation for the degree of Doctor of Philosophy.

E.E. Muschlitz, Jr.
Professor of Chemistry

I certify that I have read this study and that in my opinion it conforms to acceptable standards of scholarly presentation and is fully adequate, in scope and quality, as a dissertation for the degree of Doctor of Philosophy.

Richard A. Blue
Professor of Physics

This dissertation was submitted to the Graduate Faculty of the Department of Chemistry in the College of Arts and Sciences and to the Graduate Council, and was accepted as partial fulfillment of the requirements for the degree of Doctor of Philosophy.

June, 1975

Dean, Graduate School